Proceso de récord del *Drawdown* y gestión de riesgo de activos financieros, mediante aproximación de procesos *PDMP* y de colas pesadas

Rolando Luis Rubilar Torrealba

Supervisor: Dra. Soledad Torres

Advisor: Dr. Lisandro Fermín

Instituto de Estadística

Universidad de Valparaíso

This dissertation is submitted for the degree of

Doctor en Estadística

Acknowledgements

Para **Melisa** y **María Celeste**.

Este trabajo de tesis es dedicado a mi famila, quienes han cargado con parte importante del sacrificio durante todos estos años.

El pensamiento estadístico será algún día tan necesario para el ciudadano competente como la habilidad de leer y escribir. – H.G. Wells

Abstract

Versión en Español

Uno de los principales problemas aplicados al uso de series financieras es el control y gestión de riesgo, ya que una mala decisión de inversión puede tener fuertes repercusiones tanto a nivel microeconómico como macroeconómico. En este proyecto de investigación se propone la identificación y desarrollo de técnicas para describir el fenómeno de récords de un indicador financiero, conocido como *Drawdown*, para el control dinámico del riesgo de los activos financieros.

En primer lugar, se propone la caracterización del fenómeno de récords del *Drawdown* por medio de modelos *Piecewise Deterministic Markov Process (PDMP)* y, una vez relajados los supuestos generales, se desarrolla una aproximación del proceso por medio de distribuciones de colas pesadas, específicamente de la distribución *Poisson* fraccionaria.

En este trabajo de investigación se desarrollaron métodos de estimación apropiados, tanto al contexto de modelos *PDMP* como al contexto de colas pesadas, lo que permite una adecuada caracterización de los fenómenos financieros en el contexto de riesgo financiero.

Un tercer elemento desarrollado en este trabajo corresponde a una aplicación para la estimación de la propagación del SARS-COV-2 en la zona sur de Chile. Este trabajo utiliza herramientas desarrolladas en el programa de Doctorado que muestra la importancia una formación integral para aportar en diferentes áreas de la ciencia.

Finalmente, los desarrollos técnicos provenientes de esta investigación son aplicados para el uso práctico en la industria, entregando nuevas herramientas para la gestión adecuada del riesgo financiero.

English Version

One of the main problems applied to the use of financial series is the control and management of risk, since a bad investment decision can have strong repercussions at both microeconomic and macroeconomic levels. This research project proposes the identification and develop-

ment of techniques to describe the record phenomenon of a financial indicator, known as *Drawdown*, for the dynamic risk control of financial assets.

Firstly, the characterisation of the *Drawdown* record phenomenon by means of Piecewise Deterministic Markov Process (PDMP) models is proposed and, once the general assumptions are relaxed, an approximation of the process by means of heavy-tailed distributions, specifically the fractional Poisson distribution, is developed.

In this research work, appropriate estimation methods are developed, both in the context of *PDMP* models and in the context of heavy tails, which allow for an adequate characterisation of financial phenomena in the context of financial risk.

A third element developed in this work corresponds to an application for estimating the spread of SARS-COV-2 in southern Chile. This work uses tools developed in the PhD programme, which shows the importance of a comprehensive training to contribute to different areas of science.

Finally, the technical developments from this research are applied for practical use in industry, providing new tools for the proper management of financial risk.

Table of contents

List of figures

List of tables

Chapter 1

Introducción

El análisis del fenómeno de crisis financiera, desde la perspectiva de la investigación científica, es un tópico que ha sido popularizado durante los últimos años, especialmente desde la crisis financiera global del año 2008 (Chatzis et al. (2018), Toarna and Cojanu (2015)), siendo un área de especial interés la teoría de valores extremos dada la repercusión económica que pueden generar eventos considerados como extraños, pero que pueden tener un gran impacto en la estabilidad y desempeño de la economía global.

Autores como Longin (1996), Walter (2016), Alves and Neves (2017), entre otros, consideran la ocurrencia de eventos de muy pequeña probabilidad como un *puzzle* que debe tener una especial atención, lo cual es un cambio de paradigma a la literatura clásica que suele limitar la importancia de la ocurrencia de los eventos considerados como extremos para la modelación estadística (Granger and Orr (1972)), y por tanto, relativizan su importancia como fenómeno económico.

El análisis de valores extremos va más allá del mundo financiero. Bunde et al. (2012) indica la importancia del análisis de fenómenos extremos para poder entender la dinámica de los desastres en áreas tan diversas como climatología, salud, mercados financieros, entre otros, y de este modo, entender que no son eventos aislados, sino que son situaciones recurrentes que deben ser analizadas y gestionadas adecuadamente.

Los valores extremos son una pieza de vital importancia para el análisis de la gestión de riesgo en sus diversas áreas. Sin embargo, el vínculo entre el análisis de los eventos extremos y su utilización en la práctica profesional no es generalizada (de Carvalho (2017)), quedando un espacio importante tanto para el desarrollo de nuevas técnicas y métodos de análisis, como para la divulgación de los desarrollos en la práctica profesional.

Un elemento a considerar, es el fuerte vínculo entre los valores extremos que pueden ser observados en el mercado financiero y la gestión de riesgo de los activos. El análisis de riesgo de los activos financieros, provee una estimación de la exposición que un inversionista

adquiere al realizar una transacción y ayuda a escoger el tamaño de la inversión para encontrar un balance entre el riesgo esperado y la expectativa de rentabilidad de estos activos financieros.

En la práctica profesional el riesgo de los activos financieros debe ser medido desde diversas perspectivas, siendo la volatilidad una medida recurrente para la medición del riesgo. Sin embargo, en el contexto de eventos extremos, el uso de la volatilidad como medida del riesgo no es apropiada, debido a que no es capaz de capturar en forma adecuada (Pedersen (2019)) las estrategias de los operadores bursátiles ante situaciones extremas en los mercados financieros y, por tanto, esta medida de riesgo provee estimaciones que no representan el verdadero nivel de riesgo de los activos financieros, los que pueden provocar fuertes pérdidas económicas de los inversionistas.

Dentro de otras estrategias utilizadas en la medición del riesgo financiero podemos destacar el *Value at Risk (VaR)* (Jorion (2007), Rockafellar et al. (2000), Duffie and Pan (1997)), la que intenta capturar el riesgo asociado a la cola de la distribución de probabilidad de los retornos de los activos financieros. El *VaR* mide la máxima pérdida (o ganancia) en que puede incurrir un inversionista con cierto intervalo de confianza y puede ser obtenida por medio de la información histórica disponible.

Las estrategias mencionadas anteriormente, son capaces de medir las potenciales magnitudes de los movimientos de mercado, tal como lo mencionan Novak and Beirlant (2006). Sin embargo, la información que proviene de estas metodologías no es dinámica, lo que impide realizar gestión activa de los portafolios de inversión (Novak (2017)), siendo ésta la principal crítica y limitación de estas medidas de gestión del riesgo.

Entender el fenómeno del riesgo financiero de valores extremos desde una perspectiva dinámica, requiere el uso de otras herramientas estadísticas y matemáticas. En este sentido, la teoría de récords[1] puede ser utilizado para medir la evolución de los activos financieros en el tiempo, mediante el uso de metodologías disponibles en la práctica profesional de los operadores bursátiles o administradores de fondos.

Los administradores de los fondos de riesgo, típicamente siguen una serie de reglas que definen el comportamiento de las inversiones ante los eventos que estructuran los precios del mercado financiero, tal como lo mencionan Leal and de Melo Mendes (2005), siendo una de las estrategias la de regular las máximas pérdidas acontecidas en un horizonte de tiempo fijo o *Drawdown* (Pospisil and Vecer (2010)), modificando la estructura de incentivos de los administradores ante un nuevo récord observado.

El máximo *Drawdown* se ha transformado en una importante medida del riesgo financiero, tanto para operadores financieros, fondos de inversión y reguladores, tal como lo mencionan

[1] Para una mayor revisión bibliográfica sobre teoría de récords, podemos mencionar a Ahsanullah (2015).

de Melo Mendes and Lavrado (2017), Hsieh and Barmish (2017b), Hsieh and Barmish (2017a), Landriault et al. (2018), entre otros autores y su definición formal la podemos encontrar en Hamelink and Hoesli (2004), Carr et al. (2011) o Magdon-Ismail and Atiya (2004).

Aunque la importancia del máximo *Drawdown* ha tenido una mayor relevancia en la literatura reciente, la dinámica del máximo *Drawdown* no ha sido estudiada como un proceso estocástico, según el conocimiento del autor de este proyecto de tesis, siendo el estudio de este proceso uno de los principales aportes en este trabajo, lo cual aporta de manera complementaria a los análisis realizados por Landriault et al. (2018), Taranto and Khan (2020), Rossello and Lo Cascio (2019), Möller (2018), entre otros autores, que utilizan el máximo *Drawdown* como una medida de desempeño de los procesos estocásticos que generan series de tiempo financieras.

Este trabajo de tesis sigue la siguiente estructura:

- En el Capítulo 2 se describen una serie de elementos preliminares que serán necesarios para entender los desarrollos propios de las investigaciones científicas expuestos en los capítulos posteriores.

- El Capítulo 3 corresponde al artículo llamado *Modeling outliers in financial data using ABC estimation of fractional Poisson parameters* en el cual se desarrollan técnicas de estimación, utilizando una aproximación bayesiana conocida como*Approximate Bayesian Computation (ABC)* y el desarrollo de un nuevo test de hipótesis para el parámetro de una distribución α-estable.

- El Capítulo 4 corresponde al artículo llamado *Modeling records process with Piecewise Deterministic Markov Models*, el que desarrolla un análisis sobre el proceso de recórds del *Drawdown*, considerando procesos PDMP y desarrollando las técnicas de simulación y estimación para este proceso.

- El Capítulo 5 corresponde a un artículo llamado *Meteorological and air pollution factors on SARS-COV-2 transmission: The case of Southern Regions in Chile*, el cual realiza un análisis de los factores que inciden en la propagación de la pandemia SARS-COV-2 y que representa otras investigaciones paralelas que han sido realizadas en el contexto del programa de doctorado.

- Finalmente, el Capítulo 6 corresponde a las conclusiones y trabajo futuro de este trabajo de tesis.

Chapter 2

Preliminares

En el artículo seminal de Davis (1984), se introduce la idea de un tipo de proceso que provee una familia de modelos estocásticos con los que se puede modelar una gran variedad de aplicaciones, el cual llamó *Piecewise Deterministic Markov Processes* (PDMP).

En términos simples, un proceso PDMP corresponde a un estado de un sistema dado, por ejemplo, por un subconjunto E de los números reales. Si comienza desde un valor $x \in E$, el proceso sigue un movimiento determinístico hasta un primer salto en un tiempo T que ocurre de manera espontánea en un momento aleatorio. Estos saltos pueden aparecer como una discontinuidad en la trayectoria del proceso estocástico o como un cambio en la dinámica de la parte determinística. En ambos casos, el proceso vuelve a comenzar en su nuevo estado.

La literatura relacionada a los procesos PDMP ha tenido un importante desarrollo tanto desde una perspectiva teórica, como del desarrollo de aplicaciones en otras áreas de la ciencia. Autores como Bujorianu and Lygeros (2003), Zhang et al. (2008), Costa and Dufour (2008), Benaïm et al. (2015), Chiquet et al. (2009), Durmus et al. (2018), Verger et al. (2007), Lin and Buchler (2018), Fermín and Lévy-Véhel (2020), estudian las propiedades y alcances de los modelos PDMP, además de introducir aplicaciones en áreas tan diversas como física, investigación de operaciones, biología molecular, química, farmacología, economía y finanzas, por nombrar algunas.

Específicamente en el contexto financiero, podemos encontrar desarrollos basados en PDMP en Schäl (1998) quien utiliza los modelos PDMP para controlar el riesgo de los saltos en modelos de seguros. Bäuerle and Rieder (2010) introducen problemas de riqueza terminal y comercio en mercados que no son líquidos. En el estudio de valores extremos relacionados a modelos de seguros, podemos mencionar a Azaïs and Genadot (2018) quien realiza importantes aportes a la teoría financiera detrás de estos modelos.

Aunque los avances mencionados han representado un gran aporte desde la perspectiva teórica, se puede apreciar poco desarrollo de aplicaciones en estas áreas de la ciencia, lo que permite preveer un área de desarrollo científico en los próximos años.

Un elemento necesario para poder entender la construcción del proceso PDMP es conocer el proceso de Markov, el cual describimos a continuación.

2.1 Proceso de Markov

Un proceso de Markov puede ser descrito como un proceso estocástico $(X_t, t \geq 0)$, definido en el espacio de probabilidad $(\Omega, \mathscr{F}, P)$ con valores en E, donde E corresponde a un espacio boreliano y $\mathscr{E}$ es la σ-algebra generada por E, entonces X es un proceso de Markov si para cada instante t, s con $t \geq s$ tenemos

$$P\left(X(t+s) \in \Gamma | \mathscr{F}_t\right) = P\left(X(t+s) \in \Gamma | X(t)\right). \tag{2.1}$$

para todo $s, t \geq 0$ y $\Gamma \in \mathscr{E}$ y por tanto, todos los procesos que posean la característica de la igualdad (2.1) poseen la propiedad de Markov. La propiedad de Markov implica que, dado un proceso de Markov, el pasado y el futuro son independientes cuando el presente es conocido.

Otro punto a tener en consideración es que si $\{\mathscr{G}\}$ es una filtración con $\mathscr{F}_t \subset \mathscr{G}_t$, $t \geq 0$, entonces X es un proceso de Markov respecto a $\{\mathscr{G}\}$. Notar que (2.1) implica

$$\mathbb{E}[f(X(t))|\mathscr{F}_s] = \mathbb{E}[f(X(t))|X(s)] \tag{2.2}$$

para todo $s, t \geq 0$ y $f \in B(E)$, donde $B(E)$ representa el conjunto de funciones medibles $f : E \to \mathbb{R}$.

Definimos como *probabilidad de transición* del proceso de Markov, una función $p(s,x,t,A)$, definida en $0 \leq s \leq t < \infty$ y $A \in \mathscr{E}$ si tiene las siguientes propiedades:

1. Para s, t, x fijos, la función $A \to p(s,x,t,A)$ es una medida de probabilidad en $(E, \mathscr{E})$.
2. Para s, t, A fijos, la función $x \to p(s,x,t,A)$ es $\mathscr{E}$ medible.
3. Para todo s, x, A, la función $p(s,x,s,A) = I_A$, donde I_A corresponde a la función indicatriz.
4. Para cualquier $s \leq t$, $x \in E$ y $A \in \mathscr{E}$, tenemos

$$\mathbb{E}\left[I_A(X_t)|\mathscr{F}_s\right] = p(s, X_s, t, A), \quad c.s.$$

En base a las propiedades de la función de probabilidad de transición, podemos escribir la ecuación (2.2) como

$$\mathbb{E}[f(X_t)|X_s] = \int_E f(y)p(s,X_s,t,dy), \quad c.s. \tag{2.3}$$

Ahora, con $r \leq s \leq t$, usando la propiedad de esperanza condicional $\mathbb{E}[f(X_t)|\mathscr{F}_r] = \mathbb{E}[\mathbb{E}[f(X_t)|\mathscr{F}_s]|\mathscr{F}_r]$ y la ecuación (2.3), tenemos que

$$\mathbb{E}[f(X_t)|X_s] = \int_E \int_E f(y)p(s,z,t,dy)p(r,X_r,s,dz)$$

Tomando $f(y) = I_A$ para algún $A \in \mathscr{E}$, tenemos

$$p(r,x,t,A) = \int_E p(s,z,t,A)p(r,x,s,dz) \tag{2.4}$$

donde la ecuación (2.4) es conocida como ecuación de *Chapman-Kolgomorov*.

Una función de transición es invariante en el tiempo u homogénea si, para todos los $r,s,t, \in \mathbb{R}_+$ con $s \leq t, x \in E$ y $A \in \mathscr{E}$, tenemos

$$p(s+r,x,t+r,A) = p(s,x,t,A).$$

Conociendo las propiedades antes descritas, podemos hacer un pequeño cambio de notación donde

$$p(t,x,A) = p(0,t,x,A).$$

Definimos una familia de Markov como una colección $(\Omega, \mathscr{F}, (\mathscr{F}_t), (X_t), (P_x, x \in E))$, donde $(\Omega, \mathscr{F})$ es un espacio medible, $(\mathscr{F}_t)$ es una filtración, $(X_t, t \in \mathbb{R}_+)$ corresponde a una familia de variables aleatorias tal que X_t es $\mathscr{F}$-medible para cada t y $(P_x, x \in E)$ es una medida de probabilidad medida en $(\Omega, \mathscr{F})$ tal que (X_t) es un proceso de Markov en $(\Omega, \mathscr{F}), P_x$ con función de transición p y con distribución inicial δ_x, esto quiere decir, $P_x[X_0 = x] = 1$. Además escribiremos $\mathbb{E}_x$ como la esperanza con respecto a la medida P_x. Notar además que la medida P_x y la función de transición están relacionadas del siguiente modo

$$P_x[X_t \in A] = p(x,t,A), \quad (t,x,A) \in \mathbb{R}_+ \times E \times \mathscr{E}. \tag{2.5}$$

En una familia de Markov, solo la medida P_x depende del valor inicial $x \in E$.

Un proceso es llamado *proceso de Markov fuerte* si (x_t) es progresivamente medible con respecto a $\mathscr{F}_t$ y para cada $x \in E, A \in \mathscr{E}$, T como tiempo de parada-$\mathscr{F}_t$ y $t \geq 0$ tenemos

$$P_x[x_{T+1} \in A|\mathscr{F}_T]I_{T<\infty} = p(t, X_T, A)I_{T<\infty} \tag{2.6}$$

Esto quiere decir que la evolución del proceso después del tiempo de parada T es solo un reinicio comenzando en T.

2.2 Construcción de un modelo *PDMP*

Sea $(X_t, t \geq 0)$ un proceso de Markov con sus realizaciones continuas a la derecha y con límite a la izquierda (*cádlág*) casi seguramente. Además, el proceso X tiene valores en un subconjunto abierto $\mathscr{X} \subseteq \mathbb{R}^d$, para $d \geq 1$.

Nosotros definimos $\partial\mathscr{X}$ como la frontera de $\mathscr{X}$ y por $\overline{\mathscr{X}}$ la clausura de $\mathscr{X}$, donde la clausura es definida como $\overline{\mathscr{X}} = \{x \in X | \forall\ H(x) : H(x) \cap \mathscr{X} \neq \emptyset\}$ y $H(x)$ corresponde al entorno de x.

Definimos el semigrupo de Markov de X como una familia de operadores P_t actuando sobre funciones medibles acotadas f tal que, para todo $t > 0$ se cumple

$$P_t f(x) = \mathbb{E}\left[f(X_t)|X_0 = x\right].$$

Definimos el generador infinitesimal $\mathscr{U}$ de X el que actúa sobre las funciones f, de manerea que la siguiente definición exista

$$\mathscr{U} f(x) = \lim_{t \to 0} \frac{P_t f(x) - f(x)}{t}. \tag{2.7}$$

El operador $\mathscr{U}$ caracteriza la dinámica del proceso X y puede ser interpretado como la derivada en el tiempo del semigrupo $\partial_t P_t = \mathscr{U}$, en $t = 0$.

Dado lo anterior, el proceso PDMP es determinado por tres componentes característicos: una parte determinística del movimiento entre saltos Υ, una tasa λ de salto asociada a una distribución de probabilidad y una medida de transición o *kernel* del salto Q.

La medida de transición Q posee las siguientes características:

1. Para cada $A \in \mathscr{E}$ fijo, el mapeo $x \to Q(A;x)$ es medible.
2. $Q(\{x\};x) = 0$

A continuación consideraremos la siguiente ecuación diferencial ordinaria

$$\begin{cases} \partial_t \Phi(x,t) = F(\Phi(x,t)) \\ \Phi(x,0) = x, \end{cases} \tag{2.8}$$

con hipótesis suficientes para asegurar existencia y unicidad. Entonces, Φ es el movimiento de X, la cual dirige la dinámica del proceso entre los saltos. Además definimos los siguientes tiempos de ocurrencia de la frontera ∂E comenzando desde x con hipótesis suficientes para asegurar existencia y unicidad.

$$t^+(x) = \inf\{t > 0 : \Phi(x,t) \in \partial E\},$$
$$t^-(x) = \inf\{t > 0 : \Phi(x,-t) \in \partial E\}.$$

con la convención de $\inf\emptyset = +\infty$.

Definimos la tasa de salto $\lambda : E \to \mathbb{R}_+$, que gatilla el mecanismo de salto del proceso estocástico en una función de probabilidad.

Finalmente, Q corresponde al *kernel* de probabilidad sobre $(E \times \mathscr{E})$[1], el cual dirigirá la regla de dirección de los saltos de X, en otras palabras, Q asocia cada punto de $x \in E$ con una medida de probabilidad $Q(x,\cdot)$.

Con estas herramientas, podemos definir las trayectorias de X de modo recursivo. Dado $T_0 = 0$ y $X_0 \in \mathscr{X}$, sea S_1 una variable aleatoria positiva tal que, para todo $t > 0$,

$$P(S_1 \geq t) = \exp\left(-\int_0^t \lambda(\Phi(X_0,s)ds) I_{t<t^+(X_0)}\right), \tag{2.9}$$

Sea $T_1 = T_0 + S_1$ el tiempo del primer salto y U_1 la posición inmediatamente posterior al salto, podemos definir, para $t \in [T_0, T_1]$,

$$X_t = \begin{cases} \Phi(X_0,t) \text{ si } t \in [T_0,T_1) \\ U_1 \qquad \text{si } t = T_1. \end{cases} \tag{2.10}$$

La ecuación (2.10) puede ser expandida de manera recursiva para $t \in [T_n, T_{n+1}]$ y, de este modo, construir las trayectorias completas del proceso.

Davis (1993) en su Teorema 26.14 define para un campo vectorial F, con tasa de salto λ y *kernel* de probabilidad Q, el siguiente generador infinitesimal, para $x \in \mathscr{X}$ y $f \in \mathscr{D}(\mathscr{L})$ donde $\mathscr{D}(\mathscr{L})$ corresponde al dominio de las funciones descritas en (4.3)

$$\mathscr{U} f(x) = F(x) \cdot \nabla f(x) + \lambda(x) \int_E [f(u) - f(x)] Q(x,du). \tag{2.11}$$

[1]Para ver detalles de esta definición, revisar (Klenke, 2013, Definición 8.25).

Hay que destacar que con estas herramientas expuestas, se puede realizar una estimación de los parámetros, de los momentos, distribuciones límite y función característica del proceso por lo que, dependiendo de las necesidades del problema, se deben considerar variantes específicas del *kernel* de probabilidad Q.

A continuación se muestran ejemplos de procesos estocásticos que pueden ser modelados a través de modelos PDMP y que representan un conjunto de modelos básicos con los cuales generar aplicaciones más complejas.

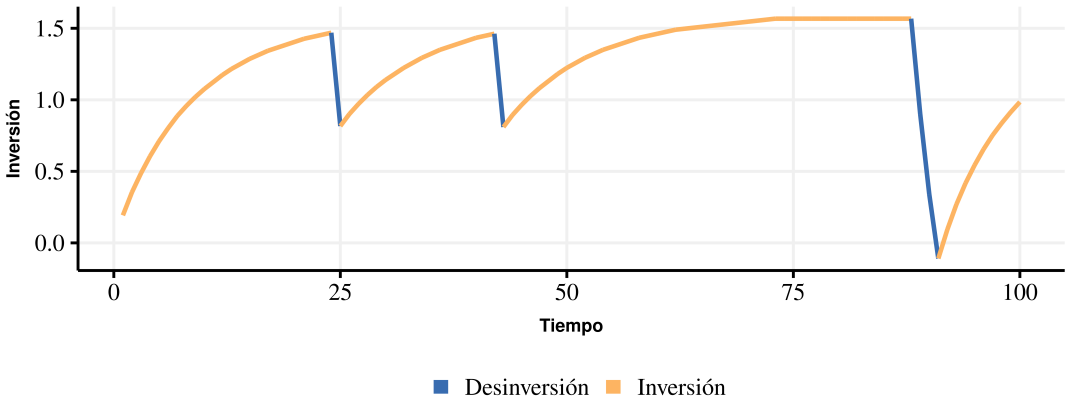

Fig. 2.1 Realización de proceso de inversión y desinversión.

La Figura 2.1 representa una realización de un proceso de inversión-desinversión de un agente económico, basado en los modelos desarrollados por Aiyagari (1994) y Huggett (1993). En estos modelos el agente económico está sujeto a condiciones durante su ciclo de vida en el cual puede perder su trabajo y, por lo tanto, su principal fuente de ingresos. Al perder su principal fuente de ingresos, el agente económico utiliza los recursos acumulados para mantener su nivel de utilidad provocando el proceso de desinversión.

2.3 Proceso de Poisson

La construcción del proceso *PDMP* y del proceso *Poisson fraccionario* tienen un estrecho vínculo con el proceso de *Poisson*, el cual fue descrito originalmente por Simeon Denis Poisson (1781-1840).

Sea $S_1, S_2, \ldots$ una sucesión de variables aleatorias independientes e identicamente distribuidas con distribución exponencial, $P(S_1 > t) = e^{-\lambda t}$ para algún $\lambda > 0$, y definimos $T_1 = S_1$, $T_i = S_1 + \ldots + S_i$ para $i \geq 2$ y $t \geq 0$. Un elemento clave de esta distribución rela-

cionada con su distribución condicional es su propiedad de pérdida de memoria, que está dada por

$$P[T > t+s|T > s] = \frac{e^{-\lambda(t+s)}}{e^{-\lambda s}} = e^{-\lambda t} \tag{2.12}$$

La condición de pérdida de memoria implica que la distribución condicional es exactamente la misma que la distribución incondicional de T.

Ahora, definimos el siguiente proceso de conteo

$$N_t = \sum_{i=1}^{\infty} I_{t \geq T_i}.$$

Las realizaciones de N_t son funciones escalonadas, con saltos de tamaño uno y continuas a la derecha para cada $T_i \in [0, \infty[$. La figura 2.2 muestra un ejemplo de realización de un proceso aleatorio N_t, donde se muestra un proceso continuo a la derecha con límite a la izquierda, con intervalos de llegada que se distribuyen exponencial.

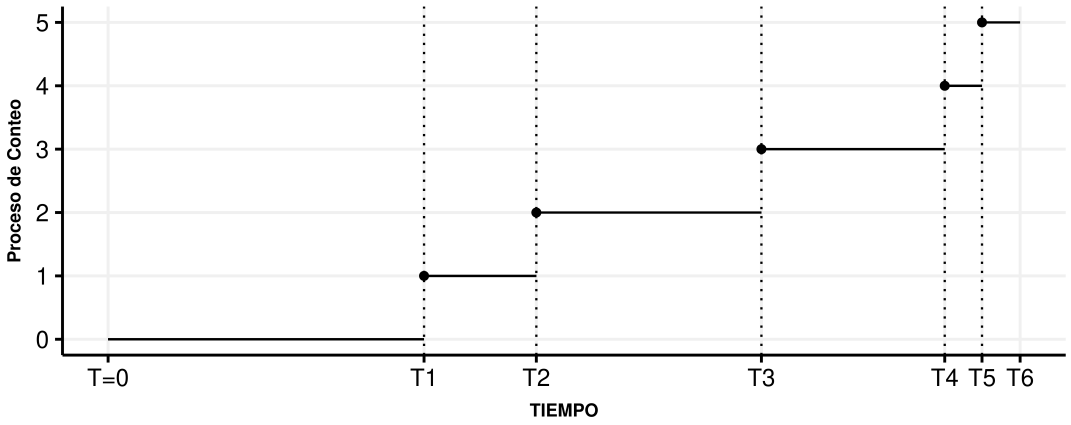

Fig. 2.2 Proceso de conteo N_t.

La distribución de la variable aleatoria N_t posee una distribución de *Poisson* con media $\mathbb{E}[N_t] = \lambda t$, la cual es definida por

$$P[N_t = n] = \frac{e^{-\lambda t}(\lambda t)^n}{n!}. \tag{2.13}$$

Definimos la filtración natural de la variable aleatoria N_T como $\mathscr{F}_t^N = \sigma\{N_s, s \leq t\}$, fijamos $t > 0$ y $T_{k(\omega)}$ sea el último salto antes de t, sea $S_1^* = T_{k(\omega)+1} - t$ y $S_i^* = T_{k(\omega)-i} - t$, $i \geq 2$. Debido a la propiedad de pérdida de memoria de la distribución exponencial descrita en

(2.12), la distribución condicional de S_1^* dado $\mathscr{F}_t^N$ es exponencial con $P[S_1^* > s|\mathscr{F}_t^N] = e^{-\mu t}$, donde μ corresponde a un parámetro de intensidad de la función.

Ahora, $N_s^* = N_{t+s} - N_t$, $s > 0$, es un proceso de *Poisson* independiente de su filtración natural $\mathscr{F}_t^N$, en otras palabras, el proceso se reinicia después de cada instante t.

En particular, N_t tiene incrementos independientes, esto implica que $(N_{t_4} - N_{t_3})$ y $(N_{t_2} - N_{t_1})$ son variables aleatorias independientes para cada $0 \leq t_1 \leq t_2 \leq t_3 \leq t_4$, por lo tanto, el proceso de *Poisson* es un proceso de Markov. Además, si f es cualquier función acotada y $t \geq s$, entonces

$$\mathbb{E}[f(N_t)|\mathscr{F}_s^N] = \sum_{k=0}^{\infty} f(k+N_s)\frac{1}{k!}e^{-\lambda(t-s)}(\lambda(t-s))^k \tag{2.14}$$

También podemos considerar el proceso de *Poisson* como parte de la familia de procesos de Markov sobre el espacio $E = \mathbb{Z} = \{0, \pm 1, \pm 2, \ldots\}$, la medida P_x sea tal que $N_0 = x \in E$ y $(N_t - x)$ es un proceso de *Poisson*. Desde la ecuación (2.14) con $s = 0$, nosotros observamos que la función de transición es

$$p(t,x,\{z\}) = \begin{cases} e^{-\mu t}\frac{1}{(z-x)!}(\mu t)^{z-x}, & z \geq x \\ 0, & z < x. \end{cases} \tag{2.15}$$

Ahora consideramos el generador de esta familia $\mathscr{U}$. Podemos observar que $\mathscr{U}f$ para pequeños valores de t es

$$\begin{aligned} P_x[N_t = x] &= 1 - \lambda t + o(t), \\ P_x[N_t = x+1] &= \lambda t + o(t), \\ P_x[N_t = x+2] &= o(t), \end{aligned}$$

donde $o(t)$ corresponde a un valor que converge a cero a medida que t tiende a infinito. Ahora, si f es una función acotada tenemos

$$\mathbb{E}_x f(N_t) = f(x)(1 - \lambda t + o(t)) + f(x+1)(\lambda t + o(t)) + o(t),$$

Entonces

$$\mathbb{E}_x f(N_t) - f(x) = \lambda t(f(x+1) - f(x)) + o(t),$$

Y, por lo tanto

$$\mathscr{U} f(x) = \lim_{t \downarrow 0} \frac{1}{t} (\mathbb{E}_x f(N_t)) = \lambda t (f(x+1) - f(x)).$$

2.4 Proceso de renovación

El proceso de renovación es un proceso de conteo, N_t, definido de forma similar al proceso de *Poisson*, con la diferencia que los tiempos entre llegadas S_i son variables aleatorias i.i.d. con alguna función de densidad ψ en $\mathbb{R}$, no necesariamente exponencial. El proceso se reinicia en cada renovación T_i. Definimos $m(t) := \mathbb{E}N_t$ comenzando en $N_0 = 0$, por lo que tenemos

$$\begin{aligned} m(t) &= \mathbb{E}N_t = \mathbb{E}\{\mathbb{E}[N_t|T_1]\}, \\ &= \mathbb{E}\{0 I_{T_1 > t} + (1 + m(t - T_1)) I_{T_1 \leq t}\}, \end{aligned}$$

Ya que T_1 tiene densidad ψ, $m(t)$ está dado por

$$m(t) = \int_0^t \psi(s) ds + \int_0^t m(t-s)\psi(s) ds, \tag{2.16}$$

El proceso de renovación no es un proceso de Markov debido a que si T_k corresponde al último salto en el tiempo antes de algún t fijo, el tiempo entre arribo residual $T_{k+1} - t$, tiene una distribución condicional dada por $\mathscr{F}_t$ que depende en el tiempo $\tau = t - T_k$ desde el último salto, a menos que el proceso sea estacionario. Con esta información nada acerca del pasado del proceso tiene alguna información relevante para predecir el futuro, ya que los futuros tiempos de arribo $S_{k+1}, S_{k+2}, \ldots$, son independientes del pasado.

Nosotros crearemos un nuevo proceso con dos componentes, $x = (N_t, \tau_t)$, donce N_t es un proceso de renovación de valores enteros y $\tau \in \mathbb{R}$ es el tiempo desde el último salto. A través de la inclusión de esta *variable suplementaria*, x_t es un proceso de Markov, o una familia de Markov si consideramos cualquier punto arbitrario de partida.

La Figura 2.3 corresponde a un proceso de renovación, donde cada salto está representado por la línea horizontal inmediatamente superior a la anterior. Notar que el tiempo τ es reiniciado en cero en cada momento que un salto sucede.

Si tomamos $\tau_t = s$, la probabilidad de observar un salto en el intervalo $]t, t+\delta]$ es $\lambda(s)\delta + o(\delta)$ y si el proceso comienza en $x = (n, \tau)$, entonces después de un corto tiempo δ si no hay salto el proceso está en $n, t+\delta$, o en el caso de que suceda un salto el proceso está en $(n+1), \delta'$ para algún $\delta' \in [0, \delta]$; otros eventos tienen probabilidad $o(\delta)$

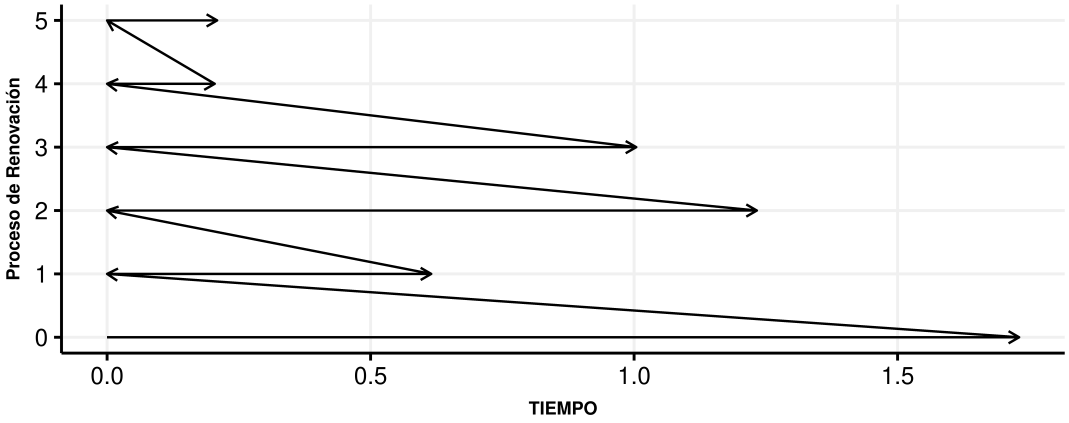

Fig. 2.3 Proceso de conteo N_t.

2.5 Proceso Poisson Fraccionario (fPp)

Un proceso de *Poisson* $N(t)$ es un proceso estocástico en un intervalo de tiempo $t \in [0,T]$, el cual es conocido por seguir una distribución de tipo *Poisson* que se describe a continuación.

$$\mathbb{P}(N(t) = n) = \exp(-\lambda t)\frac{(\lambda t)^n}{n!}, \tag{2.17}$$

donde $\lambda > 0$ corresponde a la constante de intensidad del proceso.

Junto con el supuesto de independencia y de incrementos estacionarios, la igualdad en (2.17) es suficiente para definir el proceso *Poisson* homogéneo.

El proceso de *Poisson* está intrínsecamente relacionado con la distribución exponencial. Los tiempos de llegada entre eventos sucesivos τ_i son variables aleatorias independientes y siguen una distribución de tipo exponencial. Esto quiere decir que el proceso de *Poisson* es un proceso de renovación y el tiempo de ocurrencia entre los eventos se describe como,

$$\psi(\tau) = \lambda e^{-\lambda\tau}, \quad \tau \geq 0, \quad \lambda > 0. \tag{2.18}$$

Es necesario señalar que la función de supervivencia proveniente de la función de densidad descrita en (2.18), $\Psi(\tau)$, satisface la siguiente ecuación diferencial ordinaria

$$\frac{d}{d\tau}\Psi(\tau) = -\lambda\Psi(\tau), \quad \tau > 0. \tag{2.19}$$

La generalización fraccionaria, basada en la función de probabilidad de los tiempos de llegada, planteada por Scalas et al. (2004), se escribe a continuación

$$\frac{d^\alpha}{d\tau^\alpha}\Psi(\tau) = -\Psi(\tau), \quad \tau > 0, \quad 0 < \alpha \leq 1, \tag{2.20}$$

donde el operador $d^\alpha/d\tau^\alpha$ corresponde a derivada fraccionaria de *Caputo*, la cual está definida para $0 < \alpha < 1$ y tiene la siguiente correspondencia con la derivada fraccionaria de *Riemann-Liouville*

$$\frac{d^\alpha}{dt^\alpha}f(t) = \frac{1}{\Gamma(1-\alpha)}\frac{1}{dt}\int_0^t \frac{f(\tau)}{t-\tau}^\alpha d\tau - \frac{t^{-\alpha}}{\Gamma(1-\alpha)}f(0). \tag{2.21}$$

La transformada de *Laplace* de la derivada de *Caputo* de la función $f(t)$ es

$$\mathscr{L}\left(\frac{d^\alpha}{dt^\alpha}f(t);s\right) = s^\alpha \widetilde{f}(s) - s^{\alpha-1}f(0). \tag{2.22}$$

Si aplicamos (2.22) a (2.20) obtenemos

$$\widetilde{\Psi}(s) = \frac{s^{\alpha-1}}{1+s^\alpha}, \tag{2.23}$$

y su transformada de *Laplace*, de la función de densidad

$$\widetilde{\psi}(s) = 1 - s\widetilde{\Psi}(s) = \frac{1}{1+s^\alpha}. \tag{2.24}$$

La ecuación (2.23) puede ser invertida, dando la solución de (2.20) en términos de la función *Mittag-Leffler* de parámetro α,

$$\Psi(\tau) = E_\alpha(-\tau^\alpha), \tag{2.25}$$

donde $E_\alpha(-t^\alpha)$ es la función *Mittag-Leffler* de parámetro $\alpha \in (0,1)$, y la función $E_\alpha(z)$,

definida en el plano complejo corresponde a

$$E_\alpha(z) = \sum_{n=0}^{\infty} \frac{z^n}{\Gamma(n\alpha+1)}. \tag{2.26}$$

Resultados equivalentes son descritos por Saichev and Zaslavsky (1997), Repin and Saichev (2000).

En el caso general, se puede demostrar que la densidad de los tiempos de llegada de los eventos bajo distribución exponencial fraccionaria sigue la siguiente definición

$$\psi_\alpha(t) = -\frac{d}{d\tau}E_\alpha(-\lambda t^\alpha) = \lambda t^{\alpha-1}E_\alpha(-\lambda t^\alpha), \tag{2.27}$$

La caracterización en (2.27) nos permite obtener la siguiente representación de la función de probabilidad [Saichev and Zaslavsky (1997), Repin and Saichev (2000)].

$$\psi_\alpha(t) = \frac{1}{t}\int_0^\infty e^{-x}\phi_\alpha(\lambda t/x)dx, \tag{2.28}$$

donde

$$\phi_\alpha(\xi) = \frac{\sin(\alpha\pi)}{\pi[\xi^\alpha + \xi^{-\alpha} + 2\cos(\alpha\pi)]}.$$

Cahoy (2007) nos presenta el siguiente Teorema.

Theorem 1. *El complemento de la función de distribución acumulada*

$$P(T > t) = E_\alpha(-\lambda t^\alpha), \tag{2.29}$$

puede ser representada de la siguiente forma

$$P(T > t) = \int_t^\infty e^{-\lambda t^\alpha/\tau^\alpha} g^{(\alpha)}(\tau)d\tau, \quad 0 < \alpha \leq 1,$$

donde $g^{(\alpha)}(\tau)$ es una densidad proveniente de una distribución $\alpha-$estable.

Para describir la distribución de los tiempos de arribo entre eventos, tenemos el siguiente teorema provisto por Cahoy (2007).

Theorem 2. *La variable aleatoria T que corresponde a los tiempos de arribo entre eventos tiene la misma distribución que*

$$T \stackrel{d}{=} \frac{|\ln U|^{1/\alpha}}{\lambda^{1/\alpha}} S(\alpha), \tag{2.30}$$

donde $S(\alpha)$ es una variable aleatoria distribuida de acuerdo a $g^{(\alpha)}(\tau)$, la cual corresponde a una distribución $\alpha-$estable en su cola positiva, U es uniformemente distribuida en [0,1], y U es independiente de $S(\alpha)$.

Por lo tanto, por medio de las herramientas descritas en esta sección, los tiempos de ocurrencia de los récords del *Drawdown* pueden ser caracterizados a través de la distribución *Poisson* Fraccionaria como alternativa a la utilización de modelos *PDMP*, a través del vínculo directo que poseen con las distruciones exponenciales y distribuciones $\alpha-$estables, en el contexto de larga dependencia, permitiendo capturar la tasa de ocurrencia de los fenómenos y así poder utilizar esta información para la generación de aplicaciones que permitan realizar gestión activa del riesgo por parte de los operadores financieros.

2.6 Distribución α-estable

La densidad $\alpha-$estable cumple un rol fundamental en la simulación del proceso *Poisson* fraccionario, ya que podemos definir el proceso por medio de una transformación de una distribución exponencial, multiplicada por la distribución α-estable en su parte positiva.

Lo anterior implica conocer algunas de sus características fundamentales, las cuales son descritas en forma exhaustiva por Uchaikin and Zolotarev (2011).

La densidad $\alpha-$estable definida en su parte positiva, denotada por $g^{(\alpha)}(t)$ es determinada por su transformada de *Laplace* del siguiente modo

$$\{\mathscr{L} g^{(\alpha)}(t)\}(\lambda) \equiv \widetilde{g}^{(\alpha)}(\lambda) \equiv \int_0^\infty g^{(\alpha)}(t) e^{-\lambda t} dt = e^{-\lambda^\alpha}, \tag{2.31}$$

y satisface la siguiente condición de regularidad

$$\int_0^\infty g^\alpha(t)dt = 1,$$

Otra característica relevante es que la convolución de dos densidades $\alpha-$estable definida positivas es también una densidad $\alpha-$estable definida positiva la que podemos describir a continuación

$$\int_0^t g^\alpha(t-t')g^\alpha(t')dt' = 2^{-1/\alpha}g^\alpha(2^{-1/\alpha}t),$$

y en términos de la transformada de *Laplace* tenemos

$$\widehat{g}^{(\alpha)}(\lambda)\widehat{g}^{(\alpha)}(\lambda) = \widehat{g}^{(\alpha)}(2^{1/\alpha}\lambda),$$

Por otro lado, la densidad de probabilidad de la suma la podemos caracterizar del siguiente modo. Sea $T_1, T_2, \ldots T_n$ variables aleatorias independientes e idénticamente distribuidas con $P(T_j > t) \sim at^{-\alpha}$, $t \to \infty$, entonces

$$f_{\sum T_j}(t) \sim [a\Gamma(1-\alpha)]^{1/\alpha} g^{(\alpha)}\left([\alpha\Gamma(1-\alpha)]^{1/\alpha}t\right),$$

Esta densidad posee las siguientes propiedades:

- Cuando $\alpha \to 1$, $g^\alpha(t) \to \delta(t-1)$
- Los momentos de la densidad se definen:

$$\int_0^\infty g^{(\alpha)}(t)t^\nu dt = \begin{cases} \Gamma(1-\nu/\alpha)/(\Gamma(1-\nu)), & \alpha < \nu < \infty \\ \infty, & \nu \leq \alpha \end{cases}$$

- Las densidades pueden representarse cuando $t \to 0$ de la forma

$$g^{(\alpha)}(t) = \sum_{n=1}^{\infty} \frac{(-1)^{n-1}}{n!} \frac{n\alpha}{\Gamma(1-n\alpha)} t^{-n\alpha-1}$$

- La densidad $\alpha-$estable puede ser simulada por medio de la expresión (2.32) (Weron and Weron (1995), Nolan (1997), Kanter et al. (1975), Chambers et al. (1976).

  Sean U y V variables aleatorias independientes, U uniformemente distribuida en el intervalo $(-\frac{\pi}{2}, \frac{\pi}{2})$ y V exponencialmente distribuida con media uno. Para cualquier $0 < \alpha < 1$ tenemos

$$S_\alpha = \frac{\sin(\alpha U)}{(\cos(U))^{1/\alpha}} \left(\frac{\cos(\alpha-1)U}{V}\right)^{(\alpha-1)/\alpha}, \tag{2.32}$$

Con estos elementos en consideración, tenemos disponibles herramientas para la experimentación de procesos que posean distribuciones α-estables dentro de su caracterización, como es el caso de las distribuciones *Poisson* fraccionarias que se propone como alternativa para la modelación de los tiempos de ocurrencia de los récords del *Drawdown* en el contexto de larga dependencia.

Chapter 3

Modeling outliers in financial data using ABC estimation of fractional Poisson process parameters

Abstract

In this part we develop a Bayesian approach known as the Approximate Bayesian Computation (ABC) technique to estimate the parameters defining the fractional Poisson process. In addition, we developed a test, considering the null hypothesis as the presence of long memory in the fractional Poisson process. Finally, we show a simulation study and an application to real financial time series data, to characterize the phenomenon of extreme data, delivering a new approach to characterize large losses in stock markets.

3.1 Introduction

In recent years there has been a steady increase in the areas of physics, quantum physics, mathematics (Uchaikin et al. (2008), Wang and Wen (2003)), economics and finance (Beghin and Macci (2013), Biard and Saussereau (2014)) climatology (Blender et al. (2015)), medicine (Messner et al. (2014)), and linguistics (Vasishth (2020)), which show time series exhibiting features such as long memory and jumps.

The fPp corresponds to a generalization of a Poisson process, originally introduced by Repin and Saichev (2000), Jumarie (2001), and Laskin (2003), which is characterized as a renewal process with interarrival times between events represented by Mittag-Leffler distributions (Mainardi et al. (2007), Cahoy et al. (2010), Beghin et al. (2009)). The main motivation for studying these process arises from the need to make the standard Poisson process more flexible to generate models with non-exponential, heavy-tailed interarrival time distributions.

To study fPp characteristics, it is necessary to develop statistical inference of the parameters for the Mittag-Leffler distribution. In Cahoy (2007) and Cahoy et al. (2010) the authors show us the estimation of the parameters through the method of moments under a transformation of the interarrival times events. An estimation using Monte Carlo simulations can be found in Uchaikin and Sibatov (2008).

One of the techniques used in recent years in Bayesian inference is the Approximate Bayesian Computation (ABC) method, which corresponds to a family of algorithms to

obtain the likelihood (Lintusaari et al. (2017)), when it is difficult to obtain explicitly. Thus, providing a flexible technique for parameter estimation.

This paper proposes a way of estimating the parameters that define the distribution function of a fPp by Bayesian estimation based on the **ABC** methodology and proposes the development of a new hypothesis test that allows us to test the null hypothesis that the data corresponds to a fractional Poisson process against the alternative hypothesis that it corresponds to a Poisson process in order to characterize the behavior appropriately.

The new hypothesis test makes it possible to identify the degree of regularity of the time series. In the case that the series is more irregular, it indicates that events that we can consider as normal coexist with events that we can consider as strange in the same time series, which allows modeling crisis events for the case of financial series.

Particularly, we will be interested in the study of extreme losses in the capital market as a phenomenon of high interest for portfolio management in the financial industry, providing new tools for analysis and risk management.

Our paper is organized as follows. In Section 3.2, preliminaries, we describe the fractional Poisson process as well as the estimation of the parameters by the method of moments. In Section 3.3, we consider the Bayes estimator. In Sections 3.4 we show a simulation study. In Section 3.5 we show a theoretical development of a hypothesis test to verify the degree of regularity of the time series. In 3.6 we show an application in Finance. Finally, we present our general conclusions in Section 3.7.

3.2 Preliminaries

In this section we present the basic tools and framework used in this paper. In particular, we present the fractional Poisson process (fPp) as a generalization of the Poisson process, where the interarrival times have a Mittag-Leffler distribution.

3.2.1 Fractional Poisson process

Let $\{N(t)\}_{t\geq 0}$ be a Poisson process with intensity μ. Then the probability of n elements have arrived at time t is given by

$$\mathbb{P}(N(t)=n)=\exp(-\mu t)\frac{(\mu t)^n}{n!}. \tag{3.1}$$

This is a probability distribution function because either nothing has arrived, or something must have arrived at time t.

To see what happens during a small interval Δt we write

$$\mathbb{P}(N(t+\Delta t)=0)=\mathbb{P}(N(t)=0)(1-\mu\Delta t), \tag{3.2}$$

$$\mathbb{P}(N(t+\Delta t)=n)=\mathbb{P}(N(t)=n)(1-\mu\Delta t)+\mathbb{P}(N(t)=n-1)\mu\Delta t, \quad n\geq 1. \tag{3.3}$$

On the other hand, the Poisson process is intrinsically related to the exponential distribution. The interarrival times τ, are independent random variables and follow an exponential type distribution. This means that the Poisson process is a renewal process and the interarrival times between events are i.i.d. random variables exponentially distributed with parameter μ, which we define below through

$$\psi(\tau)=\mu e^{-\mu\tau}, \quad \tau\geq 0. \tag{3.4}$$

The interarrival times distribution function ψ, represents the probability density of events occurring at $t_k=t_{k-1}+\tau$ after the previous arrived at time t_{k-1}.

The survival function of the interarrival times for the Poisson process is defined by

$$\Psi(\tau)=1-\int_0^\tau \psi(t)dt, \tag{3.5}$$

and satisfies the following ordinary differential equation

$$\frac{d}{d\tau}\Psi(\tau)=-\mu\Psi(\tau), \quad \tau>0. \tag{3.6}$$

The fractional generalization of equation (3.6), proposed by Mainardi (2020), Scalas et al. (2004), is written as follows,

$$\frac{d^\alpha}{d\tau^\alpha}\Psi(\tau)=-\Psi(\tau)=-\left(1-\int_0^\tau \mu e^{-\mu\tau}dt\right), \quad \tau>0, \quad 0<\alpha\leq 1. \tag{3.7}$$

where the operator $d^\alpha/d\tau^\alpha$ corresponds to the Caputo derivative, which is defined for any $0<\alpha<1$. We can relate this derivative with the Riemann-Liouville one. For a sufficiently well-behaved function f, the Caputo derivative is defined by the following equation

$$\frac{d^\alpha}{d\tau^\alpha}f(\tau)=\frac{1}{\Gamma(1-\alpha)}\frac{1}{d\tau}\int_0^\tau \frac{f(s)}{(\tau-s)^\alpha}ds-\frac{\tau^{-\alpha}}{\Gamma(1-\alpha)}f(0), \tag{3.8}$$

if $\alpha=1$ Equation (3.7) reduces to (3.6) .

Using the Laplace transform on $\Psi(\tau)$ we can write (3.7), in terms on the Mittag-Leffler function, Gorenflo and Mainardi (2008), with parameter α as follows.

$$\Psi(\tau) = E_\alpha(-\mu\tau^\alpha), \tag{3.9}$$

where $E_\alpha(z)$ is the Mittag-Leffler function with parameter α which is defined as

$$E_\alpha(z) = \sum_{n=0}^{\infty} \frac{z^n}{\Gamma(n\alpha+1)}, \tag{3.10}$$

then, the density of the interarrival times of events is given by

$$\psi_\alpha(\tau) = -\frac{d}{d\tau}E_\alpha(-\mu\tau^\alpha) = \mu\tau^{\alpha-1}E_\alpha(-\mu\tau^\alpha). \tag{3.11}$$

Following Repin and Saichev (2000) the Mittag-Leffler function can be expressed

$$E_\alpha(-z) = \frac{z\sin(\pi\alpha)}{\pi}\int_0^\infty \frac{x^{\alpha-1}e^{-x}dx}{x^{2\alpha}+z^2+2zx^\alpha\cos(\pi\alpha)}, \tag{3.12}$$

and following Cahoy et al. (2010), we can obtain the characterization of the $\psi_\alpha(\tau)$ as

$$\psi_\alpha(\tau) = \frac{1}{\tau}\int_0^\infty e^x\phi_\alpha(\mu t/x)dx, \tag{3.13}$$

where

$$\phi_\alpha(\xi) = \frac{\sin(\alpha\pi)}{\pi\xi[\xi^\alpha+\xi^{-\alpha}+2\cos(\alpha\pi)]}$$

The following theorems given by Cahoy (2007), describe a representation of the distribution of interarrival times in terms of the α-stable distribution.

Theorem 3. *Let τ the r.v. given in* (3.9) *corresponding the interarrivals times of the fractional Poisson process. Then*

$$\mathbb{P}(\tau > t) = E_\alpha(-\mu t^\alpha) = \int_0^\infty e^{-\mu t^\alpha/s^\alpha}g^{(\alpha)}(s)ds, \quad 0<\alpha\leq 1 \tag{3.14}$$

where $g^{(\alpha)}(\cdot)$ is the density function of a one-sided α-stable random variable. The density function of an $\alpha-$stable random variable can be defined as (see Penson and Górska (2010))

$$g^\alpha(\tau) = \frac{1}{\pi}\sum_{j=1}^{\infty}\frac{(-1)^{j+1}}{j!\tau^{1+\alpha j}}\Gamma(1+\alpha j)\sin(\pi\alpha j).$$

Theorem 4. *Let τ be the interarrival times of the fractional Poisson process given in* (3.9). *Then*

$$\tau \stackrel{d}{=} \frac{|\ln U|^{1/\alpha}}{\mu^{1/\alpha}} S(\alpha) \tag{3.15}$$

where $S(\alpha) \sim g^{(\alpha)}(\cdot)$ represents a random variable with $\alpha-$ stable distribution on its positive tail, U is a random variable uniformly distributed in $[0,1]$ and independent of $S(\alpha)$.

Figure 1 shows four realizations of fractional Poisson processes for different values of α. The first picture, $\alpha = 1$ corresponds to the standard Poisson process. As the value of α decreases, we find an increase in waiting periods for the next event.

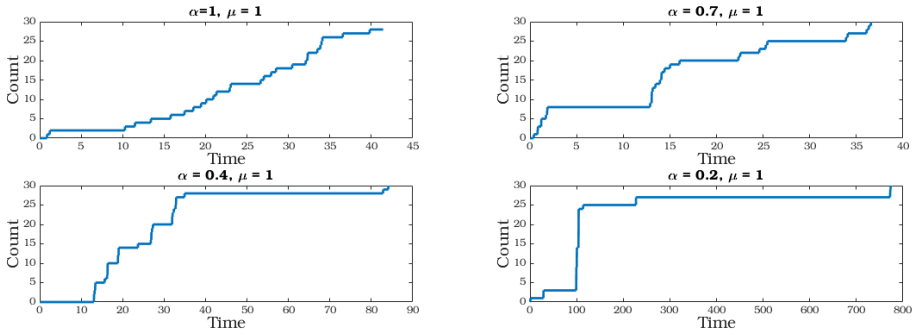

Fig. 3.1 Paths of the Fractional Poisson process with different values of α and μ. The X-axis corresponds to arrival times and the Y-axis corresponds to the counting trajectory.

3.2.2 Parameter estimation by the Moments procedure

In this section we summarize the method of moments for estimating the parameters of the fPp. Our goal is to compute a statistic that can be used to initiate computational estimation in the ABC procedure. Since the first moment does not exist for an $\alpha - stable$ distribution with $\alpha < 1$, the authors in Cahoy (2007) consider the log transformation of the random variable τ, where τ corresponds to the interarrival time.

Thus, it is possible to characterize the moments of all orders of $\ln(\tau)$, Zolotarev (1986).

$$\ln(\tau) \stackrel{d}{=} \frac{1}{\alpha} \ln\left(\frac{|\ln(U)|}{\mu}\right) + \ln\left(S(\alpha)\right), \tag{3.16}$$

where $\stackrel{d}{=}$ means equality in distribution and U, as before is a random variable uniformly distributed on $[0,1]$. Also, if $Y = -\ln(U)$ and $X = \ln(Y)$

$$\mathbb{E}[X] = \int_{\mathbb{R}} x e^{x-e^x} dx = \int_{\mathbb{R}^+} \ln(y) e^{-y} dy = -\mathscr{C}, \tag{3.17}$$

where $\mathscr{C}$ corresponds to the Euler constant as in Gasper et al. (2004). Also

$$\mathbb{E}[X^2] = \int_{\mathbb{R}} x^2 e^{x-e^x} dx = \int_{\mathbb{R}^+} \ln(y)^2 e^{-y} dy = \mathscr{C}^2 + \frac{\pi^2}{6}. \tag{3.18}$$

On the other hand, Zolotarev (1986) gives the moments for $\ln(S(\alpha))$

$$\mathbb{E}[\ln(S(\alpha))] = \mathscr{C}\left(\frac{1}{\alpha} - 1\right). \tag{3.19}$$

When we combine (3.17) with (3.19) we get

$$\mathbb{E}[\ln(\tau)] = -\frac{\ln(\mu)}{\alpha} - \mathscr{C}, \tag{3.20}$$

and

$$\mathbb{E}[\ln(\tau)]^2 = \mathbb{E}\left[\frac{1}{\alpha}\ln\left(\frac{|\ln(U)|}{\mu}\right) + \ln(S(\alpha))\right]^2, \tag{3.21}$$

after some algebraic manipulations we obtain

$$\mathbb{E}[\ln(\tau)]^2 = \frac{\pi^2}{3\alpha^2} + \frac{(\ln(\mu))^2}{\alpha^2} + \mathscr{C}^2 - \frac{\pi^2}{6} + \frac{2\mathscr{C}\ln(\mu)}{\alpha}, \tag{3.22}$$

$$\mathbb{E}[\ln(\tau)]^2 - [\mathbb{E}[\ln(\tau)]]^2 + \frac{\pi^2}{6} = \frac{\pi^2}{3\alpha^2}, \tag{3.23}$$

which implies

$$\alpha^2 = \frac{\pi^2}{3(\widehat{\sigma}^2_{\ln\tau} + \pi^2/6)}, \tag{3.24}$$

where

$$\widehat{\sigma}^2_{\ln\tau} = \mathbb{E}[\ln(\tau)]^2 - [\mathbb{E}[\ln(\tau)]]^2 = \frac{\pi^2}{3}\left(\frac{1}{\alpha^2} - \frac{1}{2}\right). \tag{3.25}$$

Thus, the estimators by the method of moments for the parameters of the process fPp are

$$\widehat{\alpha} = \frac{\pi}{\sqrt{3(\widehat{\sigma}^2_{\ln\tau} + \pi^2/6)}}, \tag{3.26}$$

and similarly, we use (3.20) to obtain the estimate of μ.

$$\widehat{\mu} = \exp(-\widehat{\alpha}(\overline{\ln(\tau)} + \mathscr{C})) \tag{3.27}$$

where $\overline{\ln(\tau)} = \frac{1}{n}\sum_{i=1}^{N} ln(\tau_i)$. The authors in Cahoy et al. (2010) prove the asymptotic normality of the parameters estimators of α and μ, thus constructing approximate confidence intervals for the estimators obtained by the method of moments. The second, third and fourth moments of the random variable $\ln(\tau)$ are defined as follows:

$$\mathbb{E}[\ln(\tau)^3] = -\frac{[\mathscr{C}\alpha+\ln(\mu)][2\mathscr{C}^2\alpha^2-\pi^2(\alpha^2-2)+2\ln(\mu)(2\mathscr{C}\alpha+\ln(\mu))]}{2\alpha^3} - 2\zeta(3)$$

$$\begin{aligned}\mathbb{E}[\ln(\tau)^4] = \frac{1}{60\alpha^4}(60\mathscr{C}^4\alpha^4 - 60\mathscr{C}^2\alpha^2(\alpha^2-2)+\pi^4(28-20\alpha^2+\alpha^4)\\ +60\ln(\mu)(2\mathscr{C}\alpha+\ln(\mu))(2\mathscr{C}^2\alpha^2-\pi^2(\alpha^2-2)+2\mathscr{C}\alpha\ln(\mu)+(\ln(\mu)^2))\\ +480\alpha^3(\mathscr{C}\alpha+\ln(\mu))\zeta(3))\end{aligned}$$

The central moments of the $\ln(\tau)$ random variable are then calculated.

$$\mu_3 = \mathbb{E}[(\ln(\tau)-\mu_{\ln(\tau)})^3] = -2\zeta(3)$$

$$\mu_4 = \mathbb{E}[(\ln(\tau)-\mu_{\ln(\tau)})^4] = \frac{\pi^4(28-20\alpha^2+\alpha^4)}{60\alpha^4}$$

Also

$$\overline{\ln(\tau)} = \frac{\sum_{j=1}^{n}\ln(\tau_j)}{n},$$

and

$$\widehat{\sigma}^2_{\ln(\tau)} = \frac{\sum_{j=1}^{n}(\ln(\tau_j)-\overline{\ln(\tau)})^2}{n}.$$

So, the central limit theorem implies

$$\sqrt{n}\begin{bmatrix}\overline{\ln(\tau)}-\mu_{\ln(\tau)}\\ \widehat{\sigma}^2_{\ln(\tau)}-\sigma^2_{\ln(\tau)}\end{bmatrix} \xrightarrow{d} N\left[\begin{bmatrix}0\\0\end{bmatrix}, \begin{bmatrix}\sigma^2_{\ln(\tau)} & \mu_3\\ \mu_3 & \mu_4-\sigma^4_{\ln(\tau)}\end{bmatrix}\right], \tag{3.28}$$

where $N[\overrightarrow{\mu},\Sigma]$ represents a multivariate normal distribution with mean $\overrightarrow{\mu}$ and covariance matrix Σ, $\xrightarrow{d}$ denote convergence in distribution as n tends to ∞. The estimates of the α and μ parameters are important for the Bayesian methodology that we will present below.

3.3 Bayesian Parameter Estimation

In this section we will proceed to estimate the parameters that define the behavior of the fPp by means of computational techniques based on Bayesian inference.

We will describe a Bayesian paradigm, in which the parameter θ itself is modeled as a random variable. The Bayesian paradigm naturally incorporates our prior belief about the unknown parameter θ, and updates this belief based on observed data.

In Bayesian analysis, before data is observed, the unknown parameter is modeled as a random variable θ having a probability distribution $\pi(\theta)$, called the prior distribution. This distribution represents our prior belief about the value of this parameter.

Conditional on θ, the observed data X is assumed to have a density $f(x/\theta)$, where $f(x/\theta)$ defines a parametric model with parameter θ. The joint distribution of θ and X is then the product $f(x,\theta) = f(x/\theta)\pi(\theta)$, and the marginal density of X (in the continuous case) is $f(x) = \int f(x,\theta)d\theta = \int f(x/\theta)f(\theta)d\theta$.

The conditional density of θ given $X = x$ is $f(\theta/x) = \frac{f(x,\theta)}{f(x)} = \frac{f(x/\theta)\pi(\theta)}{\int f(x/\theta')\pi(\theta')d\theta'}$. This is called the posterior distribution of θ. It represents our knowledge about the parameter θ after having observed the data X. We often summarize the preceding equation simply as

$$\begin{aligned} f(\theta|x) &\propto f(x/\theta) \times \pi(\theta) \\ \text{Posterior density} &\propto \text{Likelihood} \times \text{Prior density} \end{aligned} \tag{3.29}$$

where the symbol $\propto$ hides the proportionality factor which does not depend on θ.
Hereafter we refer θ as the parameter vector $\theta = (\mu, \alpha)$.

As shown in formula (3.29), the Bayesian methodology requires knowledge of the likelihood function. In the case of fPp, the interarrival times are i.i.d. but do not have a closed likelihood function.

The distribution of interarrival times τ, $F_\tau(t)$ in the fPp case, is a function of two independent random variables $F_\tau(t) = F_{(X_1,X_2)}(t)$ as it is shown in Theorem 4 (Cahoy (2007)), where $X_1 \backsim |\ln U|^{1/\alpha}/\mu^{1/\alpha}$ and $X_2 \backsim S(\alpha)$. However, we observe neither X_1 nor X_2, which generates an incomplete information problem, due to the impossibility of isolating each of the random variables that define the fractional Poisson distribution according to the definition of equation (3.15).

One way to solve this problem is developed in McLachlan and Peel (2004), where the authors provide a general strategy for the estimation of parameters with mixture type distribution, which is based on measuring the distance between the empirical ($\widehat{F_n}$) and

theoretical (F_Ψ) distributions, using the Kulback-Leibler distance (see Kullback and Leibler (1951)) defined by

$$I(\widehat{F}_n, F_\Psi) = \int \ln \left\{ \frac{d\widehat{F}_n(w)}{dF_\Psi(w)} \right\} d\widehat{F}_n(w). \tag{3.30}$$

Some alternatives that can be considered are the Wolfowitz distance, Levy distance and Cramér-von Mises distance among others, Titterington et al. (1985). The choice depends on the computational capacity and the behavior of the estimators. The general algorithm for estimation using the Kulback-Leibler distance is described below.

Algorithm 1 Kulback-Leibler distance

1. Define $n \in \mathbb{N}$ and the range of values for μ and α.
2. Define $P \in \mathbb{N}$ (points), of the value grid for μ.
3. Define $M \in \mathbb{N}$ (points), of the value grid for α.
4. For each value of μ and α, given in 1. generate $P \times M$ independent sample paths of fPp, with length n.
5. For each of the combinations of μ and α calculate the Kullback-Leibler distance, as in (3.30).
6. Choose the values of μ and α that minimizes the Kullback-Leibler distance.

One of the problems presented by the procedure using the Kulback-Leibler distance is in the definition of the precision level of the values grid on which the Kulback-Leibler distance will be evaluated. Having a mesh of size P for the parameter μ and M for the parameter α, the number of evaluations corresponds to $P \times M$, which depending on the precision to be obtained, can considerably increase the computation time.

On the other hand, this way of estimating does not provide us with information about the distributions of the parameter vector (μ, α) and therefore, does not allow us to make inference about the parameters.

One of the alternatives to avoid the complications mentioned above can be found in the development of Approximate Bayesian Computation estimation techniques.

The Approximate Bayesian Computation (ABC) technique corresponds to a series of acceptance-rejection algorithms that use a set of summary statistics from a random sample to compute the posteriori distribution, without the need to compute the likelihoods. In ABC techniques, the likelihoods are replaced by a simulation procedure.

A disadvantage of the methods based on ABC techniques is that the acceptance rate of the random sample, and therefore of the convergence speed of the algorithm, could be very low in the case that the a priori distribution is very different from the posteriori one or that the ranges in which the simulated parameters fluctuate are very different from the real ones, a situation that we do not know when using this technique with real data.

Despite the disadvantages of the method, its advantages make this technique an attractive alternative to find the posteriori distributions of the parameters on which we want to perform inference. The natural advantages of the ABC technique lie in the ease of programming, generating independent observations and the ease of adapting the technique to various contexts, which makes it possible to tackle highly complex problems that cannot be solved by other techniques.

A number of alternatives for obtaining a posteriori distribution using ABC techniques are presented in Marjoram et al. (2003). Other alternatives described in the literature can be found in Peters et al. (2012), Beaumont et al. (2009), Toni et al. (2008), Sisson et al. (2007), to name a few.

Specifically, the Sequential Monte Carlo (SMC-ABC) algorithm, described by Del Moral et al. (2006) and Beaumont (2010), is proposed for the calculation of the posteriori distributions, modifying the bandwidth selection by using the methodology described by Silverman (2018), which we show below as

$$h_{opt} = \left(\frac{4}{3n}\right)^{1/5} \sqrt{\eta^2} \tag{3.31}$$

where h_{opt} corresponds to the optimal width of the window; n represents the sample size; and η is the empirical variance of the parameter of interest.

Hereinafter we refer to $\rho(\cdot,\cdot)$ as the distance function between the original sample statistics and the simulated data sample used in the acceptance-rejection algorithm; $S_1(\cdot)$ and $S_2(\cdot)$ are the $\widehat{\alpha}$ and $\widehat{\mu}$ estimators described in equations (3.26) and (3.27), respectively of α and μ corresponding to the original random sample and the simulated sample; $K(\cdot)$ corresponds to the proposed distribution of the α or μ parameter; the vector $\varepsilon_1 = \varepsilon_{1,1}, \ldots, \varepsilon_{1,J}$ and $\varepsilon_2 = \varepsilon_{2,1}, \ldots, \varepsilon_{2,J}$ correspond to the vectors containing the decreasing sequence of values $\varepsilon_{1,j}$ and $\varepsilon_{2,j}$, $1 \leq j \leq J$, used to define the acceptance-rejection window of the algorithm, and J represents the number of iteration that are used in the algorithm.

The first part of the algorithm provides us with the initial values on which we will proceed to perform the simulations. Section 2 of the algorithm works sequentially, fixing all the parameters of the fPp distribution except for the parameters that we need to find its empirical distribution, generating a set of n elements on which the posterior distribution is calculated.

On the new parameter distribution, we obtain a value that will be kept fixed for the simulation of the new values, leaving the other parameter free to perform the same procedure of the previous parameter, repeating the sequence of the number of cycles that have been predetermined.

Algorithm 2 Sequential Monte Carlo (SMC-ABC) algorithm

1. At iteration $j = 1$,
while $i \leq n$ **do**
Simulate $\alpha_i^{(1)} \backsim \pi(\alpha)$, $\mu_i^{(1)} \backsim \pi(\mu)$ and $x_i \backsim p(x|\alpha_i^{(1)}, \mu_i^{(1)})$
if $\rho(S_1(x), S_1(y)) < \varepsilon_{1,1}$ and $\rho(S_2(x), S_2(y)) < \varepsilon_{2,1}$, **then** $i = i+1$
Set $\omega_{\alpha,i}^{(1)} = 1/n$ and $\omega_{\mu,i}^{(1)} = 1/n$
end while
Take $\eta_{\alpha,j+1}^2$ and $\eta_{\mu,j+1}^2$ as twice the empirical variance of the simulated samples.
2. At iteration $2 \leqslant j \leqslant J$,
Choose μ^* from $\pi(\mu^{(j-1)})$
while $i \leq n$ **do**
Simulate $\alpha_i^{(j)} \backsim \pi(\alpha^{(j-1)})$ and $x \backsim p(x|\alpha_i^{(j)}, \mu^*)$
if $\rho(S_1(x), S_1(y)) < \varepsilon_{1,j}$, **then** $i = i+1$
Set $\omega_{\alpha,i}^{(j)} \propto \pi(\alpha_i^{(j)}) / \sum_{h=1}^N \omega_{\alpha,h}^{(j-1)} K(\alpha_i^{(j)}|\alpha_h^{(j-1)}, \eta_{\alpha,j}^2)$
end while
Take $\eta_{\alpha,j+1}^2$ as twice the empirical variance of the $\alpha^{(j)}$
Choose α^* from $\pi(\alpha^{(j)})$
while $i \leq n$ **do**
Simulate $\mu_i^{(j)} \backsim \pi(\mu^{(j-1)})$ and $x \backsim p(x|\mu_i^{(j)}, \alpha^*)$
if $\rho(S_2(x), S_2(y)) < \varepsilon_{2,j}$, **then** $i = i+1$
Set $\omega_{\mu,i}^{(j)} \propto \pi(\mu_i^{(j)}) / \sum_{h=1}^N \omega_{\mu,h}^{(j-1)} K(\mu_i^{(j)}|\mu_h^{(j-1)}, \eta_{\mu,j}^2)$
end while
Take $\eta_{\mu,j+1}^2$ as twice the empirical variance of the $\mu^{(j)}$.

3.4 Simulation Study

In this section we will proceed to analyze the performance of the proposed method by means of simulated examples, considering four different parameter combinations shown in Table 1. For this simulation we consider random samples of size $n = 200$ for each of the defined parameter combinations, and we will consider $1,000$ samples accepted in the algorithm to generate a posteriori distribution of the parameters for each of the $J = 10$ iterations considered for this experiment.

Parameters	α	μ
$\theta_1 =$	0.3	12.0
$\theta_2 =$	0.4	7.0
$\theta_3 =$	0.5	10.0
$\theta_4 =$	0.7	5.0

Table 3.1 Experimental parameters for estimation SMC-ABC (Algorithm 2).

To run the simulations of the distributions (see eq. (3.15)) that generate the interarrival times of the fractional Poisson process, we need to simulate the stable distributions of parameter α.

In Weron and Weron (1995), Nolan (1997), Kanter et al. (1975), Chambers et al. (1976), the authors indicate the simulation process of the $\alpha - stable$ distribution, which is presented below.

Let U and V be independent random variables, U uniformly distributed in the interval $(-\frac{\pi}{2}, \frac{\pi}{2})$ and V a random variable with an exponential distribution of parameter equal to one. For any $0 < \alpha < 1$ we have

$$S_\alpha = \frac{\sin(\alpha U)}{(\cos(U))^{1/\alpha}} \left(\frac{\cos(\alpha - 1)U}{V} \right)^{(\alpha-1)/\alpha}, \tag{3.32}$$

is a random variable with $\alpha-$stable distribution.

Therefore, the complete simulation of the arrival times between events that have a fPp distribution, using (3.15) and (3.32) can be represented as

$$\tau = \frac{|\ln U_1|^{1/\alpha}}{\mu^{1/\alpha}} \frac{\sin(\alpha U_2)}{(\cos(U_2))^{1/\alpha}} \left(\frac{\cos(\alpha - 1)U_2}{V} \right)^{(\alpha-1)/\alpha} \tag{3.33}$$

In figure 3.2, for the case of α it can be observed that the distribution is concentrated near the true value although the modal value is not a precise statistic. In the case of μ the opposite is observed, a relatively large variance, but the mode is a good value of the expected value of the parameter.

In Cahoy et al. (2010) asymptotic confidence intervals are constructed for the process parameters fPp, based on the estimation by moments. These intervals allow us to have a benchmark of the procedure based on the ABC algorithm. The expression for them is given by

$$\widehat{\alpha} \pm z_{\varepsilon/2} \sqrt{\frac{\widehat{\alpha}^2(32 - 20\widehat{\alpha}^2 - \widehat{\alpha}^4)}{40n}}, \tag{3.34}$$

$$\widehat{\mu} \pm z_{\varepsilon/2} \sqrt{\frac{\widehat{\mu}^2[20\pi^4(2 - \widehat{\alpha}^2) - 3\pi^2(\widehat{\alpha}^4 + 20\widehat{\alpha}^2 - 32)(\ln\widehat{\mu})^2 - 720\widehat{\alpha}^3(\ln\widehat{\mu})\zeta(3)]}{120\pi^2 n}}, \tag{3.35}$$

where $\widehat{\mu}$ is the value estimated by the method of moments of the μ intensity, $\widehat{\alpha}$ corresponds estimator by the method of moments of the $\alpha - stable$ distribution parameter. The tail of the

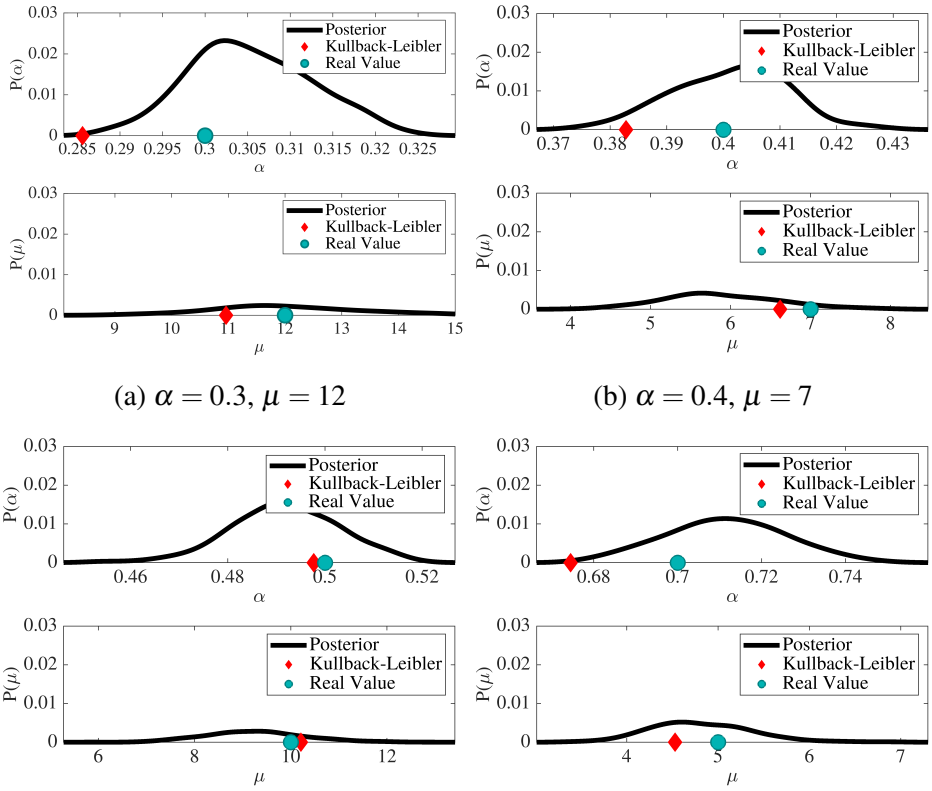

(a) $\alpha = 0.3$, $\mu = 12$ (b) $\alpha = 0.4$, $\mu = 7$

(c) $\alpha = 0.5$, $\mu = 10$ (d) $\alpha = 0.7$, $\mu = 5$

Fig. 3.2 Parameter estimation by ABC algorithm.

$z_{\varepsilon/2}$ quantile is defined by $P(Z > z_{\varepsilon/2}) = \varepsilon/2$, with $Z \stackrel{d}{=} N(0,1)$ and $\zeta(\cdot)$ corresponds to the Riemann zeta function.

To perform the comparisons between ABC procedure and method of moments, we proceed to simulate a sample of size n from a fPp with the parameters described in Table 1, considering $n = 100$, 1000 and 10000 repetitions. The 95% confidence intervals are constructed according to the specification described above (see Eq. (3.34) and (3.35)), based on moment estimation. To measure the 95% confidence interval, based on the ABC procedure, the 2.5 and 97.5 percentile of the CDF is calculated as an approximation of the $\pi(\theta)$ distribution, based on the sample data.

The following tables show the estimates obtained.

	$n = 100$		$n = 1,000$		$n = 10,000$	
	ABC	Moments	ABC	Moments	ABC	Moments
μ	(8.58 14.13)	(5.59 19.61)	(10.63 13.36)	(10.02 14.22)	(11.57 12.52)	(11.41 12.73
α	(0.25 0.37)	(0.25 0.35)	(0.28 0.32)	(0.28 0.32)	(0.29 0.31)	(0.29 0.31)

Table 3.2 95% confidence interval for a simulate fPp $(\mu, \alpha) = (12,\ 0.3)$.

	$n = 100$		$n = 1,000$		$n = 10,000$	
	ABC	Moments	ABC	Moments	ABC	Moments
μ	(5.22 10.62)	(3.81 10.68)	(6.20 7.82)	(6.00 8.09)	(6.71 7.28)	(6.67 7.33)
α	(0.34 0.48)	(0.33 0.46)	(0.37 0.42)	(0.38 0.42)	(0.39 0.41)	(0.39 0.41)

Table 3.3 95% confidence interval for a simulate fPp $(\mu, \alpha) = (7,\ 0.4)$.

	$n = 100$		$n = 1,000$		$n = 10,000$	
	ABC	Moments	ABC	Moments	ABC	Moments
μ	(7.23 13.16)	(5.28 15.65)	(9.04 11.30)	(8.49 11.61)	(9.67 10.44)	(9.56 10.55)
α	(0.42 0.59)	(0.42 0.58)	(0.47 0.53)	(0.48 0.53)	(0.49 0.52)	(0.49 0.51)

Table 3.4 95% confidence interval for a simulate fPp $(\mu, \alpha) = (10,\ 0.5)$.

	$n = 100$		$n = 1,000$		$n = 10,000$	
	ABC	Moments	ABC	Moments	ABC	Moments
μ	(3.74 7.24)	(3.21 6.92)	(4.52 5.59)	(4.43 5.59)	(4.79 5.21)	(4.81 5.18)
α	(0.60 0.82)	(0.59 0.80)	(0.67 0.74)	(0.67 0.73)	(0.69 0.71)	(0.69 0.71)

Table 3.5 95% confidence interval for a simulate fPp $(\mu, \alpha) = (5,\ 0.7)$.

The results of this simulation show that for large sample sizes, there are no significant differences between using the method of moments and using the ABC method. However, for small samples we can observe the precision loss of the moment-based estimation, observing a larger range in the confidence interval of the intensity parameter estimate μ.

The proposed procedure based on ABC parameter estimation techniques has a higher level of accuracy, providing a concrete alternative for the parameter estimation of a fPp with a fixed sample size, which is studied in various areas, such as natural sciences or financial processes.

3.5 Fractional Behavior

To identify whether a interarrival time series corresponds to the general model of fPp, we constructed a hypothesis test that allows us to identify whether the parameter associated with the fractional behavior, is contemplated within the limits in which the fractional modeling is adequate ($\alpha < 1$). We can use the well-known Delta method to characterize the behavior of the distribution of $\widehat{\sigma}^2_{\ln\tau} - \sigma^2_{\ln(\tau)}$ (See Ferguson (2017), Kulldorff (1957)).

Theorem 5. *Let g be a mapping $g : \mathbb{R}^d \to \mathbb{R}^k$ such that $\nabla g(x)$ is continuous in a neighborhood of $\mu \in \mathbb{R}^d$. If X_n is a sequence of d-dimensional random vectors such that $\sqrt{n}(X_n - \mu) \xrightarrow{d} X$, then $\sqrt{n}(g(X_n) - g(\mu)) \to \nabla g(\mu) \cdot X$.*

In particular, if $\sqrt{n}(X_n - \mu) \xrightarrow{d} N(0, \Sigma)$, where Σ is a covariance matrix, then

$$\sqrt{n}(g(X_n) - g(\mu)) \xrightarrow{d} N\left[0, \nabla g(\mu)\Sigma\nabla^t g(\mu)\right]. \tag{3.36}$$

Using (3.36), (3.28) and (3.25) we have

$$T_{(\alpha,n)} = \sqrt{n}\left(\widehat{\sigma}^2_{\ln\tau} - \frac{\pi^2}{3}\left(\frac{1}{\alpha^2} - \frac{1}{2}\right)\right) \xrightarrow{d} N\left[0, \mu_4 - \sigma^4_{\ln\tau}\right]. \tag{3.37}$$

For $\alpha = 1$, the standard Poisson case, the statistic is given by

$$T_{(1,n)} = \sqrt{n}\left(\widehat{\sigma}^2_{\ln\tau} - \pi^2/6\right) \xrightarrow{d} N\left[0, \pi^4 11/90\right]. \tag{3.38}$$

The variance

$$\sigma^2_{\ln\tau} = \frac{\pi^2}{3}\left(\frac{1}{\alpha^2} - \frac{1}{2}\right),$$

decreases as $\alpha \to 1$. Thus, for a fixed observed value of $\widehat{\sigma}^2_{\ln \tau}$, the statistic $T_{(\alpha,n)}$ increases as α increases to 1. For each sample size n the maximum value of $T_{(\alpha,n)}$, defined in (3.37), is obtained in $\alpha = 1$, the Poisson case.

Based on the statistic $T_{(\alpha,n)}$, we can obtain a relationship between the $\widehat{\alpha}$ and its true value, so the condition $T_{(\alpha,n)} \leq 0$ is equivalent to $\alpha - \widehat{\alpha} \leq 0$, which implies that we can use the statistic $T_{(\alpha,n)}$ to generate a hypothesis test for the α parameter.

Thus, the hypothesis test for the parameter $\alpha \leq \widehat{\alpha}$ is

$$\begin{aligned} H_0 &: T_{(\alpha,n)} \leq 0 \\ H_1 &: T_{(\alpha,n)} > 0 \end{aligned} \tag{3.39}$$

The null hypothesis $H_0 : T_{(\alpha,n)} \leq 0$ means that the estimated value $\hat{\alpha}$ is bigger than the proposed α. In this case we can said that the estimated process described in equation (3.15) is "more regular" (or "less fractional") than the proposal process. Otherwise, $H_1 : T_{(\alpha,n)} > 0$ means that the estimated value $\hat{\alpha}$ is smaller than the proposed α.

Therefore, once we reject H_0, for some $\alpha \in (0,1)$ we are able to find a critical value $\alpha^* < 1$ which is the smallest value of α that allows to reject H_0. In fact, we can define

$$\alpha^* = \underset{0<\alpha\leq 1}{\operatorname{argmin}} \left\{ \left| T_{(\alpha,n)} - \kappa_\varepsilon^{(n)}(\alpha) \right| \right\},$$

where $\kappa_\varepsilon^{(n)}(\alpha)$ corresponds to the rejection value located in the right tail of the empirical distribution of $T_{(\alpha,n)}$. We recall that, for a fixed observed value of $\widehat{\sigma}^2_{\ln \tau}$, the statistic $T_{(\alpha,n)}$ is an increasing function of α and the rejection value $\kappa_\varepsilon^{(n)}(\alpha)$ is a decreasing function of α. Thus, there are two cases to distinguish with respect to the value of α^*: the first case is when $\alpha^* < 1$ and we reject H_0, in this case, rejecting H_0 for a specific value of α, implies rejecting H_0 for any $\alpha' > \alpha$; the second case is when $\alpha^* = 1$, here the null hypothesis is not rejected for any value of $\alpha \in (0,1)$ and then the hypothesis that the process is Poisson is favored.

When $\alpha^* < 1$, we can conclude that the process is fractional with α less than the critical value α^*, representing the estimator with the lowest variance according to the observed data. We can find α^* using a computational procedure. We proceed as follows: we start with a value of α close to 1 that rejects the null hypothesis and test backward the H_0 for values of α until the first time we not reject the null hypothesis.

The asymptotic rejection region is the tail of the z_ε quantile of standard gaussian distribution, defined by $\mathbb{P}\left(\frac{T_{(\alpha,n)}}{\sqrt{\mu_4 - \sigma^4_{\ln \tau}}} > z_\varepsilon \right) = \varepsilon$.

In the case of small samples, the rejection region is estimated computationally. Figure 3.3 shows the computational estimation of the proposed test distribution for small samples

($n = 100$) and $\alpha = 1$, where the rejection value is located in the right tail of the empirical distribution where the $\kappa_{\varepsilon}^{(n)}(\alpha)$ quantile is defined by $\mathbb{P}(T_{(\alpha,n)} > \kappa_{\varepsilon}^{(n)}(\alpha)) = \varepsilon$. In this case Figure 3.3, allows us to have a test to verify if the process is fractional ($\alpha < 1$), however, it does not allow us to identify the degree of regularity of the process.

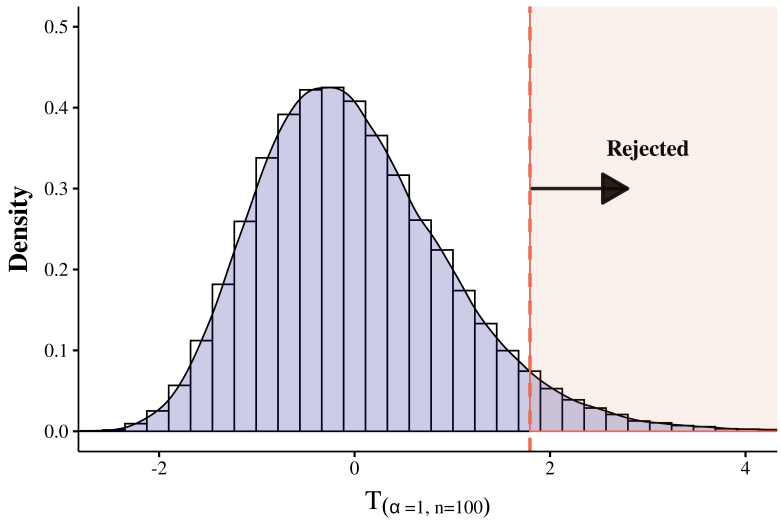

Fig. 3.3 Histogram of small sample distribution $(n = 100)$ of T, for $\alpha = 1$.

In order to identify the degree of regularity of the interarrival time series, an analysis must be performed for each possible value of α with respect to α^*. Figure 3.4 presents the probability density estimate of the statistic $T_{(\alpha,n)}$ obtained in equation (3.37) for different values of $\alpha \in [0.5, 1]$. The segmented line corresponds to the 95th percentile ($\varepsilon = 0.05$) obtained in the simulation process using $10,000$ iterations. The solid lines in the graph correspond to the observed value of the statistic $T_{(\alpha,n)}$ as a function of α, obtained from a sample path process for $\alpha = 0.75$, $\mu = 4$ and an observed value of $\widehat{\sigma}^2_{\ln \tau} = 4.2$ with a sample size of $n = 100$.

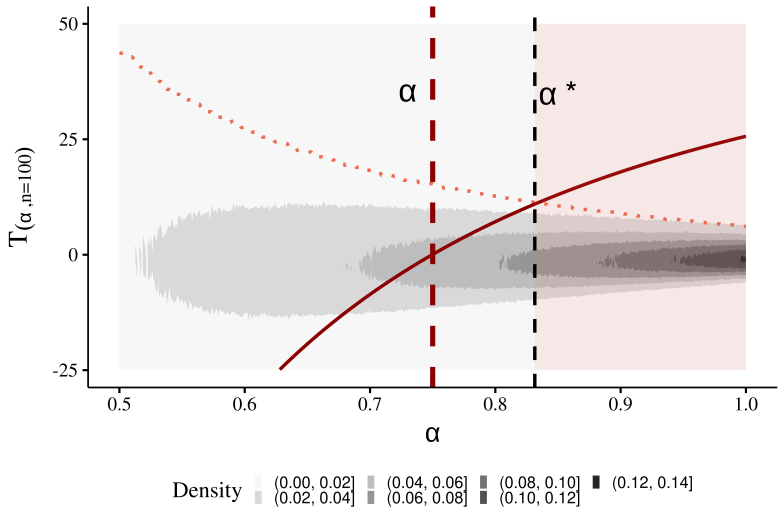

Fig. 3.4 Density of the statistic $T_{(\alpha,n)}$ for a simulated fPp process with $\alpha = 0.75$, $\mu = 4$ and an observed value of $\widehat{\sigma}^2_{\ln \tau} = 4.2$ from a sample of size 100. The segmented line corresponds to the 95th percentile. The solid line correspond to the observed value of the statistic $T_{(\alpha,n)}$ as a function of α.

Values above the segmented line correspond to the rejection region of the Test. If the solid line lies below the segmented line, then there is no evidence to reject the null hypothesis described in (3.39) for any value of $\alpha \in (0, 1)$ and $\alpha^* = 1$.

Therefore, the intersection between the segmented and solid line defines the critical value α^* for the statistic $T_{(\alpha,n)}$, for which the null hypothesis is not rejected. In this case, $\alpha^* < 1$ and corresponds to the maximum value of α that allows us to conclude that the model is a fractional Poisson process.

Figure 3.5 shows the case of a sample path process simulated with $\alpha = 0.9$, $\mu = 4$ and an observed value of $\widehat{\sigma}^2_{\ln \tau} = 2.3$ from a sample of size $n = 100$. The segmented lines corresponds to the 95th and the 99th percentile obtained in the simulation process using $10,000$ iterations. We can observe that for this sample we reject the null hypothesis for a

critical $\alpha^* < 1$ corresponding to the intersection between the 95th percentile curve and the $T_{(\alpha,n)}$ curve. However, it cannot be rejected for a 99th percentile, which implies that we cannot rule out that the series should be modelled by means of a Poisson process for that level of significance.

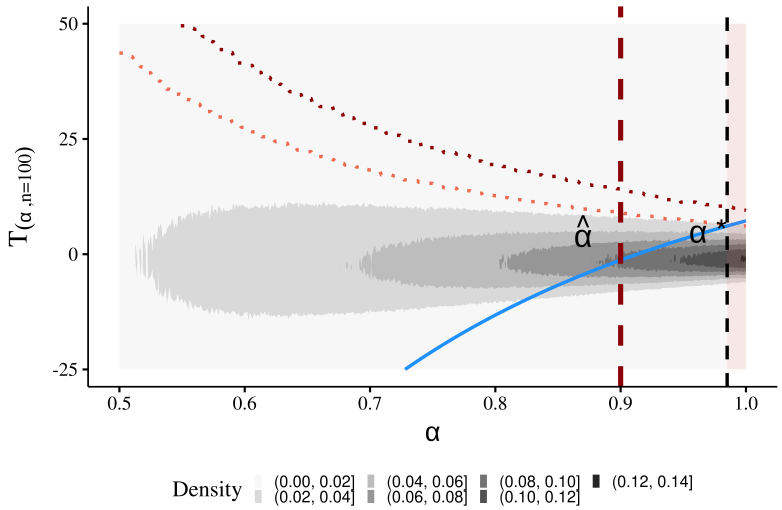

Fig. 3.5 Density of the statistic $T_{(\alpha,n)}$ for a simulated fPp process with $\alpha = 0.9$, $\mu = 4$ and an observed value of $\widehat{\sigma}^2_{\ln \tau} = 2.3$ from a sample of size 100. The segmented line corresponds to the 95th and the 99th percentile, and the solid lines correspond to the observed value of the statistic $T_{(\alpha,n)}$, as functions of α.

3.6 Application to Financial data

In recent years there has been an increase in the analysis of extreme events in the financial context which are defined for the purposes of this research as unusual observed negative returns, generally those returns that are below a threshold, as mentioned by Brogaard et al. (2018), Longin (2016), Gresnigt et al. (2015), among other authors.

One element that has received special attention is the period of incidence of extreme events and the identification of the factors that influence the occurrence of these, as shown in Bogachev and Bunde (2008) and Jiang et al. (2018).

The occurrence of extreme events is usually measured as the period of time between successive events that are below a threshold Q. One of the drawbacks in modeling these phenomena is in the analysis of the statistics for small thresholds, (Bogachev and Bunde (2008)).

The use of the fPp to analyze extreme events gives us a greater degree of flexibility for modeling, since we can consider it as a generalization of Poisson processes, which allows us to understand the behavior of the time series of financial assets in the context of extreme variations in price levels and financial crisis.

In this section we will proceed to estimate the parameters of an fPp distribution in the context of financial series of returns as an example of the ABC methodology presented in the previous sections.

Figure 3.6 exemplifies the method of computing the values considered extreme, where a return less than a defined percentile threshold $Q = 2$ of historical returns up to time t, is considered as an extreme value and the time between each of the events T_i is computed.

The first graph at the top in Figure 3.6 corresponds to the price series of the S&P500 index from January 2005 to December 2015. The second graph corresponds to the return series of the S&P500 index from the same period. The third graph corresponds to the enlargement of the segmented box in the second one, from January 2010 to October 2010, to exemplify the calculation of the time intervals (ΔT_j) between two consecutive extreme events. Finally, the last graph corresponds to the sample path of jumps process defined by the interarrival times of extreme events for the S&P500 data series.

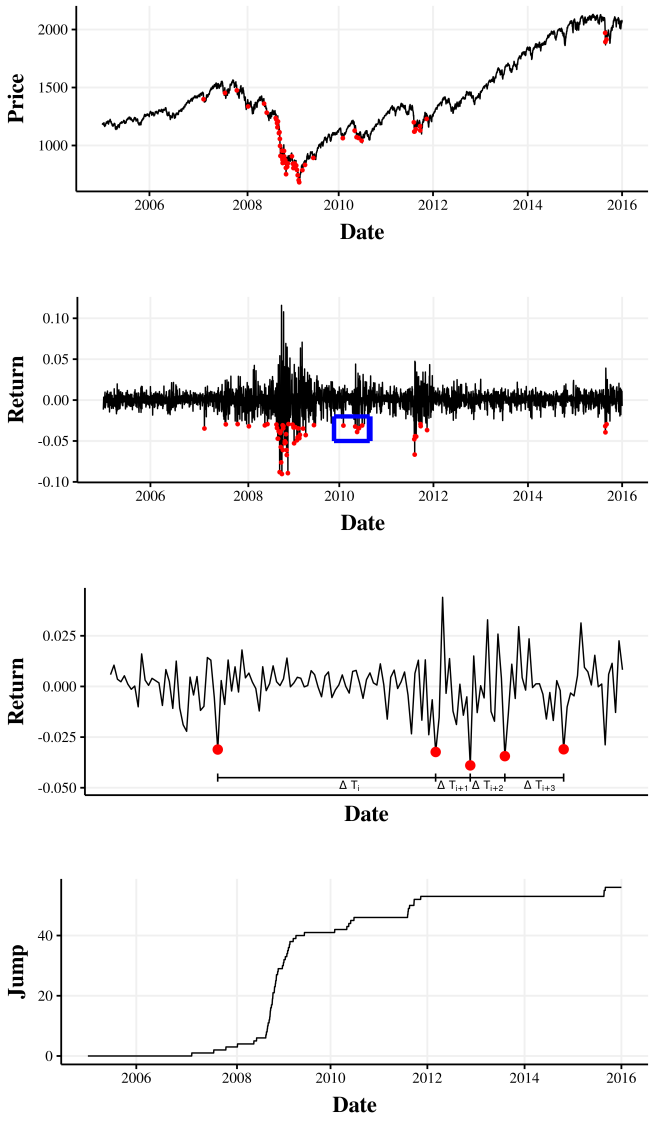

Fig. 3.6 Price, return, and extreme event interarrival times process of S&P500.

The data to be used corresponds to six financial series of returns whose characteristics are shown in the following table:

Name	N° of observations	Mean	Std. Deviation	Start	End
S&P500	17,421	2.9549e-04	0.0097	1950-01-03	2019-04-01
Nasdaq	12,145	3.5924e-04	0.0123	1971-02-05	2019-04-02
Nikey	12,599	1.4966e-04	0.0122	1970-10-12	2019-10-11
DAX	7,469	2.3875e-04	0.0138	1990-10-11	2019-10-10
Platino	12,756	1.0415e-04	0.0161	1969-01-02	2019-10-09
Coffee	11,566	3.0175e-05	0.0218	1973-08-20	2019-10-09

Table 3.6 Daily financial series.

The first column indicates the financial assets on which the measurements are made, where the S&P 500 corresponds to Standard & Poor's index of the 500 most traded stocks on the NYSE, Nasdaq corresponds to the index of the main technology companies traded on the NYSE, Nikey to the Japanese stock market index, and DAX to the German stock market index. Platinum corresponds to the price of platinum on the international market, and Coffee corresponds to the price series of coffee on the international market. The number of observations corresponds to the number of daily returns of different financial assets. The Mean column corresponds to the average returns of the price series in the analyzed period, Std. Deviation corresponds to the standard deviation of the returns of each of the financial series. Start corresponds to the start date of the data obtained from each of the financial series, End corresponds to the last period of data obtained from the financial series.

The Figure 3.7 shows the ABC estimation of the behavior of the parameters of the arrival interval between 2 extreme events for 0.5, 1, 2 percentile.

Figure 3.8 shows the use of the test developed for real time series. The S&P500 and Coffee time series are compared for the 0.5, 1 and 2 percentiles of extreme values, respectively. It can be seen that the S&P500 critical value α^* is more fractional than the case of the Coffee time series. We can also observe that for the case of the 2nd percentile of the Coffee time series, the hypothesis is rejected for all values of $\alpha \in (0,1)$, favoring the hypothesis that the process is Poisson, $\alpha = 1$.

Table 3.7 shows a summary of the main statistics obtained by means of the methodology described above. In its first column shows the observed value of the $\widehat{\sigma}^2_{\ln \tau}$, considering the 0.5, 1 and 2 percentile, respectively, for each of the time series of returns described in Table 3.6. The second column corresponds to the number of observations for each of the extreme return series. The third column $\widehat{\alpha}$ corresponds to the estimation of the parameter α by means of the ABC methodology considering a total of $10,000$ replicates. Finally, α^* corresponds to the highest value of $\alpha \in (0,1]$ such that the null hypothesis is not rejected (when $\alpha^* < 1$, this

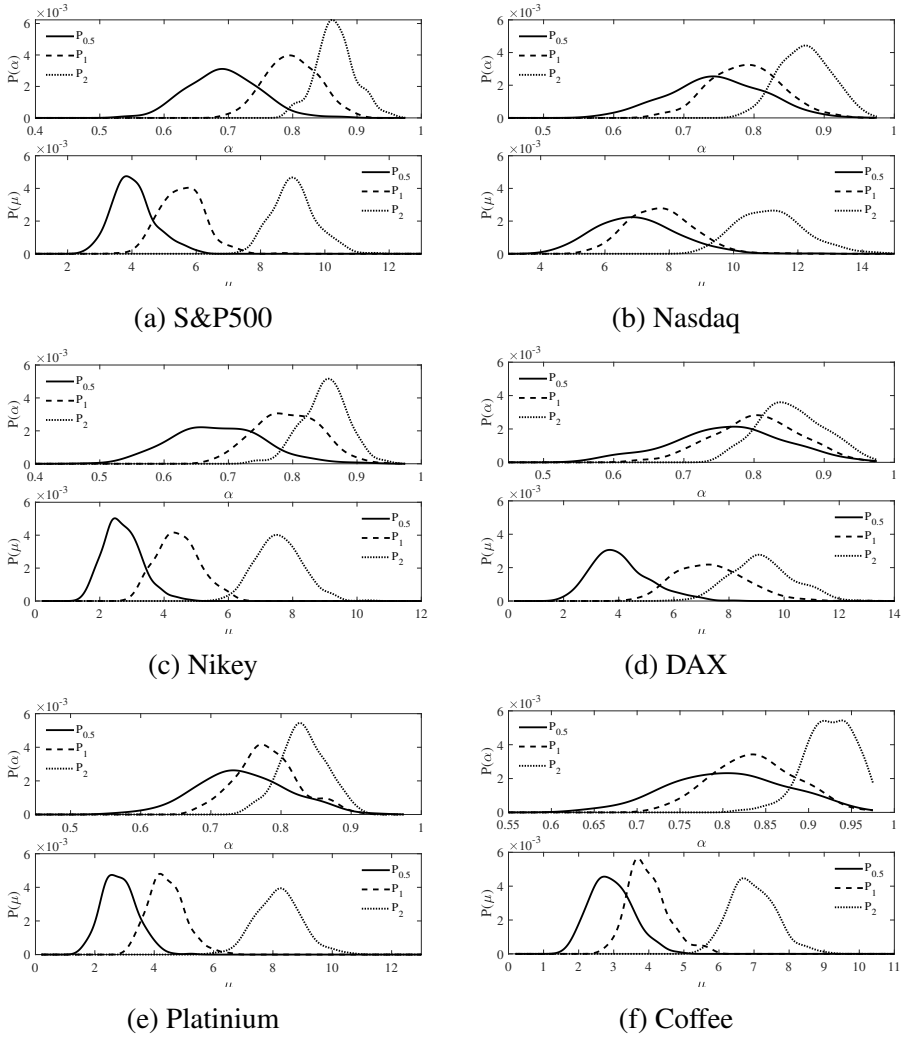

(a) S&P500 (b) Nasdaq

(c) Nikey (d) DAX

(e) Platinium (f) Coffee

Fig. 3.7 Estimation of fPp Parameters for the index returns. The first figure shows the parameter estimator distribution of the extremes values SP500 index, the second figure the Nasdaq index, the third figure the Japanese Nikey index, the fourth figure the German DAX, the fifth figure the platinum price series and the sixth figure the coffee price series.

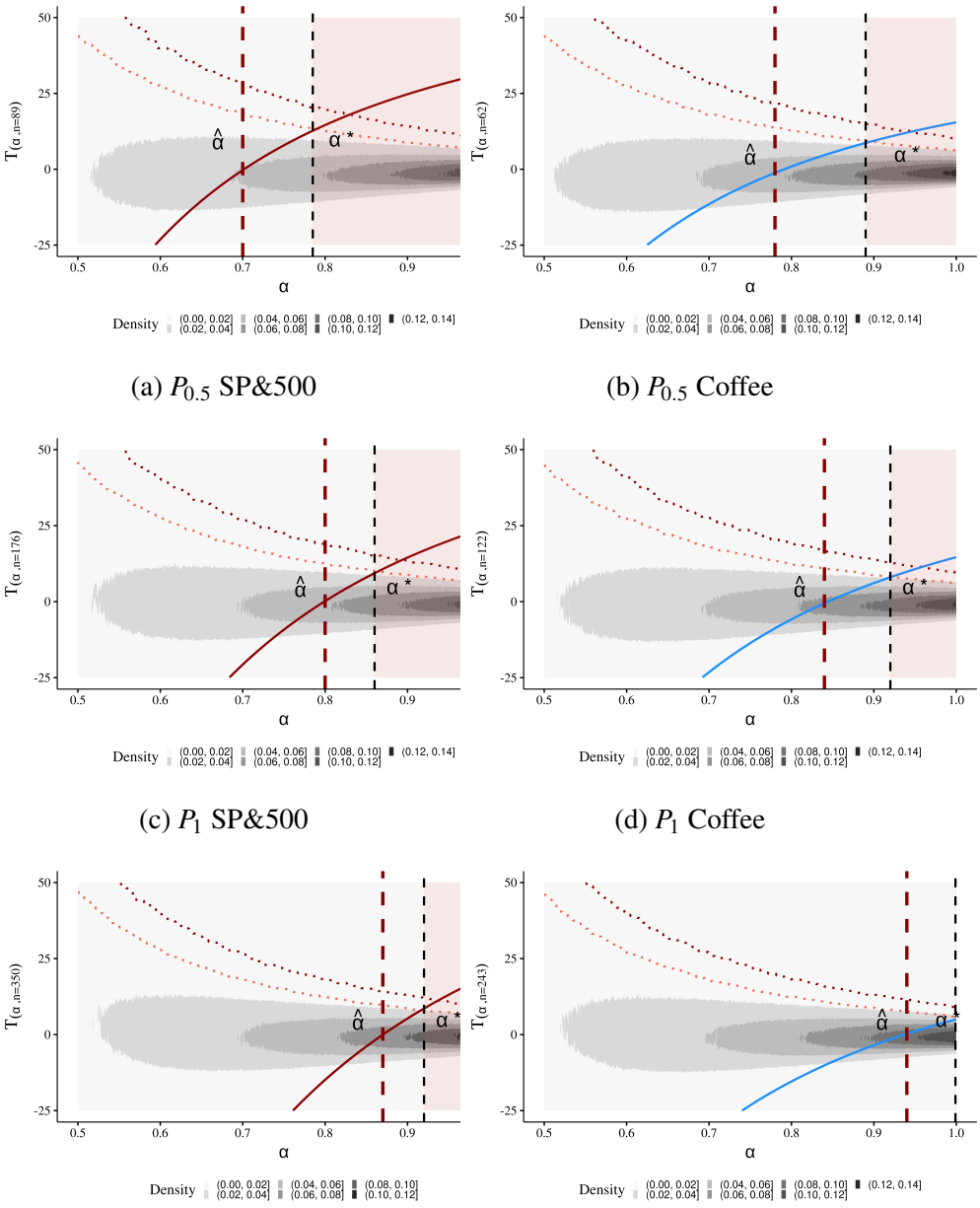

(a) $P_{0.5}$ SP&500

(b) $P_{0.5}$ Coffee

(c) P_1 SP&500

(d) P_1 Coffee

(e) P_2 SP&500

(f) P_2 Coffee

Fig. 3.8 Test of $\widehat{\alpha}$ for percentile 0.5, 1 and 2.

also corresponds to the smallest value of $\alpha \in (0,1]$ such that the null hypothesis is rejected). The value of α^* represents a threshold at which one can be assured with a $1-\varepsilon$ confidence level that the value of the true α is less than that threshold value α^*. If $\alpha^* < 1$, it implies that the financial series can be modelled as fractional.

	$P_{0.5}$				P_1				P_2			
	$\widehat{\sigma}^2_{\ln\tau}$	n	$\widehat{\alpha}$	α^*	$\widehat{\sigma}^2_{\ln\tau}$	n	$\widehat{\alpha}$	α^*	$\widehat{\sigma}^2_{\ln\tau}$	n	$\widehat{\alpha}$	α^*
S&P500	5.04	89	0.70	0.78	3.51	176	0.80	0.86	2.70	350	0.87	0.92
Nasdaq	4.61	62	0.72	0.82	3.87	123	0.76	0.85	2.74	244	0.86	0.89
Nikey	4.79	64	0.71	0.81	3.62	127	0.79	0.87	2.74	253	0.86	0.92
DAX	3.82	39	0.77	0.90	3.27	76	0.81	0.91	2.77	151	0.86	0.93
Platinum	4.13	65	0.74	0.85	3.69	129	0.78	0.86	3.13	257	0.83	0.88
Coffe	3.61	62	0.78	0.89	2.97	122	0.84	0.92	2.10	243	0.94	1

Table 3.7 $\widehat{\sigma}^2_{\ln\tau}$ corresponds to the variance of the natural logarithm of the times between extreme events of the series of returns; n corresponds to the number of observations for each of the calculated percentiles; $\widehat{\alpha}$ corresponds to the estimation by ABC method; α^* corresponds to the first value of at which the null hypothesis is not rejected with a confidence level of 95%.

It can be observed that for almost all the financial time series computed, the value of $\alpha^* < 1$, which implies the null hypothesis is not reject for $\alpha \leq \alpha^*$. Therefore these series can be modeled by a fractional Poisson process. The case of the 2nd percentile of the Coffee time series is the only case that correspond to a Poisson process ($\alpha^* = 1$).

As the event becomes less extreme (greater than the second percentile), the computed value of $\widehat{\alpha}$ begins to tend to 1, so that we can no longer characterize the event as a fractional process.

3.7 Conclusions

Through this research we have been able to characterize the parameters of an fPp by means of Aproximate Bayesian Computation (ABC) techniques, which gives us a new strategy for point estimates and inference about the behavior of the parameters that define an fPp.

The analysis using simulated data showed us that the estimation of the parameters that define the fPp, using ABC techniques, has a similar behavior to the estimation by moments, which validates the approximation presented in this work.

However, for relatively small samples, the ABC approximation is a more efficient alternative in this context, proposing closer values than the estimation by moments.

The application to time series of financial returns showed us that the process that governs the sequence of extreme events can be characterized and modeled by means of an fPp and that the more extreme the event, the smaller the α parameter that defines the fractional condition of the process, indicates that the process allows observing extreme value events or financial crises in both, the short and long term.

The development and use of the new hypothesis test described in this research work allows us to identify whether it is appropriate for a time series to be characterized as fractional. In the case that the null hypothesis is not rejected for some value of $\alpha \in (0,1)$, this time series can not be characterized as fractional, being the critical α^* value the one that represents highest value degree of non-rejected regularity for the test according to the observed data structure.

This line of development opens new possibilities for the analysis of the regularity of other types of time series, such as climatic data series, earthquakes, physics, among others, allowing a new approach to practical applications of these theoretical developments.

Chapter 4

Modeling records process with Piecewise Deterministic Markov Models

Abstract

We propose to model the records of the maximum Drawdown by means a Piecewise Deterministic Markov Process (PDMP). We derive statistical results such as the mean, variance, and characteristic function that describes the sequence of maximum Drawdown records. In addition, we developed a simulation study and techniques for estimating the parameters governing the stochastic process, using a practical example in the capital market to illustrate the procedure.

4.1 Introduction

The Piecewise Deterministic Markov Process (PDMP) are processes which was originally developed by Davis Davis (2018) and have had an important relevance in determining phenomena in different areas of science. These processes are characterised by having a certain number of states that change randomly and by having a deterministic part that evolves in each of the states of the process.

The general characteristics of PDMP processes allow to approach areas that have not been deeply developed in the literature and to generate new research opportunities. In particular, record theory allows us to understand processes that evolve over time and to understand the asymptotic behaviour of certain phenomena, where record is the largest (smallest) value in a sequence of values that are observed over time. Among recent developments, we can cite Rudnicki and Tyran-Kamińska (2015) who uses PDMP techniques to set up an analysis framework for biological systems, cell life cycle and other biological applications. Another interesting development is by Kouretas et al. (2006) who model biological networks for the study of antibiotic production. Similarly we can see developments in other areas of science such as physics, economics, among others (see Lin and Buchler (2018), Schäl (1998)).

In this part we link PDMP processes with record theory for the particular case of a risk management process known as *Drawdown*, which is widely used in the financial literature, but can be easily extended to other disciplines.

This research aims to carry out a statistical and mathematical analysis of the characteristics of the limit distribution of the process that defines the *Drawdown* records, based on the PDMP methodology, and to propose methods for estimating the parameters that determine the process.

The results of this part show a description of the mean, variance and process characteristic function of records obtained from the PDMP process. In addition, simulation techniques and estimation of the parameters of the processes that describes the model were developed, providing important tools for potential applications in different areas of science.

This paper is organized as follows. Section 4.1 presents the Introduction, the Model and preliminaries is presented in the Section 4.2. The Statistical properties of R_t process is show in Section 4.3. The Section 4.4 corresponds to the Simulation and estimation of the R_t process. In Section 4.5 we apply the methodology developed for an applied case, and the Section 4.6 corresponds to the Conclusions of this research.

4.2 Model and preliminaries

In this section, we develop the necessary elements of the stochastic process known as maximum *Drawdown*, which is linked to record theory and has a wide range of applications.

The classical theory of records consider a time series $X_0, X_1, \ldots, X_n$ of random variables that can reach a maximum (minimum) value in a period of time. We define an upper and lower record as

$$X_n > \max\{X_0, X_1, \ldots, X_{n-1}\},$$

$$X_n < \min\{X_0, X_1, \ldots, X_{n-1}\}.$$

Maximum *Drawdown* in T time can be informally defined as the largest drop from a peak of the time series to the smallest value of a valley, which implies reaching a new record in that time. Following Magdon-Ismail and Atiya (2004), we define the maximum *Drawdown* process as a process driven by a Brownian process that indicates the maximum drop observed in a period in $[0,T]$.

Let $X(t)$, $0 \leq t \leq T$, a Brownian motion with drift given by $X(t) = \sigma W(t) + \mu t$, where $\mu \in \mathbb{R}$ is the trend and $\sigma \geq 0$ is the diffusion parameter.

The mathematical definition of maximum *Drawdown* (D) is

$$D(T;\mu,\sigma) = \sup_{t\in[0,T]} \left[\sup_{s\in[0,t]} X(s) - X(t) \right], \tag{4.1}$$

with $0 \leq s \leq t \leq T$. This definition allows to characterise the maximum drop of a time series when considering a fixed value of $T > 0$.

However, we are interested in the process for each time instant over the *records* that it can reach at the maximum *Drawdown*. For this stochastic process we consider the following definition of the occurrence times of a records in the process, such that

$$T_i = \inf\{t > 0 : D(t) > D(T_{i-1}) \wedge \exists s > t, D(s) - D(t) = 0\}, \tag{4.2}$$

with $T_0 = 0$ and $i \in \mathbb{N}$, where T_i represents the ocurrence of the $i-th$ record and $D(\cdot)$ corresponds to the drawdown random variable defined in (4.1), which present a new record in the time series and, therefore, $D(T_i)$ and T_i are random variables that define a stochastic process of drawdown records that must be characterised in terms of their time evolution and distribution.

The observation of the occurrence of new records allows modeling a stochastic process that alternates in different states and thus observe the long-term behaviour of the records that are achieved. In the following subsection a model is developed that allows to characterise the evolution of the records as a stochastic process.

4.2.1 Piecewise Deterministic Markov Process

In our model we consider a Piecewise Deterministic Markov Process (PDMP) as the main tool that allows us to characterise the stochastic process. PDMP processes were first introduced by Davis Davis (2018) and which has been popularized in recent years Azais and Bouguet (2018), becoming a powerful tool for working with stochastic differential equations, specifically with processes that can change states. PDMP processes is defined as follows.

Markov Process

Let $(X_t, t \geq 0)$ a Markov process with its continuous realizations on the right-hand side and with a limit on the left-hand side (*cádlág*) almost surely. Moreover, the process X has values in an open subset $\mathscr{X} \subseteq \mathbb{R}^d$, for $d \geq 1$.

Remark 1. *We use the notation $\partial\mathscr{X}$ as a frontier of $\mathscr{X}$ and $\overline{\mathscr{X}}$ the closure of $\mathscr{X}$.For a Markov process X, we define the Markov semigroup as a family of operators P_t acting on bounded measurable functions f such that, for all $t > 0$*

$$P_t f(x) = \mathbb{E}\left[f(X_t)|X_0 = x\right],$$

and the infinitesimal generator $\mathscr{U}$ of X, acting on the functions f as

$$\mathscr{U} f(x) = \lim_{t\to 0} \frac{P_t f(x) - f(x)}{t}. \tag{4.3}$$

The operator $\mathscr{U}$ characterises the dynamics of the process and can be interpreted as the derivative in time of the semigroup $\partial_t P_t = \mathscr{U}$, at $t = 0$.

The PDMP process is determined by three characteristic components:

1. Deterministic part of the movement between jumps Υ.
2. λ jump rate associated with a probability distribution.
3. Transition measure or Q jump kernel.

In addition, the transition measure Q has the following characteristics:

1. For each fix $A \in \mathscr{E}$, mapping $x \to Q(A;x)$ is measurable.
2. $Q(\{x\};x) = 0$

Let us consider $(J_n)_{n\in\mathbb{N}}$ a time-homogeneous irreducible Markov chain taking values in the state space $K = \{1,\dots,k\}$ with initial law $\pi_i = \mathbb{P}(J_0 = i)$ for all $i \in K$ and transition probability matrix $Q = (q_{ij})_{i,j\in K}$, i.e.

$$\mathbb{P}(J_{n+1} = j | J_n = i) = q_{ij}.$$

which implies that all states with $q_{i,j} > 0$ are connected and each state can be reached by a given state i.

We denote by $(T_n)_{n\in\mathbb{N}}$ the sequence of the record ocurrence random times and $(S_n)_{n\in\mathbb{N}}$ the random interval times; i.e. $S_n = T_{n+1} - T_n$.

In addition, we define $(\nu_t)_{t\in\mathbb{R}_+}$ by

$$\nu_t = \sum_{n\geq 0} J_n \mathbb{1}_{[T_n, T_{n+1}[}(t).$$

If $(J_n)_{n\in\mathbb{N}}$ is an irredicible Markov Chain, then $(\nu_t)_{t\in\mathbb{R}}$ is an irreducible Markov process with the same initial law that your immersed Markov chain $(J_n)_{n\in\mathbb{N}}$. Here, J_n is the state taken by ν_t on $[T_n, T_{n+1}[$.

The matrix generator $A = (a_{ij})_{i,j\in K}$ of the process $(\nu_t)_{t\in\mathbb{R}_+}$ is given by

$$a_{ij} = \begin{cases} \lambda_i q_{ij} & for \quad i \neq j \\ -\lambda_i(1 - q_{ii}) & for \quad i = j \end{cases}. \tag{4.4}$$

The generator A is stable and conservative; *i.e.* $\sum_{j\in K} a_{ij} = 0$ and $a_{ij} \geq 0$ for $i \neq j$, which implies that the solutions of the system are driven by this differential operator which does not change over time and maintains stable solutions.

With these preliminaries we can define the record stochastic process $(R_t)_{t\in\mathbb{R}_+}$, which takes values on $[0,1]$ and suppose that $\mathbb{P}(R_0 = r) = 1$.

4.2.2 Definition of R_t process

We consider a PDMP process that is modeled by mean of the Markov chain $(J_n)_{n\in\mathbb{N}}$. This process makes it possible to observe the expected value of drawdown over time, allowing the development of applications that can be used in several areas of knowledge that require risk management in their analysis. The process consider the following assumptions:

Assumption 1.

i) Between two consecutive jump times T_n and T_{n+1}, the continuous time process (R_t) is constant and equal to $r_n = R_{T_n}$.

ii) The record jumps size Δ_n at the time T_n, is given by $\Delta_n = \rho(1-r_n)$, where ρ is a random variable that takes values on $[0,1]$ with probability distribution G_i, for $J_n = i \in K$. The probability distributions $(G_i)_{i\in K}$ could be different.

iii) The interval time S_n is a random variable with exponential distribution of parameter λ_i, for $i \in K$, where the jump rate λ_i of state i is a strictly positive constant.

Note that he records process increases by the value Δ_n at the time T_n. After that, the record process remains constant until the next jump T_{n+1}. Thus, the sample path of the stochastic process $(R_t, \nu_t)_{t\in\mathbb{R}_+}$ with values in $[0,1]\times K$ starting from a fixed point (r,ν) is defined in the following way, as we illustrate in Figure 4.1.

First, say that $\nu_t = J_0 = \nu$ for $t < T_1 = S_0$, where S_0 stands for the first jump time of ν_t, which has an exponential distribution of parameter λ_{J_0}, and $\nu_{T_1} = J_1$. Now, we define ρ_{J_1} as a random variable with density distribution g_{J_1}, and then we take $\Delta_1 = \rho_{J_1}(1-r)$. Then the sample path (R_t) up to the first jump time T_1 is now defined as follows:

$$\begin{aligned} R_t &= r \qquad \text{if } 0 \leq t < T_1, \\ R_{T_1} &= r + \Delta_1 \quad . \end{aligned}$$

The process now restarts from $r_1 = R_{T_1}$ according to the same recipe. Thus, we define S_1 a random variable with exponential distribution of parameter λ_{J_1}, so we take $T_2 = T_1 + S_1$. The Markov process (ν_t) jump to regime J_2 with rate $q_{J_1J_2}$, thus $\nu_{T_2} = J_2$ and $\Delta_2 = \rho_{J_2}(1-r_1)$

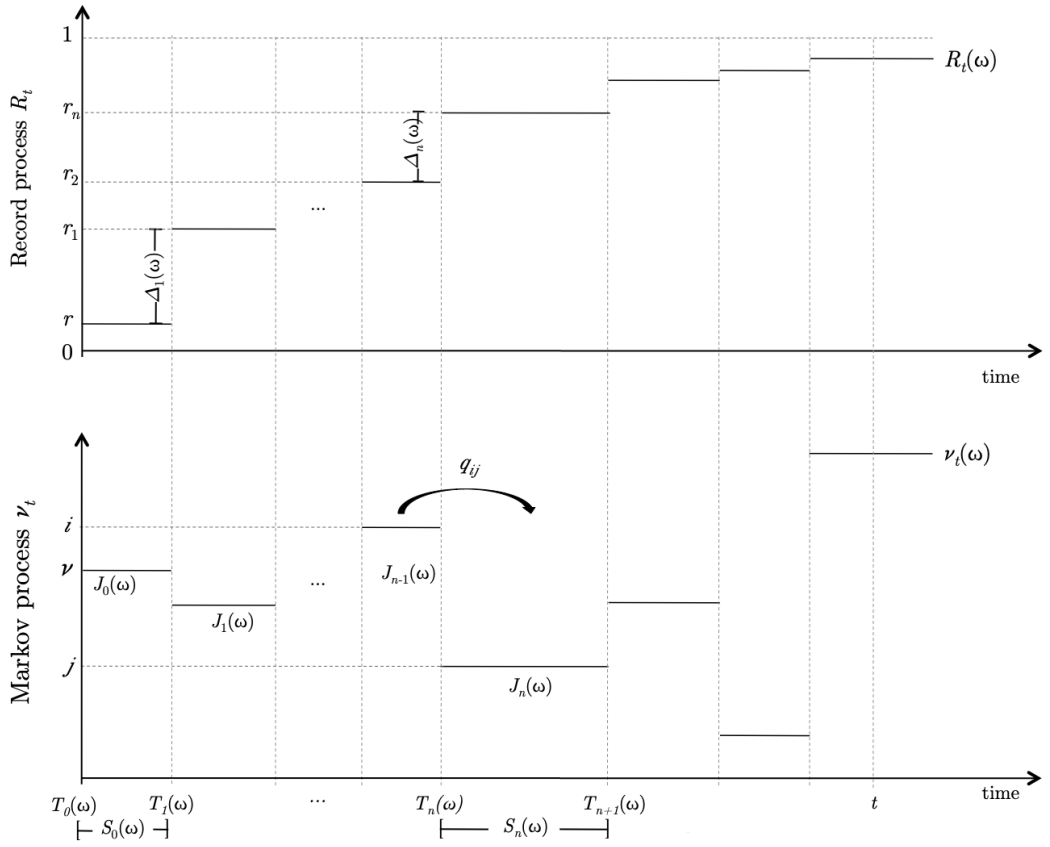

Fig. 4.1 Sample path of the PDMP process (R_t, ν_t).

where ρ_{J_2} is a random variable with probability distribution G_{J_2}. Then, the sample path (R_t) up to the second jump time, starting from r_1 at time T_1, is defined as

$$\begin{aligned} R_t &= r_1 \qquad \text{if } T_1 \le t < T_2, \\ R_{T_2} &= r_1 + \Delta_2 \quad ; \end{aligned}$$

and so on. Finally, for all $n \in \mathbb{N}$ and for $k = 1, \ldots, n$, we take $(J_k)_{k=0:n}$ a sample path of the Markov chain, S_k a random variable with exponential distribution of parameter λ_{J_k}, $T_{k+1} = T_k + S_k$, $\nu_{T_{k+1}} = J_{k+1}$, and we define $\Delta_{k+1} = \rho_{J_{k+1}}(1 - r_k)$ where $\rho_{J_{k+1}}$ is a random variable with probability distribution $G_{J_{k+1}}$ and $r_k = R_{T_k}$. Then, we have

$$R_t = r + \textstyle\sum_{k=1}^{n} \Delta_k \quad \text{if } T_n \le t < T_{n+1},$$

which can be rewritten as

$$R_t = r + \sum_{k \ge 1} \Delta_k \, \mathbb{1}\!\mathrm{l}_{(t \ge T_k)}. \tag{4.5}$$

Note that the record jump size Δ_k is a funtion of $\nu_{T_k} = J_k$ and $R_{T_{k-1}} = r_{k-1}$.

Lemma 1. *The records process* $(R_t)_{t\in\mathbb{R}_+}$ *defined in* (4.5) *with initial value* $R_0 \in [0,1[$ *satisfy*

$$R_t = R_0 + (1-R_0)R_t^0, \tag{4.6}$$

where the process $(R_t^0)_{t\in\mathbb{R}_+}$ *given by*

$$R_t^0 = \sum_{k\geq 1} \rho_{J_k} \left(\prod_{i=1}^{k-1} (1-\rho_{J_i}) \right) 1\!\!1_{(t\geq T_k)}, \tag{4.7}$$

is the records process obtained when the initial condition is zero, $R_0^0 = 0$.

Proof. R_t is given by equation (4.5) where $\Delta_k = \rho_{J_k}(1-r_k)$ are given by the following recursive equations:

$$\begin{aligned}
\Delta_1 &= \rho_{J_1}(1-R_0) \\
\Delta_2 &= \rho_{J_2}(1-R_{T_1}) = \rho_{J_2}(1-R_0-\Delta_1) = \rho_{J_2}(1-\rho_{J_1})(1-R_0) \\
\Delta_3 &= \rho_{J_3}(1-R_{T_2}) = \rho_{J_3}(1-R_0-\Delta_1-\Delta_2) = \rho_{J_3}(1-\rho_{J_2})(1-\rho_{J_1})(1-R_0) \\
&\vdots \\
\Delta_k &= \rho_{J_k}(1-R_{T_{k-1}}) = \rho_{J_k}(1-R_0-\Delta_1-\ldots-\Delta_{k-1}) = \rho_{J_k}\prod_{i=1}^{k-1}(1-\rho_{J_i})(1-R_0).
\end{aligned}$$

Then,

$$R_t = R_0 + (1-R_0)\sum_{k\geq 1} \rho_{J_k} \left(\prod_{i=1}^{k-1} (1-\rho_{J_i}) \right) 1\!\!1_{(t\geq T_k)}.$$

When $R_0 = 0$ we obtain the records process

$$R_t^0 = \sum_{k\geq 1} \rho_{J_k} \left(\prod_{i=1}^{k-1} (1-\rho_{J_i}) \right) 1\!\!1_{(t\geq T_k)}.$$

□

Considering that R_0 and ν_0 are independents, we have that the process $(R_t,\nu_t)_{t\in\mathbb{R}_+}$ is a piecewise deterministic Markov process (PDMP).

We denote by $\mathscr{M}$ the set of measurable real valued functions on $E = [0,1]\times K$ and by $\mathscr{M}_0$ the set of bounded measurable real valued function on E.

From Davis (2018), we have that the domain $\mathscr{D}(\mathscr{U})$ of the infinitesimal generator $\mathscr{U}$ of $(\nu_t,R_t)_{t\in\mathbb{R}_+}$ consists of those functions $f\in\mathscr{M}$ integrable with respect to the probability

measures G. For $f \in \mathscr{D}(\mathscr{U})$ the infinitesimal generator $\mathscr{U}$ is given by

$$\mathscr{U} f(r,\nu) = \lambda_\nu \sum_{j\in K} q_{\nu j} \int_{[0,1]} (f(r+\rho(1-r),j) - f(r,\nu))\, G_j(d\rho), \tag{4.8}$$

with $(r,\nu) \in E$.

We denote by $P : (\nu, j, r, B, t) \to P_{\nu j}(r,B,t)$ the transition probability of (R_t, ν_t); i.e.

$$P_{\nu j}(r,B,t) = \mathbb{P}(R_t \in B, \nu_t = j | R_0 = r, \nu_0 = \nu).$$

It is defined for all $r \in [0,1]$, $\nu, j \in K$, $t \in \mathbb{R}_+$ and $B \in \mathscr{B}([0,1])$, with $\mathscr{B}([0,1])$ being the Borel σ-field of $[0,1]$.

The transition probability permits to give an expression for the probability distribution of (R_t, ν_t) in the following way:

$$\mathbb{P}(R_t \in B, \nu_t = j | R_0 = r) = \sum_{\nu\in K} \pi_\nu P_{\nu j}(r,B,t). \tag{4.9}$$

For $t \in R_+$ fixed, define an operator $\mathscr{P}_t : \mathscr{M}_0 \to \mathscr{M}_0$ by the following conditional expectation given the starting point (r,ν)

$$\mathscr{P}_t f(r,\nu) = \mathbb{E}_{(r,\nu)}[f(R_t,\nu_t)] = \sum_{j\in K} \int_{[0,1]} f(r',j) P_{\nu j}(r,dr',t).$$

Here, $(\mathscr{P}_t; t \in \mathbb{R}_+)$ is the semigroup associated with the infinitesimal generator $\mathscr{U}$; (i.e $\mathscr{P}_{s+t} = \mathscr{P}_s \mathscr{P}_t$).

From Davis (2018), we recall that for t fixed, $(r,\nu) \in E$ and $f \in \mathscr{D}(\mathscr{U})$, $z(t,r,\nu) = \mathscr{P}_t f(r,\nu)$ is the unique solution of the following partial differential equation (EDP):

$$\begin{cases} \dfrac{\partial z}{\partial t}(t,r,\nu) &= \mathscr{U} z(t,r,\nu), \\ z(0,r,\nu) &= f(r,\nu). \end{cases} \tag{4.10}$$

4.3 Statistical properties of R_t process

4.3.1 Mean

First, to analyze the variability of the process we proceed to calculate the mean of the stochastic process. The mean of R_t given the starting point $R_0 = r$ is given by

$$m(t,r) = \sum_{\nu \in K} \pi_\nu m(t,r,\nu),$$

where $\pi = (\pi_\nu)_{\nu \in K}$ is the initial law of the Markov chain $(\nu_t)_{t \in \mathbb{R}_+}$ and $m(t,r,\nu) = \mathbb{E}_{(r,\nu)}[R_t]$ is the conditional expectations of R_t, given the starting point (r,ν).

Proposition 1. *The conditional expectations $m(t,r) = \mathbb{E}_r[R_t]$ of R_t, with the starting point $R_0 = r$ is given by*

$$m(t,r) = \pi e^{Bt} r + \pi \left(e^{Bt} - I\right) B^{-1} \Lambda Q \mu, \tag{4.11}$$

where $m(t,r) = (m(t,r,j))_{j \in K}$, $B = \Lambda Q(I-M) - \Lambda$, $\Lambda = diag(\lambda_j, j \in K)$, Q the transition probability matrix of the Markov chain $(\nu_t)_{t \in R_+}$ and π its initial distribution, $\mu = (\mu_j)_{j \in K}$ with $\mu_j = \int_{[0,1]} \rho G_j(d\rho)$, $M = diag(\mu_j, j \in K)$, and I is the $k \times k$ identity matrix.

Proof. We have that $m(t,r,\nu)$ is the unique solution of the system (4.10) for $f(r,\nu) = r$, then we can rewrite (4.10) as

$$\begin{cases} \dfrac{\partial m}{\partial t}(t,r,\nu) = \lambda_\nu \displaystyle\sum_{j \in K} q_{\nu j} \int_{[0,1]} \left(m(t, r+\rho(1-r), j) - m(t,r,\nu)\right) G_j(d\rho), \\ m(0,r,\nu) = r, \end{cases} \tag{4.12}$$

On the other hand, from Lemma 1

$$\begin{aligned} m(t, r+\rho(1-r), j) &= \mathbb{E}[R_t | R_0 = r+\rho(1-r), \nu_0 = j] \\ &= \mathbb{E}[\rho + (1-\rho)(r + (1-r)R_t^0) | R_0 = r+\rho(1-r), \nu_0 = j] \\ &= \mathbb{E}[r + \rho - \rho r + R_t^0 - r R_t^0 - \rho R_t^0 + \rho r R_t^0 | R_0 = r+\rho(1-r), \nu_0 = j] \\ &= \mathbb{E}[r + (1-r)R_t^0 - \rho(r + (1+r)R_t^0 - 1) | R_0 = r+\rho(1-r), \nu_0 = j] \\ &= \rho + (1-\rho)\mathbb{E}[R_t | R_0 = r, \nu_0 = j] \\ &= \rho + (1-\rho) m(t,r,j). \end{aligned} \tag{4.13}$$

Then, from (4.12) and (4.13) we have

$$\frac{\partial m}{\partial t}(t,r,\nu) = \lambda_\nu \sum_{j \in K} q_{\nu j} \left(\mu_j + (1-\mu_j) m(t,r,j) - m(t,r,\nu)\right).$$

This differential equations system can be written as a system of equations in matricial terms

$$\frac{\partial \bar{m}}{\partial t}(t,r) = \Lambda Q \mu + B \bar{m}(t,r). \tag{4.14}$$

The solution of this differential equations system is given by

$$\bar{m}(t,r) = e^{Bt}r + \left(e^{Bt} - I\right)B^{-1}\Lambda Q\mu. \tag{4.15}$$

Thus, we obtain the result given in equation (4.11) for $m(t,r) = \pi\bar{m}(t,r)$.

□

Case of one-state

In this section we develop the analytical result for the process, considering a one-state case.

Using equation (4.13), we have

$$\begin{cases} \dfrac{\partial m}{\partial t}(t,r,\nu_0) = \mu_{\nu_0}(1 - m(t,r,\nu_0)), \\ m(0,r,\nu_0) = r, \end{cases} \tag{4.16}$$

with $\mu_{\nu_0} = \int_{[0,1]} \rho G_{\nu_0}(d\rho)$, and ν_0 corresponds to the state ν_0 which remains fixed for all time t.

Regrouping terms, we have

$$\frac{\partial m}{\partial t}(t,r,\nu_0) + \mu_{\nu_0} m(t,r,\nu_0) = \mu_{\nu_0},$$

solving the differential equation we have

$$m(t,r,\nu_0) = 1 - \frac{1-r}{e^{\mu_{\nu_0} t}}, \tag{4.17}$$

providing the functional form of the process mean R_t for the case of a one-state. We can analyse the function that characterises the process, and obtain the following results

$$\begin{aligned} \lim_{t\to 0} m(t,r,\nu_0) &= r, \\ \lim_{t\to\infty} m(t,r,\nu_0) &= 1, \end{aligned} \tag{4.18}$$

describing the dynamics of the R_t process over time.

Case of two-state

This section showed how to deal with the mean of the process R_t where two-states is considered, which can be extended to n states.

From (4.14) for the two-state case, we have

$$\begin{aligned}
\frac{\partial m}{\partial t}(t,r,j) &= a\, m(t,r,j) + b\, m(t,r,i) + e \\
\frac{\partial m}{\partial t}(t,r,i) &= c\, m(t,r,j) + d\, m(t,r,i) + f \\
m(0,r,\nu_0) &= r,
\end{aligned} \tag{4.19}$$

where the coefficients are defined as follows

$$\begin{aligned}
a &= \lambda_j q_{1,1}(1-\mu_j) - \lambda_j \\
b &= \lambda_j q_{1,2}(1-\mu_i) \\
c &= \lambda_i q_{2,1}(1-\mu_j) \\
d &= \lambda_i q_{2,2}(1-\mu_i) - \lambda_i \\
e &= \lambda_j(q_{1,1}\mu_j + q_{1,2}\mu_i) \\
f &= \lambda_i(q_{2,1}\mu_j + q_{2,2}\mu_i).
\end{aligned}$$

Here λ_j, λ_i represent the jump rate from state j and i, respectively; μ_j, μ_i represent the expected value of the jump in state j and i, respectively and $q_{1,1}, q_{1,2}, q_{2,1}, q_{2,2}$ the components of the transition matrix Q for two states.

For solving numerically the system of differential equations (4.19), the Runge-Kutta method Soetaert et al. (2010) can be used. An example is given in Table 4.1, where X represents the random variable for the time between jump events subject to states i and j and ρ corresponds to the random variable for the size of the jump.

	Distribution	
	$\nu_t = i$	$\nu_t = j$
$X \sim$	$Exponential(2)$	$Exponential(1)$
$\mathbb{E}[X] =$	0.5	1.0
$\rho \sim$	$Beta(2,20)$	$Beta(2,30)$
$\mathbb{E}[\rho] =$	0.012	0.015

Table 4.1 Characteristics of the stochastic elements of the process R_t

$$Q = \begin{bmatrix} q_{1,1} & q_{1,2} \\ q_{2,1} & q_{2,2} \end{bmatrix} = \begin{bmatrix} 0.6 & 0.4 \\ 0.5 & 0.5 \end{bmatrix}, \tag{4.20}$$

In this case, the representation of the evolution of the mean for each state (v) by the Runge-Kutta method is described as

$$\begin{cases} m(t+\Delta,r,v) = m(t,r,v) + \frac{1}{6}(K_1 + 2K_2 + 2K_3 + K_4), \\ K_1 = \Delta f(t, m(t,r,v)), \\ K_2 = \Delta f(t + \frac{1}{2}\Delta, m(t,r,v) + \frac{1}{2}K_1), \\ K_3 = \Delta f(t + \frac{1}{2}\Delta, m(t,r,v) + \frac{1}{2}K_2), \\ K_4 = \Delta f(t + \Delta, m(t,r,v) + K_3). \end{cases} \tag{4.21}$$

The following figure 4.2, shows the evolution of the expected value of the process R_t, as a result of the numerically solution of the system of equations defined in (4.19) for the two-state case with initial value $r = 0$. It is observed that the mean values increase rapidly at the beginning and then decrease with time, approaching the limit 1. The figure is like the learning curve, which describes a situation in which the task may be easy to learn and the learning progression is initially rapid and fast.

The curve levels off after a certain instant t. In the graph it can be noticed that this instant $t \sim 30$ could be described as a plateau.

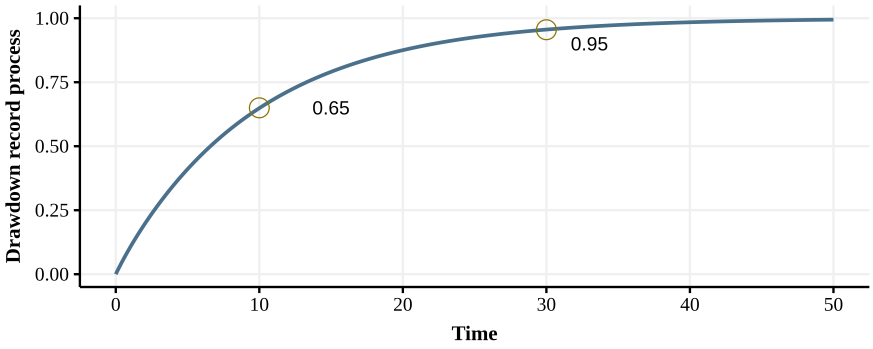

Fig. 4.2 Evolution of the expected value of R_t process.

4.3.2 Variance estimation

In this section, the variability of the record process R_t is studied, starting from the computation of the second moment given the initial point $R_0^2 = r^2$

$$m_2(t,r) = \sum_{v \in K} \pi_v m_2(t,r,v),$$

where $\pi = (\pi_\nu)_{\nu\in K}$ is the initial law of the Markov chain $(\nu_t)_{t\in\mathbb{R}_+}$ and $m_2(t,r,\nu) = E_{r,\nu}[R_t^2]$ is the conditional expectations of R_t, given the initial point (r^2,ν).

Proposition 2. *The variance of records process $(R_t)_{t\in\mathbb{R}_+}$ defined in* (4.5) *with initial value $R_0^2 = r^2$ is,*

$$\begin{aligned} Var(R_t) &= \mathbb{E}_{r,\nu}\left[R_t^2\right] - \mathbb{E}_{r,\nu}^2\left[R_t\right] \\ &= \pi e^{Ht} r^2 + \pi \int_0^t e^{-H(t-s)} \Lambda Q \mu_2 ds + \pi \int_0^t e^{H(t-s)} K \overline{m}(s,r) ds \\ &- \left(\pi e^{Bt} r + \pi \left(e^{Bt} - I\right) B^{-1} \Lambda Q \mu\right)^2 \end{aligned} \tag{4.22}$$

where $B = \Lambda Q(I-M) - \Lambda$, $\Lambda = diag(\lambda_j, j\in K)$, Q the transition probability matrix of the Markov chain $(\nu_t)_{t\in R_+}$, $H = [\lambda Q(I-2M+M_2-\Lambda)]$, $K = 2\Lambda Q(M-M_2)$, $\mu = (\mu_j)_{j\in K}$ with $\mu_j = \int_{[0,1]} \rho G_j(d\rho)$, $\mu_2 = (\mu_{2,j})_{j\in K}$ with $\mu_{2,j} = \int_{[0,1]} \rho^2 G_j(d\rho)$.

Proof. Let $f(r,\nu) = r^2$, $m_2(t,r,\nu) = \mathbb{E}_{r,\nu}[R_t^2]$. The unique solution of the system (4.10) that allow to define the behaviour of the second moment in the stochastic process R_t, considering a finite number of of states is given by

$$\begin{cases} \dfrac{\partial m_2}{\partial t}(t,r,\nu) = \lambda_\nu \displaystyle\sum_{j\in K} q_{\nu j} \int_{[0,1]} \left(m_2(t, r+\rho(1-r), j) - m_2(t,r,\nu)\right) G_j(d\rho), \\ m_2(0,r,\nu) = r^2, \end{cases} \tag{4.23}$$

From Lemma 1, we can write the second moment as

$$\begin{aligned} m_2(t, r_1+\rho(1-r), j) &= \mathbb{E}[R_t^2 | R_0 = r+\rho(1-r), \nu_0 = j] \\ &= \rho^2 + 2\rho(1-\rho) m(t,r,j) + m_2(t,r,j)(1-\rho)^2. \end{aligned} \tag{4.24}$$

Let $\mu_j = \int_{[0,1]} \rho G_j(d\rho)$, $\mu_{2,j} = \int_{[0,1]} \rho^2 G_j(d\rho)$. Combining (4.23) y (4.24), we have

$$\begin{aligned} \frac{\partial m_2}{\partial t}(t,r,\nu) &= \sum_{j=1}^{k} \lambda_\nu q_{\nu,j} (\mu_{2,j} + 2(\mu_j - \mu_{2,j}) m(t,r,j) \\ &+ (1 - 2\mu_j + \mu_{2,j}) m_2(t,r,j) - m_2(t,r,\nu)), \end{aligned}$$

which in matrix form is written as

$$\begin{aligned} \frac{\partial \overline{m}_2}{\partial t}(t,r) &= \Lambda Q \mu_2 + 2\Lambda Q(M-M_2)\overline{m}(t,r) \\ &+ \Lambda Q(I-2M+M_2)\overline{m}_2(t,r) - \Lambda \overline{m}_2(t,r). \end{aligned} \tag{4.25}$$

Let $H = [\lambda Q(I - 2M + M_2 - \Lambda)]$ y $K = 2\Lambda Q(M - M_2)$. Regrouping terms from (4.25), we get the following differential equation

$$\frac{\partial \overline{m}_2}{\partial t}(t,r) - H\overline{m}_2(t,r) = \Lambda Q\mu_2 K\overline{m}(t,r), \tag{4.26}$$

which has as a solution

$$\overline{m}_2(t,r) = e^{Ht}r^2 + \int_0^t e^{-H(t-s)}\Lambda Q\mu_2 ds + \int_0^t e^{H(t-s)}K\overline{m}(s,r)ds. \tag{4.27}$$

Finally, from (4.11) and (4.27), we obtain

$$\begin{aligned} Var(R_t) &= e^{Ht}r^2 + \int_0^t e^{-H(t-s)}\Lambda Q\mu_2 ds + \int_0^t e^{H(t-s)}K\overline{m}(s,r)ds \\ &- \left(e^{Bt}r + \left(e^{Bt} - I\right)B^{-1}\Lambda Q\mu\right)^2. \end{aligned}$$

□

Case of one-state

In this section the case of a steady state such that $\nu = \nu_0$ is presented, which shows the intuition of the results obtained for the n-state case. From equation (4.23) we have

$$\begin{aligned} \frac{\partial \overline{m}_2}{\partial t}(t,r,\nu_0) &= \lambda\mu_2 + 2\lambda(\mu - \mu_2)m(t,r,\nu_0) + \lambda(\mu_2 - 2\mu)m_2(t,r,\nu_0) \\ m_2(0,r,\nu_0) &= r^2, \end{aligned} \tag{4.28}$$

which is equivalent to

$$\frac{\partial m_2}{\partial t}(t,r,\nu_0) + c\, m_2(t,r,\nu_0) = a + b\, m(t,r,\nu_0), \tag{4.29}$$

with $a = \lambda\mu_2$, $b = 2\lambda(\mu - \mu_2)$ and $c = \lambda(2\mu - \mu_2)$. Combining equations (4.17) and (4.29), we have

$$m_2(t,r,\nu_0) = \frac{a+b}{c} + \frac{r-1}{(c-\mu)e^{ct}} + \left(r^2 - \frac{a+b}{c} - \frac{r-1}{(c-\mu)}\right)\frac{1}{e^{ct}}. \tag{4.30}$$

Therefore, the variance of the process R_t is given by

$$\begin{aligned} &Var(R_t) = \\ &\frac{a+b}{c} + \frac{r-1}{(c-\mu)e^{ct}} + \left(r^2 - \frac{a+b}{c} - \frac{r-1}{(c-\mu)}\right)\frac{1}{e^{ct}} - \left(1 - \frac{1-r}{e^{\mu_{\nu_0}t}}\right)^2 \\ &= \frac{r-1}{(c-\mu)e^{ct}} + \left(r^2 - 1 - \frac{r-1}{(c-\mu)}\right)\frac{1}{e^{ct}} + 2\frac{1-r}{e^{\mu_{\nu_0}t}} - \left(\frac{1-r}{e^{\mu_{\nu_0}t}}\right)^2 \end{aligned}$$

$$\leq \quad \frac{2(1-r)}{e^{\mu_{v_0} t}}, \tag{4.31}$$

providing the functional form of the variance of process R_t for the case of one-state. Analysing the function that characterises the second moment of the process, and obtain the following results

$$\begin{aligned} \lim_{t\to 0} m_2(t,r,v_0) &= r^2, \\ \lim_{t\to \infty} m_2(t,r,v_0) &= 1, \end{aligned} \tag{4.32}$$

describing the dynamics of the second moment of process over time, with a variance of

$$Var(R_t) \leq 2(1-r)e^{-\mu_{v_0} t}, \tag{4.33}$$

Case of two-state

In this section the variance process of R_t for the two-state case is computed, which can be extended to n different states. From (4.25) we have

$$\begin{aligned} \frac{\partial m_2}{\partial t}(t,r,j) &= a\, m_2(t,r,j) + b\, m_2(t,r,i) + c\, m_2(t,r,j) + d + e\, m(t,r,j) + f\, m(t,r.i) \\ \frac{\partial m_2}{\partial t}(t,r,i) &= g\, m_2(t,r,j) + h\, m_2(t,r,i) + k\, m_2(t,r,i) + l + n\, m(t,r,j) + p\, m(t,r,i) \\ m(0,r,v_0) &= r, \end{aligned}$$

where the coefficients are defined as follows

$$\begin{aligned} a &= \lambda_j q_{1,1}(1 - 2\mu_j + \mu_{2,j}) \\ b &= \lambda_j q_{1,2}(1 - 2\mu_i + \mu_{2,i}) \\ c &= \lambda_j \\ d &= \lambda_j(q_{1,1}\mu_{2,j} + q_{1,2}\mu_{2,i}) \\ e &= 2\lambda_j q_{1,1}(\mu_j - \mu_{2,j}) \\ f &= 2\lambda_1 q_{1,2}(\mu_i - \mu_{2,i}) \\ g &= \lambda_i q_{2,1}(1 - 2\mu_j + \mu_{2,j}) \\ h &= \lambda_i q_{2,2}(1 - 2\mu_i + \mu_{2,i}) \\ k &= \lambda_i \\ l &= \lambda_i(q_{2,1}\mu_{2,j} + q_{2,2}\mu_{2,i}) \\ n &= 2\lambda_i q_{2,1}(\mu_j - \mu_{2,j}) \end{aligned}$$

$$p = 2\lambda_i q_{2,2}(\mu_i - \mu_{2,i}).$$

Here, λ_j, λ_i represent the jump rate from state j and i, respectively; μ_j, μ_i the expected value of the jump in state j and i, respectively; $q_{1,1}, q_{1,2}, q_{2,1}, q_{2,2}$ the components of the transition matrix Q for two states. In this case, the system of differential equations can be solved by Runge-Kutta method Soetaert et al. (2010), using parameters defined in the Table 4.1. In Figure 4.3 we plot the evolution of the variance of the process R_t, with initial value $r^2 = 0$, and demonstrate convergence to zero. As illustrated in the graphics, the maximum variance is obtained around the time $t = 5$, which decays rapidly, approaching its asymptotic value equal to zero at period $t = 50$.

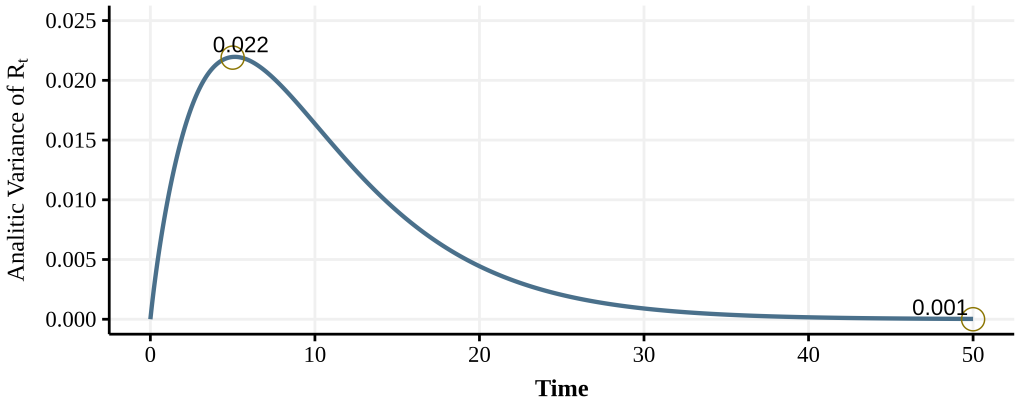

Fig. 4.3 Evolution of variance of R_t process.

Remark 2. *From Chebyshev inequality (Saw et al. (1984))*

$$\mathbb{P}(|R_t - m(t,r)| \geq t^{-\alpha}) \leq t^{2\alpha} Var(R_t), \tag{4.34}$$

for all $\alpha > 0$. *As* t *tends to infinity, equations* (4.17), (4.31), *and* (4.33) *give*

$$\mathbb{P}(|R_t - 1| \geq t^{-\alpha}) \leq 2(1-r)e^{-\mu_{v_0} t} t^{2\alpha} \to 0, \tag{4.35}$$

and therefore, the process R_t *converge in probability.*

4.3.3 Characteristic function of R_t

This section is devoted to the characteristic function of the process R_t that allows us to understand properties of the distribution the existence of a density function.

Proposition 3. *Let denote the characteristic function of the records process $(R_t)_{t\in\mathbb{R}_+}$ defined in* (4.5) *with initial value (r,ν) as $\varphi_\theta(t,r,\nu)$, then φ satisfies the following differential equation:*

$$\begin{cases} \dfrac{\partial\varphi_\theta}{\partial t}(t,r,\nu) = \lambda_\nu \displaystyle\sum_{j\in K} q_{\nu j} \int_{[0,1]} \Big(e^{i\theta\rho/(1-\rho)}\varphi_\theta(t,r,j)) - \varphi_\theta(t,r,\nu)\Big) G_j(d\rho), \\ \varphi_\theta(0,r,\nu) = \varphi, \end{cases} \tag{4.36}$$

Proof. Let φ the characteristic function of R_t i.e. $\varphi_\theta(t,r,\nu) = \mathbb{E}[e^{i\theta R_t}] = \int_0^\infty e^{i\theta R_t} f(R_t)d(R_t)$. From (4.10) φ is the unique solution of the system of equations

$$\begin{cases} \dfrac{\partial\varphi_\theta}{\partial t}(t,r,\nu) = \lambda_\nu \displaystyle\sum_{j\in K} q_{\nu j} \int_{[0,1]} (\varphi_\theta(t,r+\rho(1-r),j) - \varphi_\theta(t,r,\nu))\, G_j(d\rho), \\ \varphi_\theta(0,r,\nu) = \varphi, \end{cases} \tag{4.37}$$

In particular, we have

$$\varphi_\theta(t,r+(1-r)\rho,j) \;=\; \mathbb{E}\left[e^{i\theta R_t}|R_0 = r+\rho(1-r), \nu_0 = j\right]. \tag{4.38}$$

By Lemma 1, equation (4.38) becomes

$$\begin{aligned} \varphi_\theta(\theta,r+(1-r)\rho,j) &= \mathbb{E}\left[e^{i\theta(R_0+(1-R_0)R_t^0)}|R_0 = r+(1-r)\rho, \nu_0 = j\right] \\ &= e^{i\theta\rho}\mathbb{E}\left[e^{i\theta R_t(1-\rho)}|R_0 = r, \nu_0 = j\right]. \end{aligned} \tag{4.39}$$

By changing variables $\psi = \theta(1-\rho)$, allows us to rewrite (4.39) as

$$\varphi_\psi(\psi,r+(1-r)\rho,j) = e^{i\psi\rho/(1-\rho)}\varphi_\psi(\psi,r,j). \tag{4.40}$$

Now, combining (4.37) and (4.40) we obtain

$$\begin{cases} \dfrac{\partial\varphi_\theta}{\partial t}(t,r,\nu) = \lambda_\nu \displaystyle\sum_{j\in K} q_{\nu j} \int_{[0,1]} \Big(e^{i\theta\rho/(1-\rho)}\varphi_\theta(t,r,j)) - \varphi_\theta(t,r,\nu)\Big) G_j(d\rho), \\ \varphi_\theta(0,r,\nu) = \varphi, \end{cases}$$

from which the desired result (4.36) is obtained. □

4.3.4 Case of one-state

In this section we present the case of a steady state such that $\nu = \nu_0$, which shows the estimates for the one-state case. Let φ the characteristic function of the random variable R_t,

$$\varphi_\theta(t,r,\nu) = \mathbb{E}[e^{i\theta R_t}] = \int_0^\infty e^{i\theta R_t} f(R_t) d(R_t),$$

that has a unique solution for $\varphi_\theta(0,r,\nu) = \varphi$. The unique solution of the system (4.10) for the case of the characteristic equation that of the stochastic process R_t, considering a finite number of states with a starting point $\varphi_\theta(0,r,\nu) = \varphi$ is given by (4.37).

In particular, we have

$$\varphi_\theta(t, r+(1-r)\rho, j) = \mathbb{E}_{(r+(1-r)\rho,j)}\left[e^{i\theta R_t}\right], \tag{4.41}$$

which corresponds to the definition of the characteristic equation for the process R_t for a fixed state j. From Lemma 1, the equation (4.38) we can rewrite it as

$$\begin{aligned}\varphi_\theta(\theta, r+(1-r)\rho, j) &= \mathbb{E}_{(r+(1-r)\rho,j)}\left[e^{i\theta(R_0+(1-R_0)R_t^0)}|R_0 = r+(1-r)\rho, \nu_0 = j\right] \\ &= e^{i\theta\rho}\mathbb{E}\left[e^{i\theta R_t(1-\rho)}|R_0 = r, \nu_0 = j\right].\end{aligned}$$

Using the change of variable formula with $\psi = \theta(1-\rho)$, it allows us to rewrite (4.39) as

$$e^{i\psi\rho/(1-\rho)}\mathbb{E}\left[e^{i\psi R_t}|R_0 = r, \nu_0 = j\right],$$

$$\varphi_\psi(\psi, r+(1-r)\rho, \nu_0) = e^{i\psi\rho/(1-\rho)}\varphi_\psi(\psi, r, \nu_0). \tag{4.42}$$

Then, we can solve the following differential equation, which can be obtained from (4.37) for the case of one state

$$\begin{aligned}\frac{\partial\varphi_\theta}{\partial t}(t,r,\nu_0) &= \int_{[0,1]}\left(e^{i\theta\rho/(1-\rho)}\varphi_\theta(t,r,\nu_0) - \varphi_\theta(t,r,\nu_0)\right)G_j(d\rho), \\ \frac{\partial\varphi_\theta}{\partial t}(t,r,\nu_0) &= \int_{[0,1]}\left(\left(e^{i\theta\rho/(1-\rho)} - 1\right)\varphi_\theta(t,r,\nu_0)\right)G_j(d\rho), \\ \frac{\partial\varphi_\theta}{\partial t}(t,r,\nu_0) &= K\varphi_\theta(t,r,\nu_0),\end{aligned} \tag{4.43}$$

where K is defined as $\int_{[0,1]} \left(e^{i\theta\rho/(1-\rho)} - 1\right) G_j(d\rho)$. Finally,

$$\varphi_\theta(t, r, \nu_0) = \varphi e^{Kt}. \tag{4.44}$$

4.4 Simulation and estimation in the R_t process

In this section we proceed to perform a series of simulations in order to characterise the record phenomenon from an empirical perspective. Secondly, we present the estimation method of the process R_t for different states of the time series. This study allow us to have a concrete tool to generate applications of the stochastic R_t process.

4.4.1 Simulation of R_t process

For simulate the process R_t we will use the approximation made by Thomas Thomas (2019) for PDMP processes. We will use the theoretical development developed in previous section for two-state case to check the simulation against the analytical results. Through this application, we present a methodology that can be used in various areas of science, such as economy (see Chang (2009), Liu and Mumtaz (2011)), pharmacology (see Fermín and Lévy-Véhel (2020)), finance (see, Liu et al. (2012)).

First, we must characterise the changes of state of the process R_t for each of the jumps. Each jump of the process is characterised by a time occurrence and a jump size. Both characteristics are modelled independently by defining a transition matrix Q.

The algorithm is described below for the case when the process R_t has two-state, and the times between jumps has an exponential distribution with parameters λ_i and λ_j. When a new record is reached, the size of the jump has a Beta distribution depending on whether they belong to the ν_i or ν_j state, respectively. The parameters of the corresponding Beta distributons are (α_i, α_j) and (β_i, β_j). The extension to n-states is natural by adding sections referring to the states.

In the algorithm we can identify two cases that we can associate to each of the two states of the process. For both, we simulate the times between jumps and the size of the jump. In addition, a uniform random variable is simulated that allows us to simulate the permanence or exit of the current state in which the process R_t is.

For example, we assume a two-state matrix Q with the coefficients defined in (4.3.1). We further assume the distributions of the times between jumps and the distributions of the jumps expressed in Table 4.1.

Algorithm 3 Simulation of the R_t process for two states

Set the initial values of the process $R_0 = r$ and the initial state ν_0. Define the probabilities of the states of the transition matrix Q. Additionally it sets the time counter k and inicial time t to zero.

while $t \leq T$ **do**
  if $\nu_t = i$ **then**
    Simulate $X \sim Exponential(\lambda_i)$
    Simulate $Y \sim Beta(\alpha_i, \beta_i)$
    Simulate $u \sim Uniform(0,1)$
    if $Q(1,1) > u$ **then**
      $\nu_t = i$
    else
      $\nu_t = j$
    end if
    $t = t + X$
    $R_t = R_{t-k} + Y(1 - R_{t-k})$
    $k = X$
  else
    Simulate $X \sim Exponential(\lambda_j)$
    Simulate $Y \sim Beta(\alpha_j, \beta_j)$
    Simulate $u \sim Uniform(0,1)$
    if $Q(2,1) > u$ **then**
      $\nu_t = i$
    else
      $\nu_t = j$
    end if
    $t = t + X$
    $R_t = R_{t-k} + Y(1 - R_{t-k})$
    $k = X$
  end if
end while

Figure 4.4a shows a set of sample paths simulations to illustrate the behaviour of the process over time, considering the characteristics of the states presented above.

Similarly, figure 4.4b shows the 10,000 sample path simulation, where the dotted line corresponds to the 5th and 95th percentiles, respectively. Through this procedure we can estimate the expected value and variance of the R_t process by means of a simulation analysis.

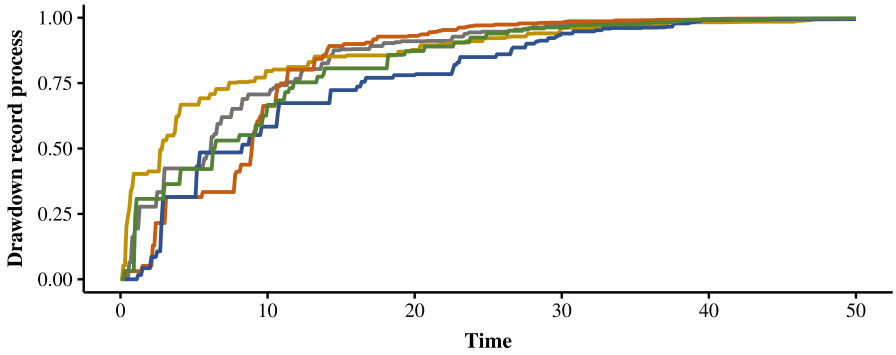

(a) Sample path of R_t process, starting in $R_0 = 0$.

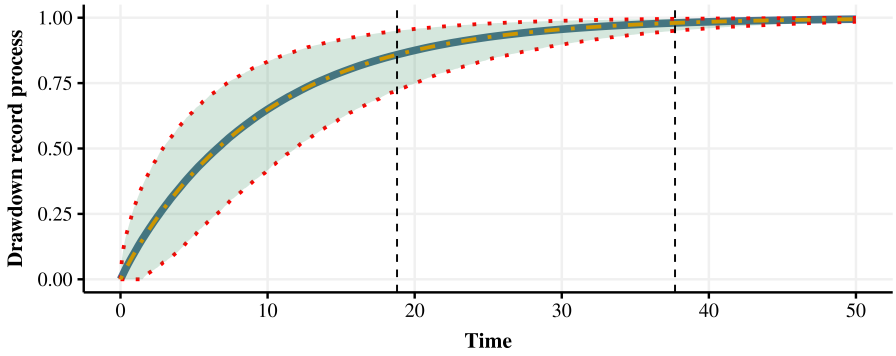

(b) Sample paths (5) of R_t process, 10000 simulations, starting in $R_0 = 0$.

Fig. 4.4 Sample path of R_t process for a sample of 10 simulate paths and a large sample of 10,000 simulate paths.

We can observe that, for this parameterisation, after time 10 approximately 90% of the paths exceed the value of 0.5, after time 20 approximately 95% of them exceed the value of 0.75, and after time 40 approximately 95% of the paths have a difference less than 0.02 at the limit 1.

On the other hand, the greatest variability of the trajectories can be observed between time 5 and 10, observing the convergence of the trajectories as time grows as shown in figure 4.4b.

To verify the efficiency of the simulation process, a dot-dashed line corresponding to the analytical mean calculated for those process parameters R_t is placed in the figure. We can see that the computational approximation of the process is very similar to the one obtained through the analytical solution.

This approach makes it possible to characterise the evolution of the main statistics of the R_t process numerically, providing a quick and simple tool for understanding the evolution of the phenomenon.

Figure 4.5a shows the evolution of the variance of 10000 simulations of R_t process, observing a convergence to zero that follows an exponential behaviour, as described in the previous sections.

Similar to Figure 4.4b, the analytical solution of the variance by means of a dot-dashed line has been used to show the efficiency of the computational process. Like the mean, the computationally estimated variance is similar to the analytically estimated variance.

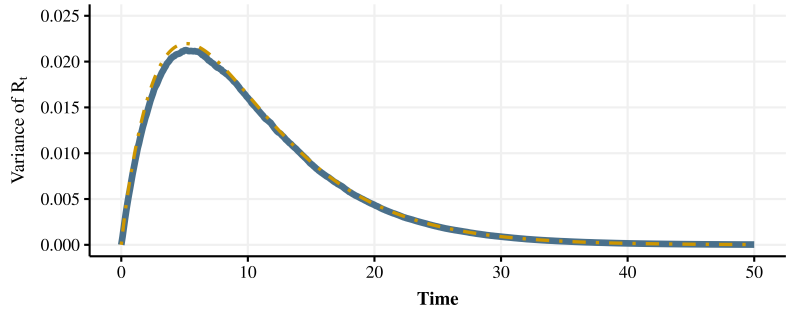

(a) Estimated variance of R_t process, 10000 simulations

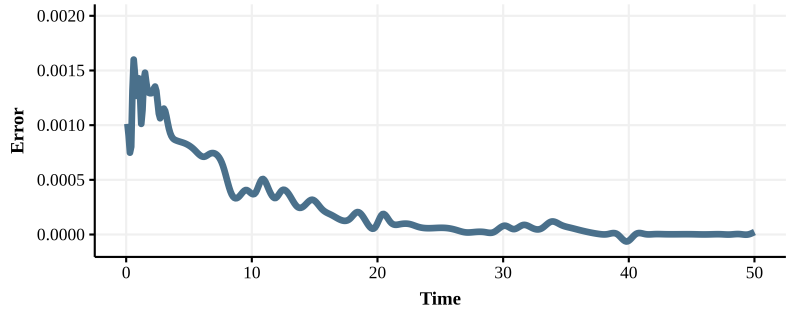

(b) Error between analytical variance and simulated process of R_t process

Fig. 4.5 Analytical and simulated variance and the error in its estimation of R_t process

In this sense, we can study the evolution of the probability density of the process R_t having a given value, as a function of time. Figures 4.6a, 4.6b, and 4.6c show the plots of the

densities of the process R_t evolves over time, showing three specific periods. The axis named density shows the relative frequency of the values taken by the R_t process for that specific time period, considering 10,000 simulated paths in the experiment.

We can observe that the variance is decreasing as time passes and the limit would be the delta function, when we consider sufficiently long time periods. The time it takes to evolve to a degenerate distribution allows to generate applications on the behaviour of the process useful for different areas of science.

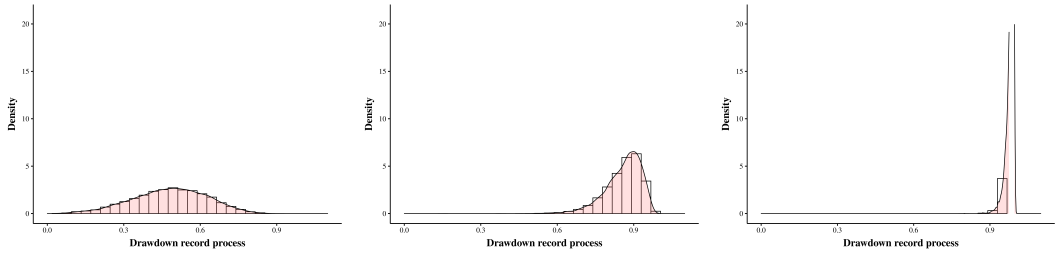

(a) Density at $T = 10$ (b) Density at $T = 20$ (c) Density at $T = 30$

Fig. 4.6 R_t process densities over time

4.4.2 Numerical approximation of the Characteristic function

From the generation of a large number of trajectories of the process R_t we can obtain the evolution of the characteristic function ($\varphi_\theta = E[e^{i\theta R_t}]$). The Figure 4.7 shows the evolution over time of the characteristic function. It can be seen that as the time of the process increases, the process becomes closer to a unit root circle, which is consistent with the characteristic function of a constant. This plot is also consistent with Figure 4.6c, showing that the limit would be the delta function, as t increase, results obtained in the previous sections on the asymptotic behavior of the R_t process.

Finally, Figures 4.8a and 4.8b show the decomposition of the process into the real and imaginary part, which converge to cosine and sine functions of amplitude one, representing the unit circle. It is worth remembering that the characteristic function associated with a constant is precisely a unit circle, as is the case here.

4.4.3 Estimation of the parameters of PDMP - R_t process

Several studies have developed estimation techniques for PDMP processes. Among which we can mention Chiquet et al. (2009), where the authors investigate some methods to estimate the parameters of the dynamical system, involving maximum likelihood estimation for the

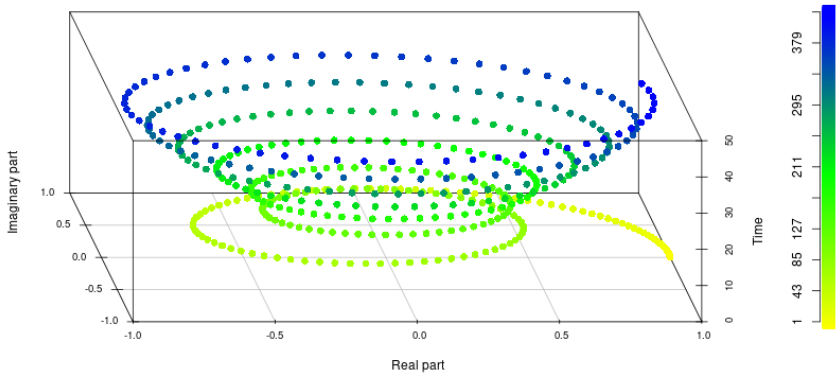

Fig. 4.7 Evolution of characteristic function φ_θ with $10,000$ simulations.

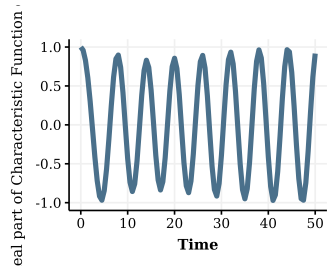

(a) Real part of φ_θ, 10000 simulations.

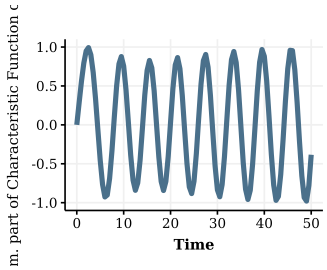

(b) Imaginary part of φ_θ, 10000 simulations.

infinitesimal generator of the underlying jump Markov process. In this article we present an estimation based on the maximum likelihood principles and distributions on jumps size of the R_t process.

Algorithm 4 shows the way to estimate the parameters of a PDMP - R_t process. Based on a specific state, the algorithm estimates the time distribution between jumps and the jump size distribution. We define the function $Par_{exp}(\cdot)$ that allows us to calculate the parameters of the exponential distribution of the vector x_i, x_j, respectively. Finally, $Par_{beta}(\cdot)$ allows us to calculate the parameters of the Beta distribution of the vector y_i, and y_j, respectively.

We define the function $Like(\cdot)$ that allows us to calculate the maximum likelihood, considering the parameters of (x_i, y_i), and of (x_j, y_j) jointly, obtaining the vector $Likelilihood_i$, and $Likelilihood_j$. Based on the above calculations. At the end, we define dif which will be a criterion for the convergence of the algorithm.

Once the distributions have been estimated and the labels of the specific state to which it belongs have been assigned, it is necessary to estimate the transition matrix Q. This estimation of the transition matrix will input a new estimation process, repeating the process until it converges.

Algorithm 4 Estimation of the states in the PDMP- R_t process with two states

Set the initial values of the labels of states of process R_t and the initial state ν_0. Define a guess of the probabilities of the states of the transition matrix Q and initial value $Likelihood_0$. Set a δ value for measure de convergence of algorithm and a value inicial $dif > \delta$ to start the iterative process. Additionally it sets the time counter k and inicial time t to zero and $s = 1$, $g = 1$, $r = 1$.

while $dif \geq \delta$ **do**
  while $t \leq T$ **do**
    if $E_r = i$ **then**
      $x_{i,s} = x_r$
      $y_{i,s} = y_r$
      $s = s + 1$
    else
      $x_{j,g} = x_r$
      $y_{j,g} = y_r$
      $g = g + 1$
    end if
    $t = t + x_r$
    $r = r + 1$
  end while
  $Likelihood_i = Like(Par_{exp}(x_i), Par_{beta}(y_i), x, y)$
  $Likelihood_j = Like(Par_{exp}(x_j), Par_{beta}(y_j), x, y)$
  $dif = Likelihood_0 - \left(\sum(Likelihood_i) + \sum(Likelihood_j)\right)$
  $Likelihood_0 = \sum(Likelihood_i) + \sum(Likelihood_j)$
end while

The first cycle generates the new classification of the labels, given the maximum likelihood calculations defined in Algorithm 4. The second cycle allows the estimation of the state matrix Q (Algorithm 5). Consider that the algorithm can be repeated until there are no variations of the state matrices and the calculated likelihoods.

Algorithm 5 Estimation of the transition matrix with two states

Set the initial values of the labels of states of process R_t and the initial state v_0. Define a guess of the probabilities of the states of the transition matrix Q and initial value $Likelihood_0$. Set a δ value for measure de convergence of algorithm and a value inicial $dif > \delta$ to start the iterative process. Additionally it sets the time counter k and inicial time t to zero and $s = 1$, $g = 1$, $r = 1$.

for $r = 1 : R$ **do**
  if $Likelihood_{i,r} > Likelihood_{j,r}$ **then**
    $E_r = i$
  else
    $E_r = j$
  end if
end for
for $r = 1 : R$ **do**
  if $E_r = i$ **then**
    $C_i = C_i + 1$
    if $E_{r+1} = i$ **then**
      $C_{i,i} = C_{i,i} + 1$
    end if
  else
    $C_j = C_j + 1$
    if $E_{r+1} = j$ **then**
      $C_{j,j} = C_{j,j} + 1$
    end if
  end if
end for
$Q_{i,i} = C_{i,i}/C_i$
$Q_{j,j} = C_{j,j}/C_j$
$Q_{i,j} = 1 - Q_{i,i}$
$Q_{j,i} = 1 - Q_{j,j}$

4.5 Financial applications

Within the strategies for managing financial risk, fund managers typically follow a set of rules that define the behaviour of investments in the face of events that structure financial market prices Leal and de Melo Mendes (2005), Power (2004), Zhang (2009).

One of the strategies for financial risk management corresponds to regulating the maximum losses occurring in a fixed time horizon or *Drawdown*. Because risk levels are dynamic, the incentive structure of managers in the face of the new *Drawdown* also changes Pospisil and Vecer (2010), leading to changes in investment decisions.

The strategies associated with the drawdown of a financial asset as a basic element for risk management generate a direct link between the price structure of financial assets with the statistical theory of extreme values, more specifically with the theory of records Embrechts et al. (2013), Gomes and Guillou (2015), assuming that the financial information of the financial asset is public knowledge for all members of the capital market.

By using various tools we can understand the evolution of the stochastic process that governs the sequence of jumps that define the drawdown. Markov chains are a fundamental tool for understanding the evolution of financial series, which have been widely used in the economic and financial literature Cui et al. (2018, 2019), Mendoza-Arriaga and Linetsky (2016).

Figure 4.9 shows the evolution of the S&P500 index which represents the 500 most traded companies on the New York Stock Exchange from 1 January 1950 to 31 December 2019, public data extracted from https://finance.yahoo.com/. The S&P500 is used as a proxy indicator for economic performance, which assumes that there is full transparency in the investment positions of each economic agent.

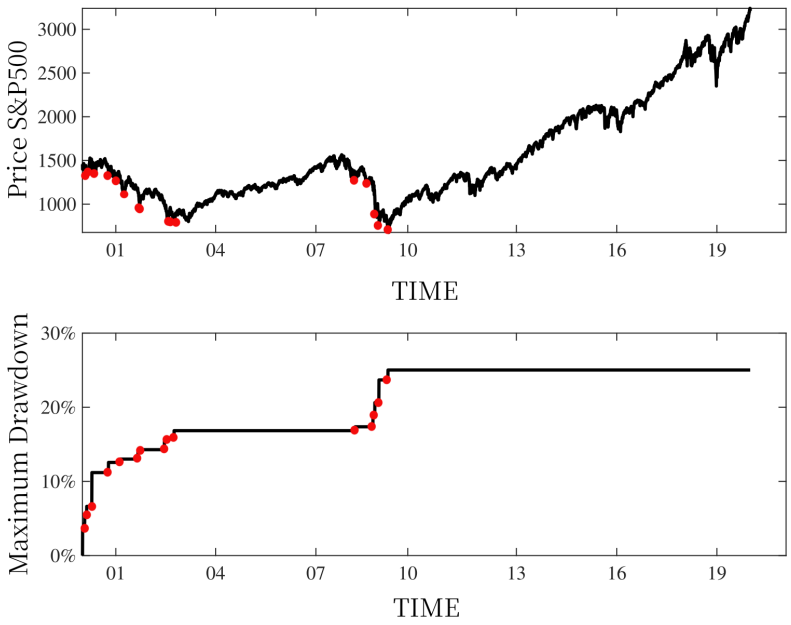

Fig. 4.9 S&P500 index and Maximum Drawdown.

When analysing the figure 4.9, we can observe periods of time in which the observation of a new record is more recurrent, while in other periods the frequency of new records is lower. The red circles highlight the moment at which a new record is set. The lower time series shows the value of the record for a period t, and the size of the jump corresponds to the difference of the record with the immediately preceding period. This suggests the existence of at least 2 different states of nature to observe a new record in this time series.

Using the Algorithms 3 and 4 on the data obtained from the drawdown process for the S&P500 time series showing the evolution of records, we have the following results: which

	Distribution	
	$\nu_t = i$	$\nu_t = j$
$X \sim$	$Exponential(0.47)$	$Exponential(5.4 \times 10^{-4})$
$\mathbb{E}[X] =$	2.095	1819
$\rho \sim$	$Beta(1.83, 145.90)$	$Beta(0.77, 47.86)$
$\mathbb{E}[\rho] =$	0.012	0.015

Table 4.2 Parameter Inference of the S&P500 -R_t process.

represent the parameter values of the estimated distributions for each of the two states present in the R_t process. In addition, by means of Algorithm xxx we can estimate the transition matrix Q. These results allow us to estimate the long-term behaviour of the time series shown in Figure 4.10 and 4.11.

$$Q = \begin{bmatrix} q_{1,1} & q_{1,2} \\ q_{2,1} & q_{2,2} \end{bmatrix} = \begin{bmatrix} 0.883 & 0.117 \\ 0.750 & 0.250 \end{bmatrix}, \tag{4.45}$$

With all the parameters obtained according to Algorithms 2 and 3 we can numerically calculate the mean and the variance of the estimated processes which we will call $\hat{R}_r$. In figures 4.10 and 4.11 we show the estimation of the mean and variance of the S&P500 - R_t process.

The time axis is being measured in days, therefore every $50,000$ observations corresponds to approximately 200 years, which means that observing financial crises that reach loss rates greater than 80% would be reached in 200 years on average and the maximum variability is reached at around $30,000$ periods, approximately 120 years.

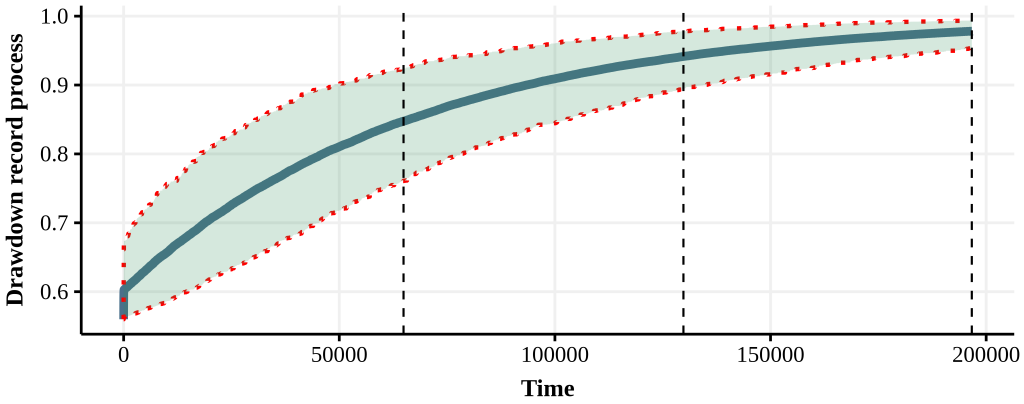

Fig. 4.10 Sample path of $\hat{R}_t$ process, 10000 simulations

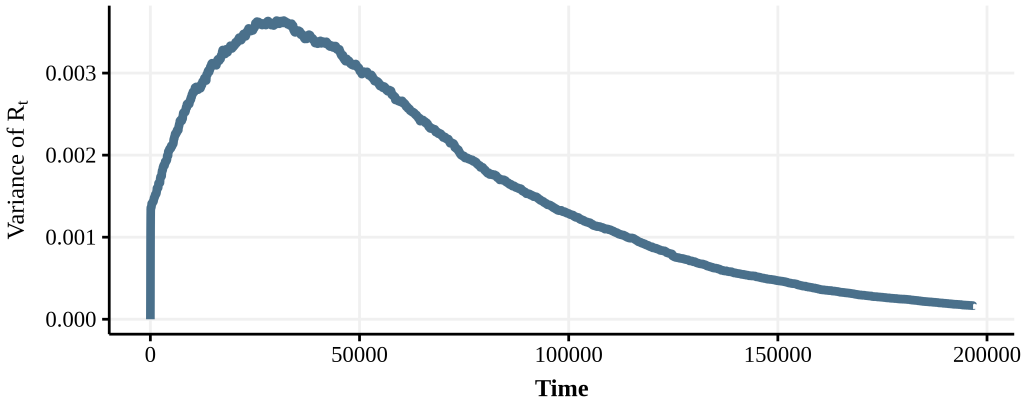

Fig. 4.11 Variance of $\hat{R}_t$ process, 10000 simulations

4.6 Conclusions

This paper developed an analysis of a record process, based on a Piecewise Deterministic Markov process, in which a finite number of states are considered and which has many applications in different areas of science.

We link PDMP processes with record theory for the process known as Drawdown, in which the maximum observed drop for a time t can be identified.

It was possible to define the characteristics that drive the Drawdown process, such as the mean, variance, and characteristic function, which provides analytical tools for defining the characteristics of the limit process, generating concrete possibilities for building applications that can be used in various areas of science.

In addition, computational estimation techniques were developed, allowing the estimation of the parameters governing a given time series, such as jump occurrence times, process jump sizes, and the state matrix, which makes it possible to simulate processes and build useful applications.

The expected future work includes the application of a generalisation of this work, considering Mittag-Leffler type distributions as the distribution of the time between jumps, which requires modifying the differential operators. In addition to considering modifications to the process, such as the possibility of the jump range being greater than one, which has other theoretical and practical implications.

Chapter 5

Meteorological and air pollution factors on SARS-COV-2 transmission: The case of Southern Regions in Chile

Abstract

There are several determinants of a population's health, including meteorological factors and air pollution. For example, it is well known that low temperatures and air pollution increase mortality rates in infant and elderly populations. With the emergence of SARS-COV-2, it is important to understand what factors contribute to its mitigation and control. There is some research in this area which shows scientific evidence on the virus's behavior in the face of these variables. This research aims to quantify the impact of climatic factors and environmental pollution on SARS-COV-2 specifically the effect on the number of new infections in different areas of Chile. At the local level, historical information available from the Department of Statistics and Health Information, the Chilean National Air Quality Information System, the Chilean Meteorological Directorate, and other databases will allow the generation of panel data suitable for the analysis. The results show the significant effect of pollution and climate variables measured in lags and will allow us to explain the behavior of the pandemic by identifying the relevant factors affecting health, using heteroskedastic models, which in turn will serve as a contribution to the generation of more effective and timely public policies for the control of the pandemic.

5.1 Introduction

Since the 2009 influenza pandemic, countries have improved and strengthened their surveillance and monitoring systems to contribute to timely health decision-making Sosa et al. (2017). In this regard, several endogenous and exogenous conditions affect the population's health. In particular, there is evidence that extreme temperatures are important health risks Basu and Samet (2002), Martens (1998), Näyhä (2005), Ren et al. (2006), Tanis and Karakaya (2021), the most studied being increased mortality due to low temperatures. On the other hand, air pollution is associated with a number of harmful effects on human health Andrée (2020), Bell et al. (2004), Samet et al. (2000), Zhang et al. (2020), Zhu et al. (2020).

Given the emergence of SARS-COV-2, it is relevant to understand what factors contribute to its mitigation and control. The main routes of transmission of the virus was person to

person through respiratory droplets, contaminated hands or surfaces Noorimotlagh et al. (2021b). To date, there is no scientific evidence in Chile on the behavior of this virus in the presence of environmental contamination. Worldwide, some studies in this area Coker et al. (2020), Gupta et al. (2021), Karan et al. (2020), Lolli et al. (2020), Xu et al. (2020), Zhang et al. (2020), Zhao et al. (2021) show scientific evidence on SARS-COV-2's behavior in the presence of these variables. Studies have shown that increased pollutant concentrations are associated with a higher daily incidence of SARS-COV-2 and an increased mortality rate Contini and Costabile (2020), Domingo and Rovira (2020), Maleki et al. (2021), Noorimotlagh et al. (2021a).

In recent years, air pollution in some areas of Chile has reached high levels, and several cities in the country have been declared saturated. In southern Chile, the main heating source used in more than 80% of homes is firewood, although, at the national level, only 33.2% of homes use it. Fifty-two percent of Chileans consider the combustion of firewood to be the worst pollutant according to the Third National Environmental Survey Enc (2018), and it is the main source of pollution due to the emission of particulate matter (PM) it generates.

In this context, the State of Chile has implemented a public program to mitigate atmospheric pollution called Atmospheric Decontamination Plans Dec (2022), environmental management instruments that, through the definition and implementation of specific measures and actions, seek to reduce the levels of atmospheric pollution to protect the health of the population.

On the other hand, meteorological factors also affect people's health. The effects of climatic variables on health is an area of knowledge that has been widely discussed Ahmadi et al. (2020), Auler et al. (2020), Bashir et al. (2020), mainly the increase in mortality caused by changes in temperature due to circulatory and respiratory diseases. Different studies Bertollini et al. (1996), Díez (1996) show that extreme temperatures are related to increased mortality rates.

In the Chilean southern there is a heterogenity of climantes ranges from temperate climates to polar. Precipitations can reach 5,000 mm per year, as a consequence of low pressures due to low pressures coming from the south pole Biblioteca del Congreso Nacional de Chile (2022). The average temperature in 2020 presented normal conditions in the southern part of the country, in cities such as Concepción, Puerto Montt and Punta Arenas the annual average temperature was 13.4 °C, 10.7 °C, and 7 °C, respectively (Figure 1). On the other hand, the total water fall was characterized by deficits in most of the area, reaching in cities such as Concepción, Puerto Montt and Punta Arenas, a total water fall of 808.8, 1352.0 and 299.6 millimeters per year (Figure 2) Dirección Meteorológica de Chile. Dirección General de Aeronáutica Civil (DGAC) (2022).

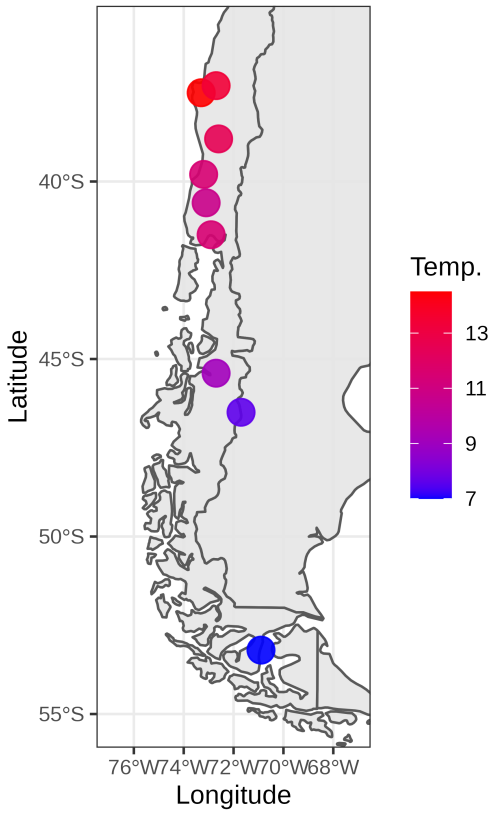

Fig. 5.1 Average Temperature in 2020.

Investigating the relationship between meteorological factors and environmental pollution with SARS-COV-2 is of utmost importance, given the lack of evidence in this regard. At the local level, it allows us to identify both the effects and the dynamics of the pandemic in highly polluted areas. It will also allow forecasts to be made for temperature increases, decreases, or climate change scenarios.

Other factors that can affect virus transmission include culture, family and housing structure, and other variables such as vaccination Ganslmeier et al. (2021), Poirier et al. (2020), Sahoo et al. (2020), GDP per capita, healthcare expenditures, strategies of pandemic management Coccia (2021b) that is, the effect of coronavirus on people's health depends on many economic, social and environmental variables Coccia (2020a, 2021c,d), Qiu et al. (2020), Sabat et al. (2020).

This research aims to quantify the impact of meteorological factors and environmental pollution on the respiratory disease SARS-COV-2 using a heteroskedastic linear regression model. Specifically, the effect on the number of new infections, the number of daily deaths in the different areas of Chile studied, and the pandemic's behavior concerning meteorological

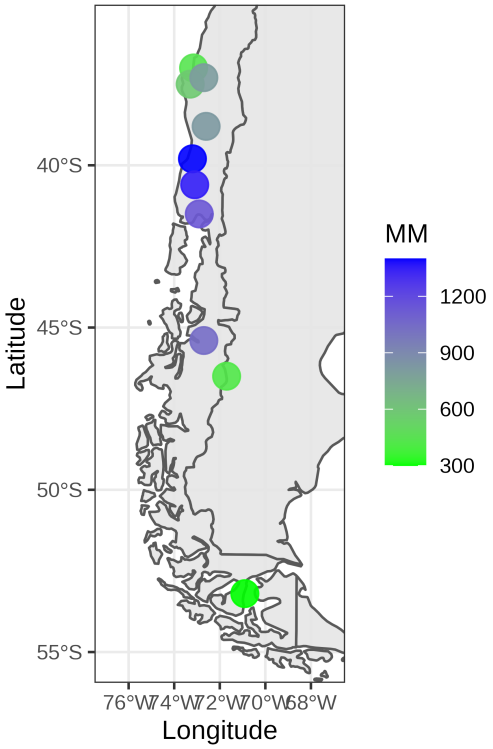

Fig. 5.2 Weather fall (mm) during 2020.

and environmental conditions. Furthermore, this study aims to help provide decision-makers with tools to improve their ability to react.

5.2 Materials and Methods

This study uses different data sources. First, the Air Quality Measurements data panel obtained from the National Air Quality Information System website SIN (2022) from March 2020 to October 2021 when most of the population had already been inoculated. In particular, information on daily concentrations ($\mu g/m^3$) of PM10 and PM2.5 from different monitoring stations located throughout the country is used. The study is carried out in six areas in southern Chile. In total, a network of approximately 60 monitoring stations is used throughout the country, those described in Table 5.1.

Secondly, the panel of meteorological data on temperature (degrees $^{\circ}C$) and rainfall (mm), obtained from the same monitoring stations or, if the information is not available, from the

Region	Municipality	Health Centre
Del Bíobío	Coronel	Hospital San José (Coronel), SAPU Lagunillas, Sapu Yobilo
	Curanilahue	Hospital Provincial Dr. Rafael Avaría (Curanilahue), SAPU Eleuterio Ramírez
	Los Ángeles	Complejo Asistencial Dr. Víctor Ríos Ruíz (Los Angeles), SAPU Paillihue, SAR Norte,
		SAR Entre Ríos, SAPU Dos de Septiembre, SAPU Nororiente, SAPU Nuevo Horizonte, SUR Santa Fe
	Laja	Hospital de Laja
	Nacimiento	Hospital de Nacimiento
De La Araucanía	Temuco	SAPU Santa Rosa, SAR Miraflores, SAPU Amanecer, SAPU Pueblo Nuevo, SAPU Villa Alegre,
		SAR Labranza, SAR Pedro de Valdivia, Hospital Dr. Hernán Henríquez Aravena (Temuco)
	Padre Las Casas	SAPU Padre Las Casas, SAPU Pulmahue, Hospital Makewe, SAR Conun Huenu, Complejo Asistencial Padre Las Casas
De Los Ríos	Valdivia	Hospital Clínico Regional (Valdivia), SAPU Las Animas, SAPU Gil de Castro, SAPU Angachilla, SAR Barrios Bajos, SAPU Niebla
	La Unión	Hospital Juan Morey (La Unión), SAR La Unión
De Los Lagos	Puerto Montt	SAPU Angelmó, SAPU Antonio Varas, SAPU Padre Hurtado, SAR Alerce, SAPU Carmela Carvajal, Hospital de Puerto Montt
	Osorno	Hospital Base de Osorno, SAPU Dr. Pedro Jáuregui, SAPU Rahue Alto, SAPU Dr. Marcelo Lopetegui Adams
De Aisén del Gral. C. Ibáñez del Campo	Coihaique	Hospital regional Coihaique, SAPU Dr. Alejandro Gutiérrez
	Aisén	Hospital de Puerto Aisén
	Cisnes	Hospital Dr. Jorge Ibar (Cisnes)
	Cochrane	Hospital Lord Cochrane
	Chile Chico	Hospital Dr. Leopoldo Ortega R. (Chile Chico)
De Magallanes y de La Antártica Chilena	Punta Arenas	Hospital D. Lautaro Navarro Avaria (Punta Arenas), SAPU Dr. Mateo Bencur, SAPU Dr. Juan Damianovic, SAPU 18 de Septiembre
	Cabo de Hornos	Hospital Comunitario Cristina Calderón de Puerto Williams
	Porvenir	Hospital Dr. Marco Antonio Chamorro (Porvenir)

Table 5.1 Health center locations by municipality and region.

Chilean Meteorological Directorate. The geographical location is shown in Figures 5.1 and 5.2.

The number of medical visits by cause and week is obtained from the Department of Health Statistics and Information DEI (2022). The data contained weekly statistical information for each of the public health centers. Finally, the health centers used here are Hospitals, Emergency Primary Care Service (SAPU) or High Resolution Primary Emergency Care Service (SAR).

Statistical Model

In this section we show the statistical model in its functional form, which we use to study the relationship between pollutants, meteorological variables and SARS-COV-2 incidence:

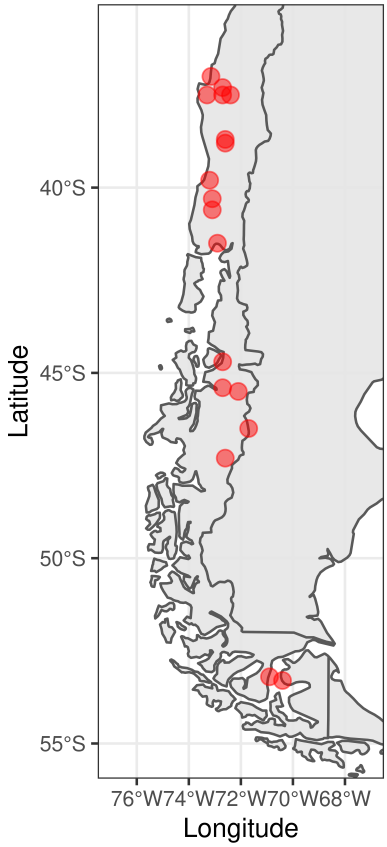

Fig. 5.3 Weather and pollutant monitoring stations.

$$y_{it} = f(MP10_{it}, L1(MP10_{it}), L2(MP10_{it}), MP2.5_{it}, L1(MP2.5_{it}), \\ L2(MP2.5_{it}), T_{it}, L1(T_{it}), L2(T_{it}), Pre_{it}, L1(Pre_{it}), L2(Pre_{it})), \quad (5.1)$$

where y_{it} corresponds to the number of new confirmed SARS-COV-2 cases, at health center i at week t; $MP10_{it}$ corresponds to the daily concentrations ($\mu g/m^3$) of PM10, at health center i, during week t; $MP2.5_{it}$ corresponds to the daily concentrations ($\mu g/m^3$) of PM2.5, at health center i at week t; T_{it} corresponds to the average ambient temperature ($^{\circ}C$) at health facility i at week t; Pre_{it} corresponds to the precipitation at health center i at week t. All the variables described are sampled in one week. Finally, L1 and L2 correspond to variables with a lag of one week and two weeks respectively.

From Equation 5.1, the following statistical models are established as a response of the dependent variable y_{it} in terms of the explanatory variables. The statistical model of Equation 5.2 corresponds to a fixed-effects model with the assumption of heteroscedasticity, where we can identify the specific factor of the week (τ_t) and of the corresponding health center for which the information for the modeling is obtained (v_i). The model is controlled by

an appropriate characterization of the model variance expressed in the Equation 5.3, using Harvey's two-step generalized least squares method Altonji and Segal (1996), Clark (1996), Greene (2018), Harvey (1976). The two-step generalized least squares method is more efficient when the correct specification of the mean and variance is not known, as in this case.

$$\begin{aligned} y_{it} = \beta_0 + \beta_1 MP10_{it} + \beta_2 L1(MP10_{it}) + \beta_3 L2(MP10_{it}) + \beta_4 MP2.5_{it} + \\ \beta_5 L1(MP2.5_{it}) + \beta_6 L2(MP2.5_{it}) + \beta_7 T_{it} + \beta_8 L1(T_{it}) + \beta_9 L2(T_{it}) + \\ \beta_{10} Pre_{it} + \beta_{11} L1(Pre_{it}) + \beta_{12} L2(Pre_{it}) + \nu_i + \tau_t + \varepsilon_{it}, \quad (5.2) \end{aligned}$$

$$\begin{aligned} \sigma_{it}^2 = \exp(\alpha_0 + \alpha_1 MP10_{it} + \alpha_2 L1(MP10_{it}) + \alpha_3 L2(MP10_{it}) + \alpha_4 MP2.5_{it} + \\ \alpha_5 L1(MP2.5_{it}) + \alpha_6 L2(MP2.5_{it}) + \beta_7 T_{it} + \alpha_8 L1(T_{it}) + \beta_9 L2(T_{it}) + \\ \alpha_{10} Pre_{it} + \alpha_{11} L1(Pre_{it}) + \alpha_{12} L2(Pre_{it}) + \delta_i + \rho_t), \quad (5.3) \end{aligned}$$

$$\varepsilon_{it} \sim N(0, \sigma_{it}^2); Cov(\varepsilon_{it}, \varepsilon_{j,s}) = 0; i \neq j; t \neq s. \quad (5.4)$$

A model that controls for heteroscedasticity has been used for this research, because a high variability of the response of geographical areas is to be expected due to region-specific socio-economic and political differences. In addition, the non-linearity of the environmental pollution variables that may be involved in the behaviour of the variance is not clear. This type of model allows us to control for heteroscedasticity effects and provides a flexible tool for the proper modelling of the data.

5.3 Results

The first statistical model is called Model 1 and considers the following explanatory variables: (i) MP2.5; (ii) L1(MP2.5); (iii) L2(MP2.5); (iv) MP10; (v) L1(MP10); (vi) L2(MP10). The second, is called Model 2 and considers in addition to the explanatory variables of Model 1 the following variables: (vii) T; (viii) L1(T); (ix) L2(T); (x) Pre; (xi) L1(Pre); (xii) L2(Pre). For both models, the health centers and the respective week are considered as fixed effects. These two models are presented as alternatives, where the second model

considers meteorological variables as a control, allowing comparison with other models presented in recent literature. The fundamental reason for exposing these two models is that meteorological information is not available for all localities that have health centres, so a robustness analysis is required to validate the effects of the environmental pollution variables.

Table 5.2 shows the ordinary linear regression (OLS) analysis of Models 1 and 2. For both models, it is observed that the variables of interest are not significant, although the coefficient of determination (R^2) shows values 0.5913 for Model 1 and 0.572 for Model 2, which represents the proportion of the variance that we are able to explain by OLS models.

Observing a relatively high R^2, a high F-statistic, but no significance of any of the variables for the two models, gives us signs that we have some problems with the modelling of the phenomenon. We analyze the heteroscedasticity effect of the study variables. For this, the Breusch-Pagan test which has a χ^2 distribution, is applied to evaluate the heteroscedasticity effect in the linear regression model. Rejection of the null hypothesis implies that the homoscedasticity hypothesis is rejected and therefore a model that controls for variance is preferred. It can be observed that the null hypothesis of non-heteroscedasticity for both models is rejected. Therefore, the model must consider the effect that the variables may have on the variance of the linear model. Table 5.3 shows linear regression considering the effects of heteroscedasticity on Models 1 and 2, respectively. The same variables in Models 1 and 2 without heteroscedasticity are considered.

The likelihood ratio test for $\log(\sigma^2) = 0$ presented in Table 5.3 which is distributed χ^2, indicates that the null hypothesis that the variance is constant is rejected, therefore, the model that considers heteroscedasticity is appropriate for both models.

Finally, based on the Breush-Pagan test and and the constant variance test presented in Table 5.2 and 5.3 respectively, we conclude that it is better to consider the model that considers heteroscedasticity than an ordinary linear model (OLS).

The analysis of the model considering heteroscedasticity shows that the pollution variables MP2.5, L2(MP2.5), MP10, and L2(MP10) are significant for both models.

For the case of Model 2, the variables L1(T) and L2(T) are also significant. The variables MP2.5, L1(MP2.5), and MP10 are significant in the variance modeling for Model 1, while for Model 2, the variables MP10, and L1(T) are significant.

5.4 Discussion

In the present study, the potential effects of meteorological variables and air pollution on the incidence of SARS-COV-2 are preliminary evaluated, since the arrival of the virus in Chile, week by week, from march 2020 to october 2021. Chile is located in the southern

		Lineal Regresion	
Variable	OLS Estimator	Model 1	Model 2
MP2.5	$\hat{\beta_1}$	0.002796 ns	0.0030147 ns
L1(MP2.5)	$\hat{\beta_2}$	-0.000096 ns	-0.0005504 ns
L2(MP2.5)	$\hat{\beta_3}$	-0.000715 ns	-0.0009616 ns
MP10	$\hat{\beta_4}$	-0.001568 ns	-0.0017679 ns
L1(MP10)	$\hat{\beta_5}$	0.0003358 ns	0.0002483 ns
L2(MP10)	$\hat{\beta_6}$	0.001201 ns	0.0012701 ns
T	$\hat{\beta_7}$		-0.0034373 ns
L1(T)	$\hat{\beta_8}$		-0.0321138 ns
L2(T)	$\hat{\beta_9}$		-0.0298265 ns
Pre	$\hat{\beta_{10}}$		-2.13e-43 ns
L1(Pre)	$\hat{\beta_{11}}$		3.02e-44 ns
L2(Pre)	$\hat{\beta_{12}}$		-1.14e-43 ns
Constant		4.39259***	5.80982***
N		2343	2008
Week		Fixed	Fixed
Center		Fixed	Fixed
R^2		0.5913	0.5720
F-statistic		25.88	21.01
Breusch–Pagan test			
$\chi^2(1)$		2282.29	2062.60
Prob> χ^2		< 0.001	< 0.001

* $p < 0.10$, ** $p < 0.05$, *** $p < 0.01$, ns=non-significant

Table 5.2 Parameter estimate and significance level.

		Lineal Regresion		$\log(\sigma^2)$	
Variable	Estimators	Model 1	Model 2	Model 1	Model 2
MP2.5	$\hat{\beta_1}$ and $\hat{\alpha_1}$	0.00191**	0.00238**	0.00996*	0.00837 ns
L1(MP2.5)	$\hat{\beta_2}$ and $\hat{\alpha_2}$	0.000269 ns	-0.000363 ns	-0.0110*	-0.00716 ns
L2(MP2.5)	$\hat{\beta_3}$ and $\hat{\alpha_3}$	-0.00192**	-0.00188*	-0.00117 ns	-0.000835 ns
MP10	$\hat{\beta_4}$ and $\hat{\alpha_4}$	-0.00129*	-0.00176**	-0.00878*	-0.0102**
L1(MP10)	$\hat{\beta_5}$ and $\hat{\alpha_5}$	0.000467 ns	0.00104 ns	0.00527 ns	0.00396 ns
L2(MP10)	$\hat{\beta_6}$ and $\hat{\alpha_6}$	0.00205**	0.00174**	-0.00114 ns	0.00241 ns
T	$\hat{\beta_7}$ and $\hat{\alpha_7}$		0.00308 ns		-0.0358 ns
L1(T)	$\hat{\beta_8}$ and $\hat{\alpha_8}$		-0.0201**		-0.0124 ns
L2(T)	$\hat{\beta_9}$ and $\hat{\alpha_9}$		-0.0271***		-0.0765*
Pre	$\hat{\beta_{10}}$ and $\hat{\alpha_{10}}$		-1.06e-43 ns		2.12e-43 ns
L1(Pre)	$\hat{\beta_{11}}$ and $\hat{\alpha_{11}}$		-8.76e-44 ns		-3.08e-43 ns
L2(Pre)	$\hat{\beta_{12}}$ and $\hat{\alpha_{12}}$		-1.05e-43 ns		4.08e-43 ns
Constant		4.673***	5.700***	3.571***	6.250***
N		2343	2008	—	—
Week		Fixed	Fixed	Fixed	Fixed
Center		Fixed	Fixed	Fixed	Fixed
Likelihood Ratio Test for $\log(\sigma^2) = 0$					
χ^2		1165.12	991.62	-	-
Prob> χ^2		< 0.001	< 0.001	-	-

* $p < 0.10$, ** $p < 0.05$, *** $p < 0.01$, ns=non-significant

Table 5.3 Parameter estimate and significance level of the regression considering heteroscedasticity.

hemisphere, and present relevant meteorological differences when compared to Europe and Asia.

In general, based on data from in six regions in southern Chile, our results show that new cases of SARS-COV-2 have a strong association with temperature and air pollution. In addition, the results show the lagged effects of temperature and pollution variables affecting the temporal dynamics of SARS-COV-2 cases.

In particular, the results of the model considering heteroscedasticity show that low temperatures affect the incidence of new infections in the subsequent weeks, which may be due to the incubation period of the virus. Precipitation is not shown to be related to the disease. Other studies have similar conclusions about the seasonality of coronavirus infections, showing a negative association between temperature and virus incidence, that is, low temperatures are associated with increased risks of SARS-COV-2 incidence Ganslmeier et al. (2021), Nottmeyer et al. (2023).

In relation to air pollution, our results show a strong association with the incidence of SARS-COV-2. Specifically, coarse particle (PM10) affects the number of diagnoses in the subsequent week, while fine particulate matter (PM2.5) affects the number of diagnoses in the same week. The latter may be because the smaller size of this pollutant allows it to penetrate directly into the airways reaching the lungs and alveoli Gil (2007). Particulate matter is a mixture of solid and liquid particles found in the air, some of these particles are large and dark enough to be seen with the naked eye (PM10 whose diameter is less than 10 micrometers) while others can only be detected with a microscope (PM2.5 whose diameter is less than 2.5 micrometers) Agency. Due to their small size they can be inhaled and cause cardiovascular and respiratory diseases throughout the community that is exposed to the emissions. Smaller particulate matter can enter the respiratory tract and reach the lungs, alveoli, and can sometimes reach the bloodstream Gil (2007). Pevious studies have found similar results, including the impacts of air pollution and weather conditions on the incidence of COVID-19 Akan (2022), Jiang et al. (2020), and the relationship between high air pollution and low wind speeds that can favor the spread of COVID-19 and other infectious diseases Coccia (2020b, 2021a).

Different studies out the effect of lockdow revealed a reduction in the concentration of PM2.5, PM10 and other gaseous pollutans Chauhan and Singh (2020), Collivignarelli et al. (2020), Li et al. (2020), Mandal and Pal (2020), Nakada and Urban (2020), Sharma et al. (2020), Srivastava (2021) while, in the case of ozone, its concentration increased, thus having a curative effect on the ozone layer Collivignarelli et al. (2020), Li et al. (2020), Nakada and Urban (2020), Sharma et al. (2020), Srivastava (2021). The reduction in the air pollution due to lockdow show a decrease in mortality and morbidity, and with them a number of health and

economic benefits associated with these measures Cui et al. (2020). These lessons allow us to face the great challenge of advancing in the reduction of atmospheric pollution through the use of technologies to increase remote working Nakada and Urban (2020), remote education, and other services.

These results show that permanent control and prevention of environmental pollution play a vital role in controlling the health crisis and minimizing the impact on people's health. Although the study was carried out in the southern part of the country, the relationship found between the incidence of SARS-COV-2 and air pollution is evident. Others important lessons learned during the pandemic include avoiding overburdening health services and reducing transmission Canals (2020).

5.5 Conclusion

This study brings novelty in the field of environment SARS-COV-2 viral disease environment for nine regions of southern Chile, a country located in the southern hemisphere. We have included lagged variables for both meteorological and pollution variables, and controls by statistical week, and health centers, which allows us to capture any variation that exist in time and space caused by possible differences in health policies specific to each geographical area.

The results obtained in this study are consistent with the findings of other investigators about the relationship between the incidence of SARS-COV-2 with temperature and air pollution (PM10 and PM2.5). On the one hand, low temperatures are related to an increase in new cases in the following weeks.

Furthermore, air pollution is positively related to the incidence of the virus. Specifically, coarse particles affect the number of diagnoses in the following week, while fine particles affect the incidence in the same week.

Future studies are planned on mortality levels related to SARS-COV-2 and its relationship with climatic and pollution variables. These studies will also include new pollutants, other socioeconomic variables (population, distance between cities, income, among others) and the study area will extend to the entire country, where the climates and pollution factors vary greatly. Finally, it is interesting to study how vaccination has affected incidence and mortality levels related to the pandemic.

Chapter 6

Conclusiones y trabajo futuro

6.1 Conclusiones

En esta tesis se presentaron desarrollos teóricos y computacionales del fenómeno estocástico que gobierna el proceso de récord del *Drawdown*. En particular, se presentaron dos aproximaciones, una basada en procesos *PDMP* y otra por medio de una distribución Poisson fraccionaria.

A continuación se presentan los resultados más relevantes obtenidos en esta investigación.

- Se ha podido caracterizar los parámetros de una fPp por medio de técnicas de Approximate Bayesian Computation (ABC), lo cual nos entrega una nueva estrategia de estimación puntual e inferencia sobre el comportamiento de los parámetros que definen a una fPp.

- El análisis por medio de datos sintéticos, nos mostró que la estimación de los parámetos que definen la fPp, por medio de técnicas de ABC tiene un comportamiento similar a la estimación por momentos, lo cual valida la aproximación presentada en el actual trabajo.

- Para muestras relativamente pequeñas, la aproximación por ABC propone bandas de confianza de valores de los parámetros más estrechas que la estimación por momentos, siendo una alternativa más eficiente en este contexto.

- La aplicación a series de retornos financieros, nos mostró que el proceso que gobierna la sucesión de eventos extremos, puede ser caracterizada y modelada por medio de una fPp y que mientras más extremo es el evento, el parámetro α que define la condición fraccionaria del proceso, es menor.

- Se analizó el proceso de récord del *Drawdown*, por medio de un proceso Markoviano, considerando un número finito de estados.
- Se caracterizaron los estadísticos de media, varianza y función característica del proceso de récord del *Drawdown*.
- Se desarrollaron técnicas de simulación y estimación del proceso de récord, considerando un proceso Markoviano con un número finito de estados.

6.2 Trabajo Futuro

Dentro de las investigaciones esperadas en trabajos próximos, podemos considerar las extensiones de las investigaciones presentadas en este trabajo de tesis, dentro de las cuales podemos mencionar las siguientes.

- Generalización de los procesos PDMP, considerando procesos de larga memoria, lo que puede implicar la pérdida de las características Markovianas y necesidad de desarrollos teóricos en cuanto a los operadores diferenciales, técnicas de estimación y simulación de los procesos.
- Utilización de las técnicas desarrolladas sobre estimación y simulación de distribuciones Mittag-Leffler en otras áreas de la ciencia, como Sismología, Climatología, Física y Economía.
- Por medio de los conocimientos generales adquiridos en el programa de doctorado, desarrollar líneas de investigación en otras áreas de la ciencia como Inteligencia Artificial, Economía Aplicada, Finanzas, Medio Ambiente, entre otras.

References

Tercera encuesta nacional de medio ambiente y cambio climático. https://mma.gob.cl/encuestas-nacionales-del-medio-ambiente/, 2018. Accessed: 2022-03-01.

Department of health statistics and information. https://deis.minsal.cl/, 2022. Accessed: 2022-03-01.

Atmospheric decontamination plans. https://ppda.mma.gob.cl/, 2022. Accessed: 2022-03-01.

National air quality information system. https://sinca.mma.gob.cl/, 2022. Accessed: 2022-03-01.

U. E. P. Agency. Conceptos básicos sobre el material particulado (pm, por sus siglas en inglés). https://espanol.epa.gov/espanol/efectos-delmaterial-particulado-pm-sobre-la-salud-y-el-medioambientel. Accessed: 2022-07-14.

M. Ahmadi, A. Sharifi, S. Dorosti, S. J. Ghoushchi, and N. Ghanbari. Investigation of effective climatology parameters on covid-19 outbreak in iran. *Science of the total environment*, 729:138705, 2020.

M. Ahsanullah. *Records via probability theory*. Springer, 2015.

S. R. Aiyagari. Uninsured idiosyncratic risk and aggregate saving. *The Quarterly Journal of Economics*, 109(3):659–684, 1994.

A. P. Akan. Transmission of covid-19 pandemic (turkey) associated with short-term exposure of air quality and climatological parameters. *Environmental Science and Pollution Research*, 29(27):41695–41712, 2022.

J. G. Altonji and L. M. Segal. Small-sample bias in gmm estimation of covariance structures. *Journal of Business & Economic Statistics*, 14(3):353–366, 1996.

I. F. Alves and C. Neves. Extreme value theory: an introductory overview. *Extreme events in finance: A handbook of extreme value theory and its applications*, pages 53–95, 2017.

B. P. J. Andrée. Incidence of covid-19 and connections with air pollution exposure: evidence from the netherlands. *World Bank Policy Research Working Paper*, (9221), 2020.

A. Auler, F. Cássaro, V. Da Silva, and L. Pires. Evidence that high temperatures and intermediate relative humidity might favor the spread of covid-19 in tropical climate: a case study for the most affected brazilian cities. *Science of the Total Environment*, 729: 139090, 2020.

R. Azais and F. Bouguet. *Statistical Inference for Piecewise - deterministic Markov Processes*. John Wiley & Sons, 2018.

R. Azaïs and A. Genadot. Level crossings and absorption of an insurance model, 2018.

M. F. Bashir, B. Ma, B. Komal, M. A. Bashir, D. Tan, M. Bashir, et al. Correlation between climate indicators and covid-19 pandemic in new york, usa. *Science of The Total Environment*, 728:138835, 2020.

R. Basu and J. M. Samet. Relation between elevated ambient temperature and mortality: a review of the epidemiologic evidence. *Epidemiologic reviews*, 24(2):190–202, 2002.

N. Bäuerle and U. Rieder. Optimal control of piecewise deterministic markov processes with finite time horizon. *Modern trends in controlled stochastic processes: theory and applications*, 123:143, 2010.

M. A. Beaumont. Approximate bayesian computation in evolution and ecology. *Annual review of ecology, evolution, and systematics*, 41:379–406, 2010.

M. A. Beaumont, J.-M. Cornuet, J.-M. Marin, and C. P. Robert. Adaptive approximate bayesian computation. *Biometrika*, 96(4):983–990, 2009.

L. Beghin and C. Macci. Large deviations for fractional poisson processes. *Statistics & Probability Letters*, 83(4):1193–1202, 2013.

L. Beghin, E. Orsingher, et al. Fractional poisson processes and related planar random motions. *Electronic Journal of Probability*, 14:1790–1826, 2009.

M. L. Bell, A. McDermott, S. L. Zeger, J. M. Samet, and F. Dominici. Ozone and short-term mortality in 95 us urban communities, 1987-2000. *Jama*, 292(19):2372–2378, 2004.

M. Benaïm, S. Le Borgne, F. Malrieu, and P.-A. Zitt. Qualitative properties of certain piecewise deterministic markov processes. In *Annales de l'IHP Probabilités et statistiques*, volume 51, pages 1040–1075, 2015.

R. Bertollini, D. Lebowitz, R. Saracci, and D. A. Savitz. Environmental epidemiology, 1996.

R. Biard and B. Saussereau. Fractional poisson process: long-range dependence and applications in ruin theory. *Journal of Applied Probability*, 51(3):727–740, 2014.

Biblioteca del Congreso Nacional de Chile. Clima y vegetación. chile nuestro país. https://www.bcn.cl/siit/nuestropais/clima.htm, 2022. Accessed: 2022-07-18.

R. Blender, C. Raible, and F. Lunkeit. Non-exponential return time distributions for vorticity extremes explained by fractional poisson processes. *Quarterly Journal of the Royal Meteorological Society*, 141(686):249–257, 2015.

M. I. Bogachev and A. Bunde. Memory effects in the statistics of interoccurrence times between large returns in financial records. *Physical Review E*, 78(3):036114, 2008.

J. Brogaard, A. Carrion, T. Moyaert, R. Riordan, A. Shkilko, and K. Sokolov. High frequency trading and extreme price movements. *Journal of Financial Economics*, 128(2):253–265, 2018.

M. L. Bujorianu and J. Lygeros. Reachability questions in piecewise deterministic markov processes. In *International Workshop on Hybrid Systems: Computation and Control*, pages 126–140. Springer, 2003.

A. Bunde, J. Kropp, and H.-J. Schellnhuber. *The science of disasters: climate disruptions, heart attacks, and market crashes*. Springer Science & Business Media, 2012.

D. O. Cahoy. *Fractional Poisson process in terms of alpha-stable densities*. PhD thesis, Case Western Reserve University, 2007.

D. O. Cahoy, V. V. Uchaikin, and W. A. Woyczynski. Parameter estimation for fractional poisson processes. *Journal of Statistical Planning and Inference*, 140(11):3106–3120, 2010.

M. Canals. Conceptos para una buena toma de decisiones en la pandemia covid-19 en chile. *Revista chilena de infectología*, 37(2):170–172, 2020.

P. Carr, H. Zhang, and O. Hadjiliadis. Maximum drawdown insurance. *International Journal of Theoretical and Applied Finance*, 14(08):1195–1230, 2011.

J. M. Chambers, C. L. Mallows, and B. Stuck. A method for simulating stable random variables. *Journal of the american statistical association*, 71(354):340–344, 1976.

K.-L. Chang. Do macroeconomic variables have regime-dependent effects on stock return dynamics? evidence from the markov regime switching model. *Economic Modelling*, 26 (6):1283–1299, 2009.

S. P. Chatzis, V. Siakoulis, A. Petropoulos, E. Stavroulakis, and N. Vlachogiannakis. Forecasting stock market crisis events using deep and statistical machine learning techniques. *Expert systems with applications*, 112:353–371, 2018.

A. Chauhan and R. P. Singh. Decline in pm2. 5 concentrations over major cities around the world associated with covid-19. *Environmental research*, 187:109634, 2020.

J. Chiquet, N. Limnios, and M. Eid. Piecewise deterministic markov processes applied to fatigue crack growth modelling. *Journal of Statistical Planning and Inference*, 139(5): 1657–1667, 2009.

T. E. Clark. Small-sample properties of estimators of nonlinear models of covariance structure. *Journal of Business & Economic Statistics*, 14(3):367–373, 1996.

M. Coccia. Factors determining the diffusion of covid-19 and suggested strategy to prevent future accelerated viral infectivity similar to covid. *Science of the Total Environment*, 729: 138474, 2020a.

M. Coccia. How (un) sustainable environments are related to the diffusion of covid-19: the relation between coronavirus disease 2019, air pollution, wind resource and energy. *Sustainability*, 12(22):9709, 2020b.

M. Coccia. The effects of atmospheric stability with low wind speed and of air pollution on the accelerated transmission dynamics of covid-19. *International Journal of Environmental Studies*, 78(1):1–27, 2021a.

M. Coccia. High health expenditures and low exposure of population to air pollution as critical factors that can reduce fatality rate in covid-19 pandemic crisis: a global analysis. *Environmental Research*, 199:111339, 2021b.

M. Coccia. The impact of first and second wave of the covid-19 pandemic in society: comparative analysis to support control measures to cope with negative effects of future infectious diseases. *Environmental Research*, 197:111099, 2021c.

M. Coccia. The relation between length of lockdown, numbers of infected people and deaths of covid-19, and economic growth of countries: Lessons learned to cope with future pandemics similar to covid-19 and to constrain the deterioration of economic system. *Science of The Total Environment*, 775:145801, 2021d.

E. S. Coker, L. Cavalli, E. Fabrizi, G. Guastella, E. Lippo, M. L. Parisi, N. Pontarollo, M. Rizzati, A. Varacca, and S. Vergalli. The effects of air pollution on covid-19 related mortality in northern italy. *Environmental and Resource Economics*, 76(4):611–634, 2020.

M. C. Collivignarelli, A. Abbà, G. Bertanza, R. Pedrazzani, P. Ricciardi, and M. C. Miino. Lockdown for covid-2019 in milan: What are the effects on air quality? *Science of the total environment*, 732:139280, 2020.

D. Contini and F. Costabile. Does air pollution influence covid-19 outbreaks?, 2020.

O. L. V. Costa and F. Dufour. Stability and ergodicity of piecewise deterministic markov processes. *SIAM Journal on Control and Optimization*, 47(2):1053–1077, 2008.

L. Cui, J. Zhou, X. Peng, S. Ruan, and Y. Zhang. Analyses of air pollution control measures and co-benefits in the heavily air-polluted jinan city of china, 2013–2017. *Scientific reports*, 10(1):1–10, 2020.

Z. Cui, C. Lee, and Y. Liu. Single-transform formulas for pricing asian options in a general approximation framework under markov processes. *European Journal of Operational Research*, 266(3):1134–1139, 2018.

Z. Cui, J. L. Kirkby, and D. Nguyen. A general framework for time-changed markov processes and applications. *European Journal of Operational Research*, 273(2):785–800, 2019.

M. H. Davis. Piecewise-deterministic markov processes: a general class of non-diffusion stochastic models. *Journal of the Royal Statistical Society: Series B (Methodological)*, 46 (3):353–376, 1984.

M. H. Davis. *Markov models & optimization*, volume 49. CRC Press, 1993.

M. H. Davis. *Markov models & optimization*. Routledge, 2018.

M. de Carvalho. Statistics of extremes: Challenges and opportunities. *Extreme Events in Finance. Wiley Handb. Finance Eng. Econom*, pages 195–213, 2017.

B. V. de Melo Mendes and R. C. Lavrado. Implementing and testing the maximum drawdown at risk. *Finance Research Letters*, 22:95–100, 2017.

P. Del Moral, A. Doucet, and A. Jasra. Sequential monte carlo samplers. *Journal of the Royal Statistical Society: Series B (Statistical Methodology)*, 68(3):411–436, 2006.

F. B. Díez. Meteorología y salud. la relación entre la temperatura ambiental y la mortalidad. *Rev Esp Salud Pública*, 70(3):251–259, 1996.

Dirección Meteorológica de Chile. Dirección General de Aeronáutica Civil (DGAC). Reporte climático. https://climatologia.meteochile.gob.cl/publicaciones/reporteClimatologico/reporteClimatologico-2020.pdf, 2022. Accessed: 2022-07-18.

J. L. Domingo and J. Rovira. Effects of air pollutants on the transmission and severity of respiratory viral infections. *Environmental research*, 187:109650, 2020.

D. Duffie and J. Pan. An overview of value at risk. *Journal of derivatives*, 4(3):7–49, 1997.

A. Durmus, A. Guillin, and P. Monmarché. Piecewise deterministic markov processes and their invariant measure. *arXiv preprint arXiv:1807.05421*, 2018.

P. Embrechts, C. Klüppelberg, and T. Mikosch. *Modelling extremal events: for insurance and finance*, volume 33. Springer Science & Business Media, 2013.

S. N. Ethier and T. G. Kurtz. *Markov processes: characterization and convergence*, volume 282. John Wiley & Sons, 2009.

T. S. Ferguson. *A course in large sample theory*. Routledge, 2017.

L. J. Fermín and J. Lévy-Véhel. Variability and singularity arising from a piecewise-deterministic markov process applied to model poor patient compliance in the multi-iv case. *Journal of Applied Statistics*, 47(13-15):2525–2545, 2020. doi: 10.1080/02664763.2019.1711030. URL https://doi.org/10.1080/02664763.2019.1711030.

M. Ganslmeier, D. Furceri, and J. D. Ostry. The impact of weather on covid-19 pandemic. *Scientific reports*, 11(1):1–7, 2021.

G. Gasper, M. Rahman, and G. George. *Basic hypergeometric series*, volume 96. Cambridge university press, 2004.

C. L. Gil. Las pm 2.5 y su impacto sobre la salud. el caso de la ciudad de madrid. *Ecosostenible*, (35):32–37, 2007.

M. I. Gomes and A. Guillou. Extreme value theory and statistics of univariate extremes: a review. *International statistical review*, 83(2):263–292, 2015.

R. Gorenflo and F. Mainardi. Fractional calculus: integral and differential equations of fractional order. *arXiv preprint arXiv:0805.3823*, 2008.

C. W. Granger and D. Orr. "infinite variance" and research strategy in time series analysis. *Journal of the American Statistical Association*, 67(338):275–285, 1972.

W. Greene. *Econometric Analysis*. Pearson, 2018.

F. Gresnigt, E. Kole, and P. H. Franses. Interpreting financial market crashes as earthquakes: A new early warning system for medium term crashes. *Journal of Banking & Finance*, 56: 123–139, 2015.

A. Gupta, H. Bherwani, S. Gautam, S. Anjum, K. Musugu, N. Kumar, A. Anshul, and R. Kumar. Air pollution aggravating covid-19 lethality? exploration in asian cities using statistical models. *Environment, Development and Sustainability*, 23(4):6408–6417, 2021.

F. Hamelink and M. Hoesli. Maximum drawdown and the allocation to real estate. *Journal of Property Research*, 21(1):5–29, 2004.

A. C. Harvey. Estimating regression models with multiplicative heteroscedasticity. *Econometrica: Journal of the Econometric Society*, pages 461–465, 1976.

C.-H. Hsieh and B. R. Barmish. On drawdown-modulated feedback control in stock trading. *IFAC-PapersOnLine*, 50(1):952–958, 2017a.

C.-H. Hsieh and B. R. Barmish. On inefficiency of markowitz-style investment strategies when drawdown is important. In *2017 IEEE 56th Annual Conference on Decision and Control (CDC)*, pages 3075–3080. IEEE, 2017b.

M. Huggett. The risk-free rate in heterogeneous-agent incomplete-insurance economies. *Journal of economic Dynamics and Control*, 17(5-6):953–969, 1993.

Y. Jiang, X.-J. Wu, and Y.-J. Guan. Effect of ambient air pollutants and meteorological variables on covid-19 incidence. *Infection Control & Hospital Epidemiology*, 41(9): 1011–1015, 2020.

Z.-Q. Jiang, G.-J. Wang, A. Canabarro, B. Podobnik, C. Xie, H. E. Stanley, and W.-X. Zhou. Short term prediction of extreme returns based on the recurrence interval analysis. *Quantitative Finance*, 18(3):353–370, 2018.

P. Jorion. *Value at risk: the new benchmark for managing financial risk*. The McGraw-Hill Companies, Inc., 2007.

G. Jumarie. Fractional master equation: non-standard analysis and liouville–riemann derivative. *Chaos, Solitons & Fractals*, 12(13):2577–2587, 2001.

M. Kanter et al. Stable densities under change of scale and total variation inequalities. *The Annals of Probability*, 3(4):697–707, 1975.

A. Karan, K. Ali, S. Teelucksingh, and S. Sakhamuri. The impact of air pollution on the incidence and mortality of covid-19. *Global Health Research and Policy*, 5(1):1–3, 2020.

A. Klenke. *Probability theory: a comprehensive course*. Springer Science & Business Media, 2013.

P. Kouretas, K. Koutoumpas, and J. Lygeros. Parameter identification for piecewise deterministic markov processes: A case study on a biochemical network. *IFAC Proceedings Volumes*, 39(5):172–178, 2006.

S. Kullback and R. A. Leibler. On information and sufficiency. *The annals of mathematical statistics*, 22(1):79–86, 1951.

G. Kulldorff. On the conditions for consistency and asymptotic efficiency of maximum likelihood estimates. *Scandinavian Actuarial Journal*, 1957(3-4):129–144, 1957.

D. Landriault, B. Li, and D. Li. Optimal investment to minimize the expected cumulative drawdown. 2018.

N. Laskin. Fractional poisson process. *Communications in Nonlinear Science and Numerical Simulation*, 8(3-4):201–213, 2003.

R. P. C. Leal and B. V. de Melo Mendes. Maximum drawdown: Models and applications. *The Journal of Alternative Investments*, 7(4):83–91, 2005.

L. Li, Q. Li, L. Huang, Q. Wang, A. Zhu, J. Xu, Z. Liu, H. Li, L. Shi, R. Li, et al. Air quality changes during the covid-19 lockdown over the yangtze river delta region: An insight into the impact of human activity pattern changes on air pollution variation. *Science of the Total Environment*, 732:139282, 2020.

Y. T. Lin and N. E. Buchler. Efficient analysis of stochastic gene dynamics in the non-adiabatic regime using piecewise deterministic markov processes. *Journal of The Royal Society Interface*, 15(138):20170804, 2018.

J. Lintusaari, M. U. Gutmann, R. Dutta, S. Kaski, and J. Corander. Fundamentals and recent developments in approximate bayesian computation. *Systematic biology*, 66(1):e66–e82, 2017.

P. Liu and H. Mumtaz. Evolving macroeconomic dynamics in a small open economy: An estimated markov switching dsge model for the uk. *Journal of Money, Credit and Banking*, 43(7):1443–1474, 2011.

X. Liu, D. Margaritis, and P. Wang. Stock market volatility and equity returns: Evidence from a two-state markov-switching model with regressors. *Journal of Empirical Finance*, 19(4):483–496, 2012.

S. Lolli, Y.-C. Chen, S.-H. Wang, and G. Vivone. Impact of meteorological conditions and air pollution on covid-19 pandemic transmission in italy. *Scientific reports*, 10(1):1–15, 2020.

F. Longin. *Extreme events in finance: A handbook of extreme value theory and its applications*. John Wiley & Sons, 2016.

F. M. Longin. The asymptotic distribution of extreme stock market returns. *Journal of business*, pages 383–408, 1996.

M. Magdon-Ismail and A. F. Atiya. Maximum drawdown. *Risk Magazine*, 17(10):99–102, 2004.

F. Mainardi. Why the mittag-leffler function can be considered the queen function of the fractional calculus? *Entropy*, 22(12):1359, 2020.

F. Mainardi, R. Gorenflo, and E. Scalas. A fractional generalization of the poisson processes. *arXiv preprint math/0701454*, 2007.

M. Maleki, E. Anvari, P. K. Hopke, Z. Noorimotlagh, and S. A. Mirzaee. An updated systematic review on the association between atmospheric particulate matter pollution and prevalence of sars-cov-2. *Environmental research*, 195:110898, 2021.

I. Mandal and S. Pal. Covid-19 pandemic persuaded lockdown effects on environment over stone quarrying and crushing areas. *Science of the Total Environment*, 732:139281, 2020.

X. Mao. *Stochastic differential equations and applications*. Elsevier, 2007.

P. Marjoram, J. Molitor, V. Plagnol, and S. Tavaré. Markov chain monte carlo without likelihoods. *Proceedings of the National Academy of Sciences*, 100(26):15324–15328, 2003.

W. J. Martens. Climate change, thermal stress and mortality changes. *Social science & medicine*, 46(3):331–344, 1998.

G. McLachlan and D. Peel. *Finite mixture models*. John Wiley & Sons, 2004.

R. Mendoza-Arriaga and V. Linetsky. Multivariate subordination of markov processes with financial applications. *Mathematical Finance*, 26(4):699–747, 2016.

M. J. Messner, P. Berger, and S. P. Nappier. Fractional poisson—a simple dose-response model for human norovirus. *Risk Analysis*, 34(10):1820–1829, 2014.

P. M. Möller. Drawdown measures and return moments. *International Journal of Theoretical and Applied Finance*, 21(07):1850042, 2018.

L. Y. K. Nakada and R. C. Urban. Covid-19 pandemic: Impacts on the air quality during the partial lockdown in são paulo state, brazil. *Science of the Total Environment*, 730:139087, 2020.

S. Näyhä. Environmental temperature and mortality. *International Journal of Circumpolar Health*, 64(5):451–458, 2005.

J. P. Nolan. Numerical calculation of stable densities and distribution functions. *Communications in statistics. Stochastic models*, 13(4):759–774, 1997.

Z. Noorimotlagh, N. Jaafarzadeh, S. S. Martínez, and S. A. Mirzaee. A systematic review of possible airborne transmission of the covid-19 virus (sars-cov-2) in the indoor air environment. *Environmental research*, 193:110612, 2021a.

Z. Noorimotlagh, S. A. Mirzaee, N. Jaafarzadeh, M. Maleki, G. Kalvandi, and C. Karami. A systematic review of emerging human coronavirus (sars-cov-2) outbreak: focus on disinfection methods, environmental survival, and control and prevention strategies. *Environmental Science and Pollution Research*, 28(1):1–15, 2021b.

L. Nottmeyer, B. Armstrong, R. Lowe, S. Abbott, S. Meakin, K. M. O'Reilly, R. von Borries, R. Schneider, D. Royé, M. Hashizume, et al. The association of covid-19 incidence with temperature, humidity, and uv radiation–a global multi-city analysis. *Science of The Total Environment*, 854:158636, 2023.

S. Novak. Measures of financial risk. *Extreme Events in Finance*, page 215, 2017.

S. Novak and J. Beirlant. The magnitude of a market crash can be predicted. *Journal of banking & finance*, 30(2):453–462, 2006.

L. H. Pedersen. *Efficiently inefficient: how smart money invests and market prices are determined*. Princeton University Press, 2019.

K. Penson and K. Górska. Exact and explicit probability densities for one-sided lévy stable distributions. *Physical review letters*, 105(21):210604, 2010.

G. W. Peters, Y. Fan, and S. A. Sisson. On sequential monte carlo, partial rejection control and approximate bayesian computation. *Statistics and Computing*, 22(6):1209–1222, 2012.

C. Poirier, W. Luo, M. S. Majumder, D. Liu, K. D. Mandl, T. A. Mooring, and M. Santillana. The role of environmental factors on transmission rates of the covid-19 outbreak: an initial assessment in two spatial scales. *Scientific reports*, 10(1):1–11, 2020.

L. Pospisil and J. Vecer. Portfolio sensitivity to changes in the maximum and the maximum drawdown. *Quantitative Finance*, 10(6):617–627, 2010.

M. Power. The risk management of everything. *The Journal of Risk Finance*, 2004.

Y. Qiu, X. Chen, and W. Shi. Impacts of social and economic factors on the transmission of coronavirus disease 2019 (covid-19) in china. *Journal of Population Economics*, 33(4): 1127–1172, 2020.

C. Ren, G. M. Williams, and S. Tong. Does particulate matter modify the association between temperature and cardiorespiratory diseases? *Environmental health perspectives*, 114(11): 1690–1696, 2006.

O. Repin and A. Saichev. Fractional poisson law. *Radiophysics and Quantum Electronics*, 43(9):738–741, 2000.

R. T. Rockafellar, S. Uryasev, et al. Optimization of conditional value-at-risk. *Journal of risk*, 2:21–42, 2000.

D. Rossello and S. Lo Cascio. A refined measure of conditional maximum drawdown. *A Refined Measure of Conditional Maximum Drawdown (July 31, 2019)*, 2019.

R. Rudnicki and M. Tyran-Kamińska. Piecewise deterministic markov processes in biological models. In *Semigroups of operators-theory and applications*, pages 235–255. Springer, 2015.

I. Sabat, S. Neumann-Böhme, N. E. Varghese, P. P. Barros, W. Brouwer, J. van Exel, J. Schreyögg, and T. Stargardt. United but divided: Policy responses and people's perceptions in the eu during the covid-19 outbreak. *Health Policy*, 124(9):909–918, 2020.

P. K. Sahoo, M. A. Powell, S. Mittal, and V. Garg. Is the transmission of novel coronavirus disease (covid-19) weather dependent? *Journal of the Air & Waste Management Association*, 70(11):1061–1064, 2020.

A. I. Saichev and G. M. Zaslavsky. Fractional kinetic equations: solutions and applications. *Chaos: An Interdisciplinary Journal of Nonlinear Science*, 7(4):753–764, 1997.

J. M. Samet, F. Dominici, F. C. Curriero, I. Coursac, and S. L. Zeger. Fine particulate air pollution and mortality in 20 us cities, 1987–1994. *New England journal of medicine*, 343 (24):1742–1749, 2000.

J. G. Saw, M. C. Yang, and T. C. Mo. Chebyshev inequality with estimated mean and variance. *The American Statistician*, 38(2):130–132, 1984.

E. Scalas, R. Gorenflo, and F. Mainardi. Uncoupled continuous-time random walks: Solution and limiting behavior of the master equation. *Physical Review E*, 69(1):011107, 2004.

M. Schäl. On piecewise deterministic markov control processes: control of jumps and of risk processes in insurance. *Insurance: Mathematics and Economics*, 22(1):75–91, 1998.

S. Sharma, M. Zhang, J. Gao, H. Zhang, S. H. Kota, et al. Effect of restricted emissions during covid-19 on air quality in india. *Science of the total environment*, 728:138878, 2020.

B. W. Silverman. *Density estimation for statistics and data analysis*. Routledge, 2018.

S. A. Sisson, Y. Fan, and M. M. Tanaka. Sequential monte carlo without likelihoods. *Proceedings of the National Academy of Sciences*, 104(6):1760–1765, 2007.

K. Soetaert, T. Petzoldt, and R. W. Setzer. Solving differential equations in r: package desolve. *Journal of statistical software*, 33:1–25, 2010.

P. Sosa, P. Couto, A. Rodriguez, M. Charles, J. Leite, and R. Paleker. Sistemas de vigilancia de influenza y otros virus respiratorios en las américas. *Washington, DC: Organización Panamericana de la Salud*, 2017.

A. Srivastava. Covid-19 and air pollution and meteorology-an intricate relationship: A review. *Chemosphere*, 263:128297, 2021.

C. Tanis and K. Karakaya. Investigating the impacts of air quality and weather indicators on the spread of sars-cov-2 in istanbul, turkey. *Thermal Science*, 25(4 Part A):2755–2765, 2021.

A. Taranto and S. Khan. Drawdown and drawup of bi-directional grid constrained stochastic processes. *Journal of Mathematics and Statistics*, 16(1):182–197, 2020.

N. Thomas. *Stochastic numerical methods for Piecewise Deterministic Markov Processes: applications in Neuroscience*. PhD thesis, Sorbonne université, 2019.

D. M. Titterington, A. F. Smith, and U. E. Makov. *Statistical analysis of finite mixture distributions*. Wiley,, 1985.

A. Toarna and V. Cojanu. The 2008 crisis: Causes and future direction for the academic research. *Procedia Economics and Finance*, 27:385–393, 2015.

T. Toni, D. Welch, N. Strelkowa, A. Ipsen, and M. P. Stumpf. Approximate bayesian computation scheme for parameter inference and model selection in dynamical systems. *Journal of the Royal Society Interface*, 6(31):187–202, 2008.

V. Uchaikin and R. Sibatov. A fractional poisson process in a model of dispersive charge transport in semiconductors. *Russian Journal of Numerical Analysis and Mathematical Modelling*, 23(3):283–297, 2008.

V. V. Uchaikin and V. M. Zolotarev. *Chance and stability: stable distributions and their applications*. Walter de Gruyter, 2011.

V. V. Uchaikin, D. O. Cahoy, and R. T. Sibatov. Fractional processes: from poisson to branching one. *International Journal of Bifurcation and Chaos*, 18(09):2717–2725, 2008.

S. Vasishth. Using approximate bayesian computation for estimating parameters in the cue-based retrieval model of sentence processing. *MethodsX*, 7:100850, 2020.

P. Verger, J. Tressou, and S. Clemencon. Integration of time as a description parameter in risk characterisation: application to methyl mercury. *Regulatory Toxicology and Pharmacology*, 49(1):25–30, 2007.

C. Walter. The extreme value problem in finance: Comparing the pragmatic program with the m andelbrot program. *Extreme events in Finance: A handbook of extreme value theory and its applications*, pages 25–51, 2016.

X.-T. Wang and Z.-X. Wen. Poisson fractional processes. *Chaos, Solitons & Fractals*, 18(1): 169–177, 2003.

A. Weron and R. Weron. Computer simulation of lévy α-stable variables and processes. In *Chaos—The interplay between stochastic and deterministic behaviour*, pages 379–392. Springer, 1995.

R. Xu, H. Rahmandad, M. Gupta, C. DiGennaro, N. Ghaffarzadegan, H. Amini, and M. S. Jalali. The modest impact of weather and air pollution on covid-19 transmission. *Available at SSRN 3593879*, 2020.

H. Zhang. Effect of derivative accounting rules on corporate risk-management behavior. *Journal of accounting and economics*, 47(3):244–264, 2009.

H. Zhang, F. Dufour, Y. Dutuit, and K. Gonzalez. Piecewise deterministic markov processes and dynamic reliability. *Proceedings of the Institution of Mechanical Engineers, Part O: Journal of Risk and Reliability*, 222(4):545–551, 2008.

Z. Zhang, T. Xue, and X. Jin. Effects of meteorological conditions and air pollution on covid-19 transmission: Evidence from 219 chinese cities. *Science of the total environment*, 741:140244, 2020.

C. Zhao, X. Fang, Y. Feng, X. Fang, J. He, and H. Pan. Emerging role of air pollution and meteorological parameters in covid-19. *Journal of Evidence-Based Medicine*, 2021.

Y. Zhu, J. Xie, F. Huang, and L. Cao. Association between short-term exposure to air pollution and covid-19 infection: Evidence from china. *Science of the total environment*, 727:138704, 2020.

V. M. Zolotarev. One-dimensional stable distributions, translations of mathematical monographs, vol. 65. *American Mathematical Society*, 1986.